UNIVERSITY OF HAWAII
LIBRARY
Jun 10 '60

The
Philosophical Magazine

FIRST PUBLISHED IN 1798

A Journal of Theoretical
Experimental and Applied Physics

Vol. 5 January 1960 No. 49
Eighth Series

25s. 0d., plus postage
Annual Subscription £13 10s. 0d., payable in advance

ALERE FLAMMAM

Printed and Published by
TAYLOR & FRANCIS LTD
RED LION COURT, FLEET STREET, LONDON, E.C.4

THE PHILOSOPHICAL MAGAZINE

Editor
Professor N. F. Mott, M.A., D.Sc., F.R.S.

Editorial Board
Sir Lawrence Bragg, O.B.E., M.C., M.A., D.Sc., F.R.S.
Sir George Thomson, M.A., D.Sc., F.R.S.
Professor A. M. Tyndall, C.B.E., D.Sc., F.R.S.

Authors wishing to submit papers for publication in the Journal should send manuscripts directly to the Publishers.

Manuscripts should be typed in *double* spacing on one side of quarto (8 × 10 in.) paper, and authors are urged to aim at absolute clarity of meaning and an attractive presentation of their texts.

References should be listed at the end in alphabetical order of authors and should be cited in the text in terms of author's name and date. Diagrams should normally be in Indian ink on white card, with lettering in soft pencil, the captions being typed on a separate sheet.

A leaflet giving detailed instructions to authors on the preparation of papers is available on request from the Publishers.

Authors are entitled to receive 25 offprints of a paper in the Journal free of charge, and additional offprints can be obtained from the Publishers.

The *Philosophical Magazine* and its companion journal, *Advances in Physics*, will accept papers for publication in experimental and theoretical physics. The *Philosophical Magazine* publishes contributions describing new results, letters to the editor and book reviews. *Advances in Physics* publishes articles surveying the present state of knowledge in any branch of the science in which recent progress has been made. The editors welcome contributions from overseas as well as from the United Kingdom, and papers may be published in English, French and German.

THE

PHILOSOPHICAL MAGAZINE

A JOURNAL OF THEORETICAL, EXPERIMENTAL AND APPLIED PHYSICS

First Published in 1798

[EIGHTH SERIES—VOL. 5]

Direct Observations of the Annealing of Prismatic Dislocation Loops and of Climb of Dislocations in Quenched Aluminium†

By J. Silcox and M. J. Whelan
Crystallographic Laboratory, Cavendish Laboratory,
Cambridge, England

[Received September 16, 1959]

Abstract

A high temperature stage fitted to a Siemens Elmiskop 1 electron microscope has been used to study directly the annealing of prismatic dislocation loops in thin foils prepared from quenched and aged bulk specimens of aluminium. In the temperature range 170–200°c the loops are observed to shrink and eventually to disappear. Observations on dislocations other than loops also present in the thin foils show that they become smoother while the loops are disappearing. The results are interpreted in terms of climb of dislocations by vacancy emission, and in the case of loops in thin foils, where vacancy supersaturation effects are thought to be negligible, the climb rate is governed by the line tension and curvature of the loops. The radius r of a loop as a function of time t is given by the theoretical expression $r=r_0[1-(t/\tau)]^{1/2}$ where τ is the lifetime of a loop of initial radius r_0. The temperature dependence is primarily $\tau=\tau_0 \exp(E/kT)$ where E is the activation energy of self diffusion. Comparison with experiment gives estimates of the activation energy in the range 1·2–1·3 ev.

Annealing experiments with bulk material have been carried out in parallel with the above experiments. They show that the loops anneal out in the same temperature range. The details are different however owing to vacancy supersaturation effects. Larger loops appear to grow at the expense of smaller ones. The theory gives a qualitative explanation of the annealing of electrical resistivity in quenched aluminium observed by other workers, although the shape of the isothermal annealing curve is difficult to predict quantitatively, owing to its dependence on the complex annealing behaviour of loops in bulk material. The experiments also suggest that the temperature rise of thin foils examined in the electron microscope due to heating by the electron beam is very small.

§ 1. Introduction

When a metal is rapidly cooled from high temperatures large numbers of vacant lattice sites in excess of the equilibrium concentration may be quenched-in. The changes in physical properties produced by quenching and the variation of these changes on subsequent annealing are therefore interpreted in terms of the properties and behaviour of vacancies (Maddin and Cottrell 1955, Bauerle and Koehler 1957, Koehler *et al.* 1957, Panseri and Federighi 1958, Federighi 1959, DeSorbo and Turnbull 1959, Kimura *et al.* 1959 a, b, Meshii and Kauffman 1959, for review see Cottrell 1957). An investigation of the annealing out of the increase in electrical resistivity of aluminium produced by quenching has recently been carried out by Panseri and Federighi (1958) and by Federighi (1959). These workers showed the presence of two stages in the isochronal annealing curves of specimens quenched from temperatures greater than ~400°C. The first stage took place in a few minutes at room temperature (Wintenberger 1957, Bradshaw and Pearson 1957, DeSorbo and Turnbull 1959) and was associated by Panseri and Federighi with the movement of vacancies to form clusters of some unspecified type. The second stage occurred at temperatures at which self-diffusion is important and was therefore associated with the dispersal of the clusters.

---

† Communicated by the Authors.

Recent observations (Hirsch, Silcox, Smallman and Westmacott 1958) using the transmission electron microscope technique, have revealed the presence of small prismatic dislocation loops in thin foils of aluminium prepared from quenched and aged bulk material. These are thought to be produced by the condensation of excess vacancies into disc-like cavities which subsequently collapse to form loops of whole dislocation line. However, as was pointed out by Federighi (1959), the identification of these loops with the clusters postulated by Panseri and Federighi was not unambiguous. Thus it was possible that while a fraction of the vacancies formed dislocation loops, another fraction formed clusters so small that they are not detected on transmission electron micrographs. Stage II of the resistivity annealing curves could then be associated with the annealing of small vacancy clusters and not necessarily with the disappearance of loops. It is therefore necessary to decide this point by experiment. Two types of experiment may be carried out using the transmission electron microscope. In the first a high temperature stage in the microscope is used to observe the annealing out phenomena directly in the thin foils. The behaviour of the loops on annealing can therefore be studied in detail. In the second, the annealing treatment is carried out on bulk material which is subsequently thinned and examined in the electron microscope. This paper describes the results of both types of experiment for aluminium and discusses their physical significance.

§ 2. EXPERIMENTAL TECHNIQUE

Aluminium of Johnson-Matthey 'specpure' quality, nominally 99·99% pure, and in the form of foil 0·003 in. thick, was quenched from about 600°C by dropping under gravity from a vertical tube furnace into iced brine. The foil was then allowed to age at room temperature for several hours. The foils were thinned by electropolishing in an 80% ethyl alcohol – 20% perchloric acid bath (Tomlinson 1958). Observations were recorded on photographic plates in the usual way, and also in some of the high-temperature stage experiments by direct ciné-photography of the fluorescent screen of the electron microscope using equipment described by Whelan *et al.* (1957). For the bulk material experiments a quenched and aged foil was cut into two parts. One part was thinned and examined directly to establish the existence of loops. The other part was annealed in an oil bath for six minutes prior to thinning and examination. Annealing temperatures of 100, 160, 170, 180, 190, 200, 210 and 220°C were employed.

Examination was carried out with a Siemens Elmiskop 1 electron microscope operating at 100 kv.

Figures 1 (*a*), (*b*) and (*c*) show the main details of the high temperature stage used for annealing the thin foils during observation. The specimen holder (fig. 1 (*a*) and (*b*)) is similar in shape to the conventional holder and is inserted through the airlock into the bore of the objective pole-piece in the usual manner. The specimen holder contains a two-pin socket E, insulated from the body of the holder and carrying a filament type specimen support AB. This support consists of two 0·4 mm diameter platinum legs B spot-welded to a 200 mesh stainless steel grid A and secured in the socket by two screws D. The grids are cut from RCA $\frac{1}{8}$ in. diameter stainless steel specimen supports. The spacing between the platinum legs at the grid is 1·5 mm, and the width of the grid is such that seven strands of wire conduct the heating current. Direct current is passed through the grid by means of a two-pin plug A at the end of a long rod inserted through the hole in the objective lens normally occupied by the stereo-drive (fig. 1 (*c*)). With this equipment therefore it is not possible to tilt the object during observation. The rod can move to follow the stage movement and can be withdrawn to an inoperative position when the specimen is removed. The instrument also requires a modified stage carriage (not shown) similar to the conventional carriage but without the stereo-mechanism. More complete details of this equipment have been reported by Whelan (1958).

The specimens are mounted by removing the end cap C in fig. 1 (*a*). The grid is dipped in a dilute solution of polybutene in xylol, which acts as an adhesive ; excess solution is blotted off and the specimen is placed in the centre of the grid as in fig. 1 (*b*).

The compact design of the stage prevents measurement of the temperature of the grid during observation. However grid temperature versus heating current curves have been determined by calibration of individual specimen supports in a high vacuum system. A Pt, Pt–13% Rh thermocouple of 48 s.w.g. (supplied by Johnson-Matthey) was placed as closely as possible to the centre of the grid. Millivolt readings were converted to degrees centigrade using Johnson-Matthey conversion tables. Measurements were reproducible to about ±2°C at 170°C. The current required to heat the centre of an average grid to 200°C was about 1·1 amp, the working temperature being attained a few seconds after switching on. The variation of temperature over the grid was not investigated. However, in a few cases a grid was recalibrated with a new thermocouple after use. The temperature usually differed slightly from the previous

Fig. 1

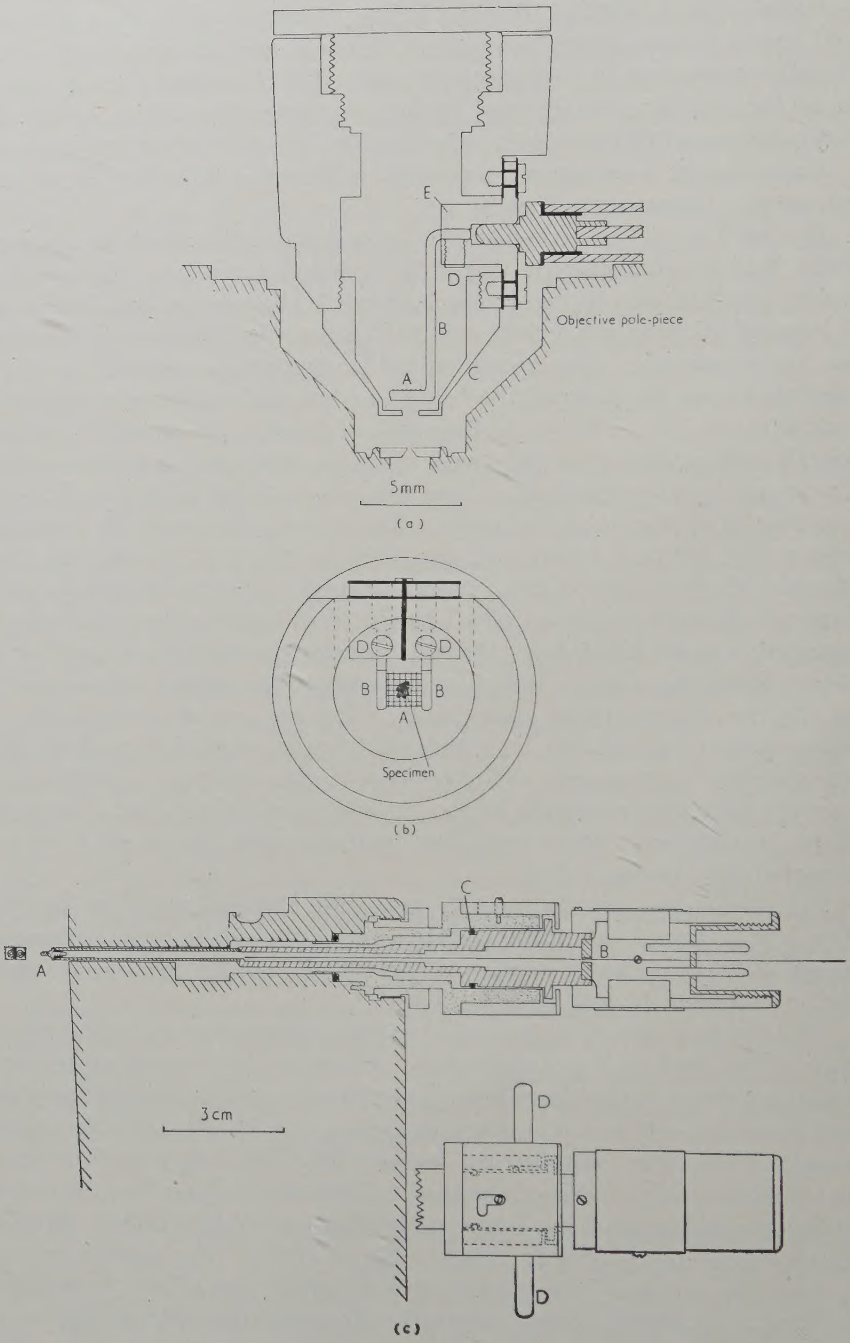

High temperature stage for the Elmiskop 1.

estimate. From such measurements the inaccuracy in stage temperature obtained from heating current in this way is very roughly estimated to be about ± 10°C. This does not include of course any rise of temperature of the thin foil due to heating by the electron beam. To minimize this last effect the double condenser was used with an illuminating spot about 10 μ diameter, with a 600 μ diameter aperture in condenser 2, and with a total beam current $\sim 15\ \mu\text{A}$.

§ 3. EXPERIMENTAL RESULTS

3.1. *High Temperature Stage Experiments*

When a specimen containing loops is heated in the electron microscope the loops are observed to shrink and eventually to disappear completely. The loops begin to shrink at a noticeable rate at a stage temperature of about 170°C; the rate of shrinking increases rapidly with increasing temperature. For example, timed sequences of micrographs and ciné-sequences have shown that the rates of decrease of radius of a loop about 250 Å radius are about 0·2, 1·5, and 33 Å sec^{-1} at temperatures ~ 170, 200 and 220°C respectively. This shrinking is quite distinct from the process of prismatic slip observed by Hirsch, Silcox, Smallman and Westmacott (1958). Figure 2 (*a*), (*b*), (*c*) and (*d*) (Pl. 1) is a sequence of micrographs taken on photographic plates at an estimated stage temperature of 187°C. The time interval between successive micrographs was not recorded but is estimated to be about one minute. Most of the loops in fig. 2 (*a*) diminish in size and disappear during the sequence; loop A remains through the whole sequence although diminished in size. In general in the thin foils, loops which are originally round remain round as they shrink, i.e. there is no tendency to form angular shapes. Also all the loops (large and small) appear to shrink in the thin foils. There is no tendency for large loops to grow at the expense of small ones.

The rate at which a loop shrinks is not uniform but is a function of its radius. A small loop shrinks much faster than a large loop, i.e. the rate of shrinking of a loop is accelerated as it grows smaller. Figure 3 (Pl. 2) is a sequence of micrographs taken on photographic plates of a loop shrinking at a stage temperature of 197°C; the times in seconds at which these exposures were made are marked on each micrograph. The loop lies on an inclined plane, and the distance between the more steeply inclined and less visible parts of the loop (Hirsch, Howie and Whelan 1958, 1959) has been taken as a measure of the loop diameter. Figure 4 shows a plot of loop radius versus time. There is some uncertainty in the exact position of the centre of the dislocation line as judged from the contrast and this is indicated by the vertical spread in the points on fig. 4. However, the relative positions of the points are probably more accurate. With single exposures on photographic plates it is not possible to record the shrinking at very small radius owing to its rapidity. However using ciné-techniques the steep slope of the radius-time curve at small radius has been verified, although it is difficult to determine its functional form with accuracy.

The observations suggest that the loops are acting as vacancy sources, i.e. that the vacancies which condensed to form the loops after quenching are dispersing. Assuming that the only force acting to aid climb is that due to the line tension and curvature of the loop, the theory given in detail in §4 suggests that the radius time curve of a shrinking loop should be approximately a parabola. Accordingly such a curve has been fitted to the experimental points of fig. 4 and the points are seen to be consistent with this curve. The dislocation loops are therefore climbing by vacancy diffusion in a sense to annihilate themselves. These results may be taken as direct proof of the hypothesis of climb of dislocations. Figure 5 (*a*), (*b*), (*c*) and (*d*) (Pl. 3) shows a sequence of micrographs from a region containing both loops and irregular dislocations (e.g. fig. 5 (*a*) at A). During the sequence, while the loops are disappearing, the irregular dislocations assume a noticeably smoother shape (e.g. at A). This effect has been observed a number of times and is thought to be due at least partly to climb.

Fig. 4

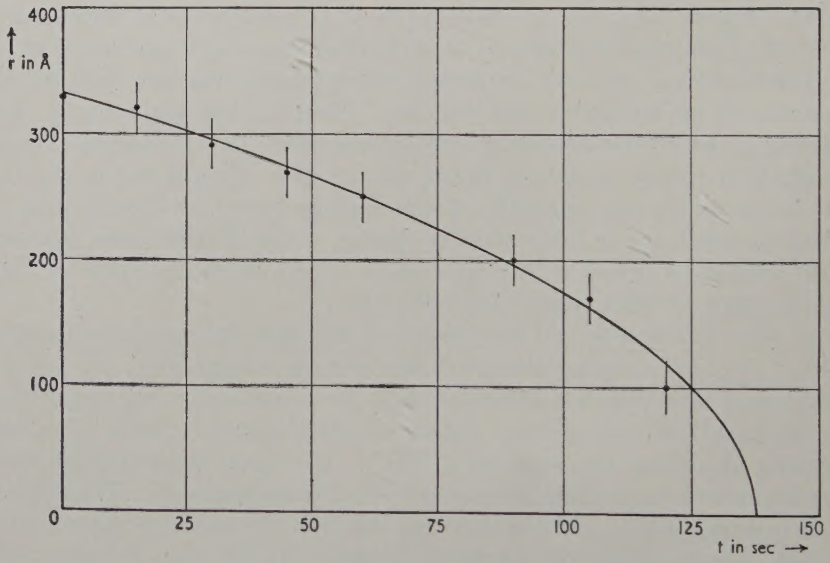

Radius versus time plot for the loop in fig. 3. A parabola has been fitted to the experimental points.

Relatively little slip of the loops has been observed. Occasionally however a loop has been observed to jump suddenly as a whole over a small distance, presumably along its slip cylinder, after it has shrunk to a very small size before it finally disappears. The explanation of this effect is not known with certainty; however prismatic slip is a very rapid way of transferring the last remaining vacancies as a whole to the surface as a nearby sink.

3.2. *Bulk Material Experiments*

The density of loops in the quenched and aged specimens is $\sim 6 \times 10^{14}\,\mathrm{cm}^{-3}$ assuming a foil thickness of ~ 1000 Å. No noticeable change was observed in thin foils prepared from bulk material which had been annealed for six minutes at temperatures below 180°C. In specimens annealed at 180°C the density decreased slightly to $\sim 1{\cdot}3 \times 10^{14}\,\mathrm{cm}^{-3}$. A reduction in loop density was quite marked in foils annealed at 190°C and 200°C in which the densities were about 5×10^{13} and $5 \times 10^{12}\,\mathrm{cm}^{-3}$ respectively. These figures should be regarded as order of magnitude estimates only since variations were observed from specimen to specimen and from point to point on any one specimen. For reliable estimates of loop densities the foil thickness must be determined (for example from the projected width of a slip trace left by a dislocation moving on a $\{111\}$ plane). It has not always been possible to determine the foil thickness in this way, and an average thickness ~ 1000 Å has been assumed. Experience has shown that the foil-thickness in areas transparent to electrons is usually of this order. The change in number of loops on micrographs from as-quenched material and from material annealed at 190°C and 200°C is too large to be attributed to differences of foil thickness.

Figure 6 (*a*) (Pl. 4) shows a micrograph of a foil prior to annealing and fig. 6 (*b*) (Pl. 4) and fig. 6 (*c*) (Pl. 5) show micrographs of foils annealed at 190°C. Several large loops can be seen in these micrographs. This increase in size accompanying the decrease in loop density is also apparent in the micrograph of a foil annealed at 200°C shown in fig. 6 (*d*) (Pl. 5). In specimens annealed at 210°C and higher temperatures no loops were observed. The conclusion drawn from these results is that in bulk material large loops grow at the expense of smaller loops; eventually however they too either shrink and disappear or become large enough to be incorporated in the dislocation network of the crystal.

Sometimes the larger loops left in bulk material after annealing have angular shapes (e.g. figs. 6 (*b*) and (*c*) at A). Such loops may be parallelograms with edges in close packed directions although no experimental confirmation of this has been attempted. The shape of a large loop which has grown from a small one by vacancy absorption presumably depends on the detailed mechanism of growth of a loop (see § 4.1).

§ 4. THEORETICAL INTERPRETATION

4.1. *Climb of Dislocation Loops*

The observations leave little doubt that climb of the dislocation loops is occurring and it is therefore convenient to discuss the various factors which govern the climb of a prismatic loop. Friedel (1956) has considered the climb of a dislocation due to vacancy diffusion in terms of the movement of jogs. He gives the following expression for the velocity of a jog along the dislocation line:

$$v_{\mathrm{c}} = \frac{z\nu_{\mathrm{a}}b}{\sin\psi}\exp\left\{-\frac{(E_{\mathrm{f}}+E_{\mathrm{m}})}{kT}\right\}\left[\exp\left(\frac{F_{\mathrm{c}}b^2}{kT}\right)-\exp\left(\frac{F_{\mathrm{s}}b^2}{kT}\right)\right] \qquad (1)$$

where $z \sim 11$ (of the order of the atomic coordination number of the lattice), ν_{a} is an atomic frequency (of order 10^{13}); ψ is the angle between the Burgers vector **b** and the dislocation line; E_{f} is the formation energy and E_{m} the activation energy of movement of a vacancy; $E=E_{\mathrm{f}}+E_{\mathrm{m}}$ is the activation energy of self-diffusion; kT is the usual Boltzmann temperature factor; while F_{c} and F_{s} are forces per unit length acting on the dislocation line tending to make it climb out of its slip plane. F_{c} is a force due to an applied stress or due to the stress fields of other segments of dislocation. F_{s} is a chemical stress due to a deviation of the concentration of vacancies from the equilibrium value at temperature T. F_{s} is equal to

$$\frac{kT}{b^2}\log\frac{c}{c_0} \quad . \ . \ . \ . \ . \ . \ . \ . \ . \ . \ . \quad (2)$$

where c and c_0 are the actual and equilibrium concentrations of vacancies at temperature T.

Fig. 7

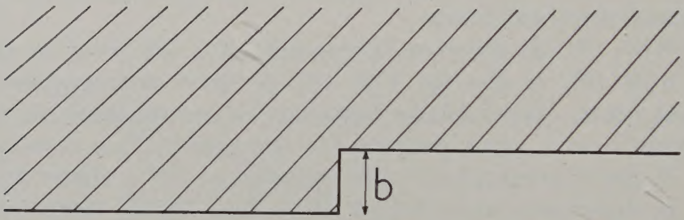

Climb of an edge dislocation by jog movement (following Friedel 1956).

Equation (1) may be given a simple physical interpretation. Consider an edge dislocation containing a jog in a simple cubic lattice as in fig. 7; the extra half plane of atoms is shown shaded. Under the action of a suitable force F_{c} tending to make the dislocation climb the jog will emit vacancies and will move to the right with an average velocity given by the left-hand term in the square brackets of eqn. (1) together with the factor outside the brackets. However vacancies will tend to recombine with the jog which will therefore move to the left, and this is taken into account by the right-hand term in the square brackets. The resultant velocity of the jog is the difference between these two terms. (The formula assumes that the force F_{c} does not affect the probability that a vacancy will combine with the jog, i.e. that the energy barrier to be surmounted when a vacancy combines with a jog is independent of the force F_{c}.) Clearly the rate of climb of the dislocation normal to its slip plane in fig. 7 is

$$v = v_{\mathrm{c}}\,b/x$$

where x is the average distance between jogs. b/x is called the concentration of jogs c_c by Friedel. c_c is a dimensionless quantity equal to unity for an edge dislocation in a simple cubic lattice running at 45° to its glide plane.

For a circular prismatic loop lying in a (111) plane in a face centred cubic metal such as aluminium the jog concentration will vary round the loop as shown schematically in fig. 8. c_c will be of the order of unity at the segments of the loop lying between close packed direction in the (111) plane (i.e. at the corners of the inscribed hexagon in fig. 8). The jogs on these segments will run along the loop in the directions indicated with arrows and will annihilate with jogs moving in opposite directions from the other joggy segments. Thus there is a tendency to produce a hexagonal loop lying inside the original circular loop as in fig. 8. However new jogs are expected to nucleate easily at the corners of the hexagon since this requires no additional line energy. The equilibrium form of the loop as it shrinks will be governed by the rate at which jogs are nucleated and the rate at which material is redistributed along the dislocation, i.e. on the rate of

Fig. 8

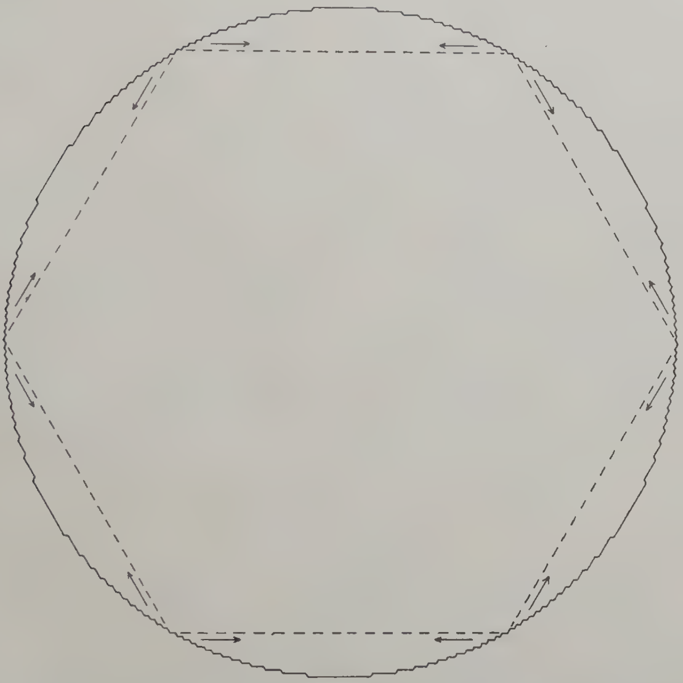

Circular dislocation loop in a $(1\bar{1}1)$ plane. The loop represents a disc of vacancies. The sides of the inscribed hexagon are parallel to close packed directions. The highest jog density occurs at the corners of the hexagon. Climb of the dislocation loops occurs by movement of jogs of opposite sign from adjacent corners and subsequent annihilation.

diffusion between jogs. This is a theoretical problem involving jog kinetics analogous to the type of problem discussed by Frank (1958) and Cabrera and Vermilyea (1958) for crystal growth kinetics. A similar theory could probably be applied to a shrinking loop, although the solution is not obvious. The experimental observations show however that as a circular loop shrinks it remains roughly circular, and this implies that jogs are nucleated and move at a rate sufficient to maintain a circular shape. It is worth noting here that in the converse process (i.e. when a small loop grows by absorption of vacancies as in the bulk material experiments) the details may be different, as a little consideration of fig. 8 suggests. In this case new jogs will ultimately have to be nucleated by condensation of vacancies. This will involve an increase in dislocation line energy and is therefore likely to be a difficult process. The dislocation loop will therefore tend to have a low concentration of jogs, i.e. to be angular with sides parallel to close packed directions. This is probably the explanation of the parallelogram shaped loops visible in figs. 6 (*b*) and (*c*).

Detailed considerations of fig. 8 show that for a loop in a (111) plane of a face centred cubic lattice the maximum rate of change of radius of the loop is $\frac{1}{2}v_c$, where v_c is measured along close packed directions, i.e. $c_c \sim \frac{1}{2}$. In this theory for simplicity it will be assumed that the loops are circular and lie in planes perpendicular to the axis of the glide cylinder (i.e. in (110) planes). Thus all segments of a loop are edge dislocations ($\sin\psi = 1$), and no dissociation into partial dislocations will occur. An average value of jog concentration $c_c \sim \frac{1}{2}$ will also be assumed to hold for all segments of a circular loop. For a loop lying in a (111) plane the situation is not expected to differ much from this provided dissociation into partial dislocations can be neglected. The rate of shrinkage of the loop will then be given by

$$\frac{dr}{dt} = -\frac{1}{2}v_c \qquad \ldots \ldots \ldots \ldots \qquad (3)$$

where r is the radius of the loop at time t.

It should also be mentioned here that eqns. (1) and (3) give the climb rate of a dislocation assuming that vacancy emission (or absorption) is the rate determining process. This will be the case if vacancies diffuse rapidly to sinks (such as free surfaces, grain boundaries, or other dislocations). If the diffusion is not sufficiently rapid a local supersaturation will be set up at the dislocation which will suppress the emission. The rate of climb in this case will be determined by transport of vacancies away from the dislocation by diffusion (the 'saturation' case discussed by Friedel 1956). The solution of this problem is complicated and depends on the geometrical conditions in any particular case (i.e. on the nature and distribution of sinks). This point is discussed in § 4.4 and in the Appendix.

4.2. *The Effect of Up-quenching*

During the annealing process the climb rate of a loop will be determined by the factor in square brackets in eqn. (1). It is assumed that both in the bulk material and in the thin foil experiments the metal is not under any form of stress. In thin foils stresses may be produced by electron bombardment in the electron microscope; these however will be neglected since little prismatic slip was observed with low electron beam intensity. Neglecting forces between loops, the only elastic force acting on a segment of loop will be that due to its line tension and curvature. This force tends to contract the loop. As far as the chemical stresses are concerned the experiments can be visualized as follows. The foil containing loops is assumed to have a concentration of vacancies equal to the equilibrium value at room temperature. The foil is then up-quenched from room temperature to about 180°C. This gives rise to an undersaturation of vacancies. Consequently the initial chemical stress is not equal to zero and acts in a direction tending to shrink the loops. A simple calculation shows however that to restore equilibrium only about one vacancy per loop is required (assuming a loop concentration of $\sim 10^{14}\ \mathrm{cm}^{-3}$) and equilibrium is rapidly attained, i.e. $F_{\mathrm{S}}=0$.

Once vacancies are being produced by the dislocation loops it becomes necessary to consider the rate at which they are absorbed by sinks. There will now be a supersaturation of vacancies and a chemical stress will build up in opposition to the line tension stress, i.e. vacancies will tend to condense on the loops again. The discussion of this problem will be deferred to § 4.4 At present it will be assumed that vacancies are removed by sinks faster than they are produced by loops so that the chemical stress is small, i.e. the right-hand term in the square bracket of eqn. (1) is very nearly unity. This is thought to be the case in the thin foil annealing experiments where the foil surface is a very effective vacancy sink (see § 4.4 and Appendix).

4.3. *Climb of Loops in Thin Foils*

An approximate expression for the force F_{C} due to the line tension and curvature of a loop is (Frank 1950, Franz and Kröner 1955)

$$F_{\mathrm{C}}=\frac{Gb}{4\pi(1-\sigma)}\,\frac{\log\ (r/b)}{(r/b)} \quad . \quad . \quad . \quad . \quad . \quad . \quad . \quad . \quad (4)$$

where the radius of the dislocation core is taken as b, G is the shear modulus and σ is Poisson's ratio. (The core energy of the dislocation is neglected in this expression.) Putting $F_{\mathrm{S}}=0$ in eqn. (1) the radius r of a loop as a function of time t is given by

$$\frac{dr}{dt}=-\tfrac{1}{2}z\nu_{\mathrm{a}}b\exp\left(-\frac{E}{kT}\right)\left[\exp\left(\frac{F_{\mathrm{C}}b^2}{kT}\right)-1\right]. \quad . \quad . \quad . \quad (5)$$

With $G=2{\cdot}53\times10^{11}$ dynes cm^{-2} at 161°C, $b=2{\cdot}86\ \mathrm{\AA}$, $\sigma=\frac{1}{3}$ and $k=0{\cdot}86\times10^{-4}$ ev degree C^{-1}, the reciprocal of the function in square brackets has been plotted as a function of r/b for temperatures of 161°C and 200°C in fig. 9. The curves approach infinity near $r/b=1$ but this corresponds to a range of r/b where the expression (4) is no longer valid. In the range of loop radius of interest therefore $[\exp(F_{\mathrm{C}}b^2/kT)-1]$ may be approximated by $\alpha b/r$ where $\alpha\sim72$ at 161°C and ~64 at 200°C. dr/dt is therefore only slightly dependent on temperature through the factor α and depends mainly on temperature through the term $\exp(-E/kT)$ in eqn. (5)†.

Fig. 9

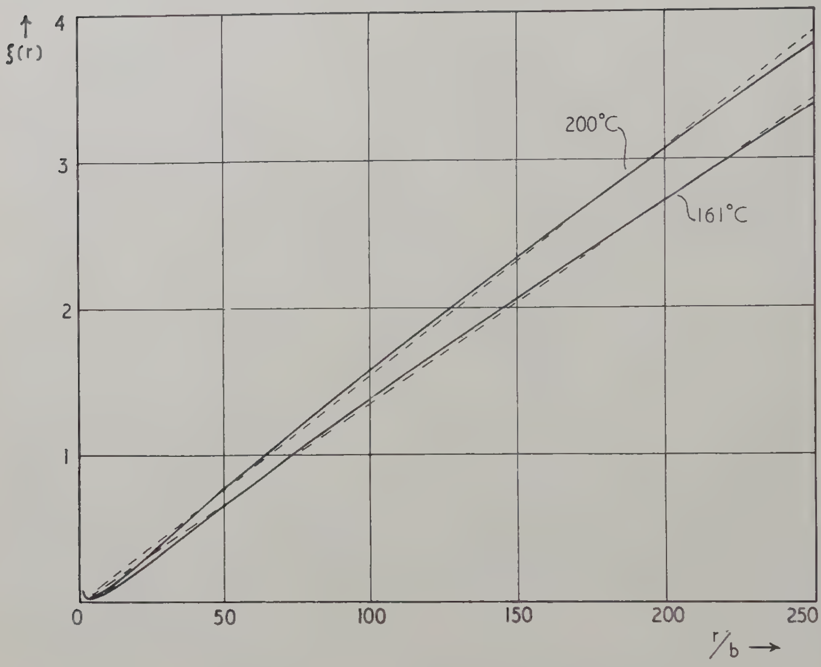

——— $\xi(r)$ ---- linear approximation

Plot of the function

$$\xi(r)=\left[\exp\left(\frac{Gb^3}{4\pi kT(1-\sigma)}\cdot\frac{\log(r/b)}{(r/b)}\right)-1\right]^{-1}$$

as a function of r/b. Note that the function is approximately linear over the range of r/b of interest.

Then
$$\frac{dr}{dt}=-\tfrac{1}{2}z\nu_a b^2\alpha\exp\left(-\frac{E}{kT}\right)\cdot\frac{1}{r}. \qquad (6)$$

Equation (6) can be integrated to give

$$r=r_0(1-t/\tau)^{1/2} \qquad (7)$$

where r_0 is the initial radius of the loop at $t=0$

$$\tau=\tau_0\exp(E/kT) \qquad (8)$$

and where
$$\tau_0=r_0^2/(z\nu_a\mathbf{b}^2\alpha). \qquad (9)$$

---

† *Note added in proof.*—Calculations show that an increase of the core radius of the dislocation has a similar effect on $\xi(r)$ as an increase of temperature, e.g. at 161°c and 200°c changing the core radius to $2b$ causes α to decrease by about 10%.

Equation (7) shows that the radius–time curve of a shrinking loop should be parabolic as shown in the curve fitted to the experimental points of fig. 4. These points were obtained from the loop in fig. 3 climbing at ~197°c. In this case $r_0 \sim 330$ Å, $\tau \sim 138$ sec, $kT \sim 0{\cdot}0405$ ev. Substituting these figures in eqns. (8) and (9) with $z \sim 11$, $\nu_a \sim 10^{13}$, $\alpha \sim 64$, E is found to be 1·29 ev. The error in E due to 10°c error in temperature estimation is about 2%. The result also assumes the value of ν_a. The activation energy depends logarithmically on this factor and is relatively insensitive to it. Errors due to rises in temperature of the foil in the electron beam are not known but are thought to be small (see § 6). Other estimates of E from the rate of shrinkage of certain loops (for which complete radius–time curves were not obtained) gave values lying in the range 1·2 to 1·3 ev. Although these values of the activation energy cannot be claimed to be accurate owing to assumed factors and to uncertainty in the accuracy of the temperature, the values are consistent with those obtained by other workers: Bradshaw and Pearson (1957) give 1·2 ev; Federighi (1959) gives 1·33 ± 0·05 ev; DeSorbo and Turnbull (1959) give 1·31 ± 0·08 ev; while Spokas (reported by Federighi 1959) has obtained 1·4 ± 0·1 ev.

The rates of decrease of radius of a loop of radius 250 Å can now be calculated from eqn. (6). Assuming $\alpha \sim 70$ for all temperatures of interest, and taking $E = 1{\cdot}32$ ev (the average of the values quoted by Federighi and De Sorbo and Turnbull), the calculated rates are ~0·13, ~1·3, ~4 Å sec^{-1} at temperatures of 170, 200 and 220°c respectively. Considering the errors involved in estimating temperature and in assumed factors these rates are in good agreement with the observed rates mentioned in § 3.1.

The observations are therefore consistent with the theory of shrinking of loops by climb. The temperature dependence of the rates is best illustrated by considering the lifetimes τ obtained from eqn. (8) of a loop of radius ~140 Å. This is the average loop radius of the distribution shown in fig. 10, which is a histogram of loop sizes for a typical specimen quenched from 600°c (this histogram was obtained from fig. 1 of Hirsch, Silcox, Smallman and Westmacott (1958)). τ has the following values for several temperatures (α has been taken ~120 at 20°c and ~70 for all other temperatures):

T°c	20	160	170	180	190	200	210	220
τ	230 years	11·6 min	5·2 min	2·3 min	1·2 min	35 sec	17·5 sec	8·8 sec

It is seen that the loops will shrink at a noticeable rate for temperatures greater than ~170°c which is precisely the range in which the loops are observed to anneal out in the thin foils.

Equation (6) can be written as follows (the plane of the loop is perpendicular to the glide cylinder)

$$\frac{d}{dt}(\sqrt{2\pi r^2 b^2}) = -\sqrt{2}\pi z \nu_a \alpha \exp\left(-\frac{E}{kT}\right). \quad . \quad . \quad . \quad (10)$$

The left-hand side of (10) is the rate at which the number of vacancies forming the loop decreases (volume per vacancy$=b^3/\sqrt{2}$). The rate of emission of vacancies from the loop is then

$$\frac{dN}{dt}=\sqrt{2}\pi z\nu_{\mathrm{a}}\alpha\exp\left(-\frac{E}{kT}\right) \quad . \quad . \quad . \quad . \quad . \quad . \quad (11)$$

and this is independent of loop size. It is seen therefore that at a fixed temperature the rate of change of area of a loop is constant.

Fig. 10

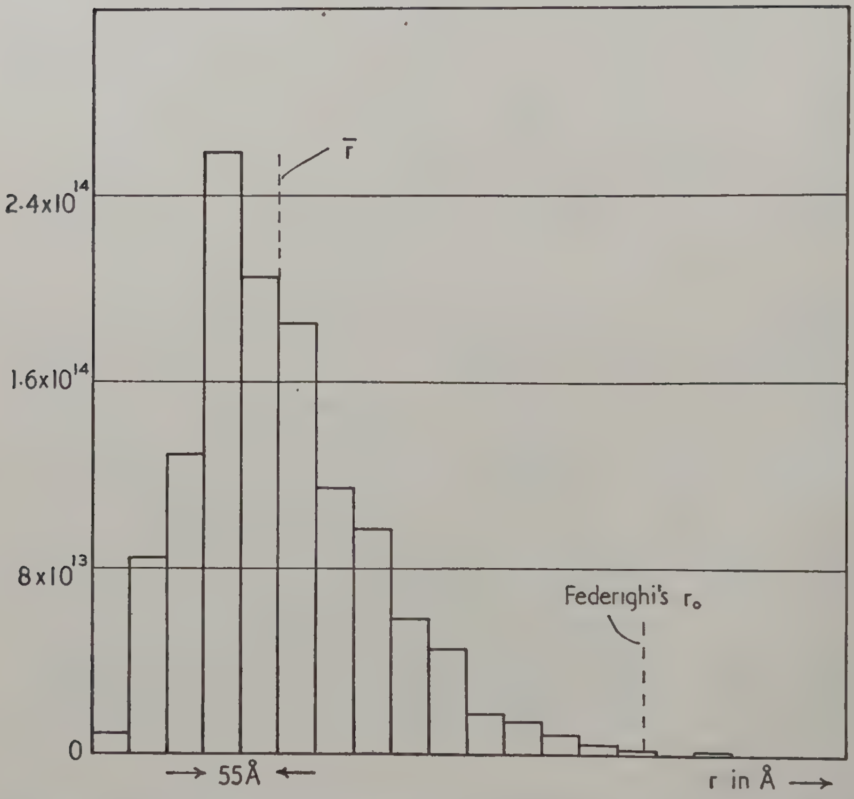

Histogram of loop sizes for the micrograph of fig. 1 of Hirsch, Silcox, Smallman and Westmacott (1958) taken from aluminium quenched from ~600°c. The average loop radius is 138 Å. The ordinate is loop density in number cm^{-3}, assuming a foil thickness of 1000 Å. See text for discussion of the radius r_0 derived from Federighi's results.

Attempts to verify the form of eqn. (7) are inaccurate for the following reasons. The dislocation core itself is not imaged in the electron microscope but its strain field gives rise to a diffraction image lying to one side of the core (Hirsch, Howie and Whelan 1958, 1959). There is therefore an inherent inaccuracy in the measurement of loop diameters owing to the uncertainty in position of the dislocation. In addition, during heating, the specimen may tilt, thus altering the contrast. The observations reported in figs. 3 and 4 are therefore considered to be in satisfactory agreement with theory.

4.4. *Annealing of Loops in the Bulk Material*

So far the chemical stress due to the vacancy supersaturation produced by vacancies released from loops has been neglected. In general it is not permissible to neglect this effect in experiments with the bulk material as the following considerations show. First consider the number of vacancies in equilibrium at various temperatures T in a cube of aluminium 1000 Å edge; this is approximately the volume occupied by a single loop in a region of typical loop density. Using the formula of Bradshaw and Pearson (1957) for vacancy concentration the following figures are obtained.

T°c	Equilibrium number of vacancies per cube 1000 Å edge
600	2×10^{4}
200	4
170	1·1
20	4×10^{-5}

The equilibrium number of vacancies near each loop in the annealing range (170–200°c) is therefore of order unity, so that even if only a few vacancies per loop remain in the vicinity of the loop (or of other loops) appreciable supersaturation occurs. The degree of supersaturation will be determined by several factors including the rate at which vacancies are produced by loops, the rate at which they move, and the nature and distribution of vacancy sinks (isolated dislocation lines, free surfaces and grain boundaries). The detailed solution of this problem is complicated. However some simple generalizations can be made. The number of jumps, n, made by a vacancy in time t is (Cottrell 1957)

$$n=z\nu_{\mathrm{a}}t\exp\left(-\frac{E_{\mathrm{m}}}{kT}\right)$$

and the mean square distance moved, assuming a random walk process, is

$$\overline{\Delta x^2}=b^2z\nu_{\mathrm{a}}t\exp\left(-\frac{E_{\mathrm{m}}}{kT}\right). \quad . \quad . \quad . \quad . \quad . \quad . \quad (12)$$

Then the time taken for a vacancy to move to a sink at a distance l from the loop at which it originates is

$$t_l\sim(l^2/b^2z\nu_{\mathrm{a}})\exp\left(\frac{E_{\mathrm{m}}}{kT}\right) \quad . \quad . \quad . \quad . \quad . \quad . \quad (13)$$

Equation (11) also shows that if supersaturation effects are neglected the time interval t_{s} between emission of successive vacancies by a loop is on average

$$t_{\mathrm{s}}\sim(\sqrt{2\pi z\nu_{\mathrm{a}}\alpha})^{-1}\exp\left(\frac{E_{\mathrm{m}}+E_{\mathrm{f}}}{kT}\right). \quad . \quad . \quad . \quad . \quad . \quad (14)$$

Then
$$t_l/t_s \sim \sqrt{2\pi} l^2 \alpha b^{-2} \exp\left(-\frac{E_f}{kT}\right). \quad . \quad . \quad . \quad . \quad . \qquad (15)$$

Now for thin foils the surface is a very effective vacancy sink; l is then about the average distance of a loop from the surface, i.e. ~1000 Å. In bulk material however a vacancy may have to move about 1 to 10 μ before it encounters a sink such as a grain boundary or dislocation line (ignoring other loops which may act as sinks). The following are typical values of t_l/t_s for aluminium at various temperatures obtained from eqn. (15) assuming $\alpha \sim 70$, $E_f = 0{\cdot}76$ ev.

T°c	$l = 1000$ Å	$l = 1\,\mu$	$l = 10\,\mu$
170	$8{\cdot}7 \times 10^{-2}$	8·7	870
200	3×10^{-1}	30	3000
220	$6{\cdot}6 \times 10^{-1}$	66	6600

It can be seen that for thin foils ($l \sim 1000$ Å), a vacancy from a loop will on average reach the surface before the next vacancy is emitted by the same loop. The figures therefore suggest that the vacancy supersaturation will be small and that the chemical stress can be neglected in this case. The theory of the previous paragraph is therefore expected to hold for thin foils.

For loops in the interior of grains in bulk material however ($l \sim 10\,\mu$), t_l/t_s is large and increases with increasing annealing temperature. In this case supersaturation effects are expected to be important because vacancies are formed at loops at a rate greater than the rate at which they move to sinks. The effect of a vacancy supersaturation may be illustrated by using eqns. (1) and (2) to write eqn. (3) in the form

$$\frac{dr}{dt} = -\tfrac{1}{2} z \nu_a b \exp\left(-\frac{E}{kT}\right)\left[\frac{\alpha b}{r} - \frac{\Delta c}{c_0}\right] \quad . \quad . \quad . \quad . \quad . \qquad (16)$$

where $\Delta c = c - c_0$. The rate of change of radius of a loop will therefore depend on the local supersaturation of vacancies and it is readily seen that a loop of radius less than $r_c = \alpha c_0 b/\Delta c$ will shrink while a loop of radius greater than r_c will grow. The large loops therefore grow at the expense of the small loops which disappear giving rise to a lower concentration of larger loops. This conclusion is in agreement with the observations on bulk material annealed at 190°c and 200°c (fig. 6) where a definite difference in the diameter and density of the loops in the as-quenched and annealed specimens was detected.

In general local time-dependent inhomogeneities in vacancy concentration are to be expected. However the main physical features of the process as a whole can be illustrated in the following manner assuming a homogeneous supersaturation Δc. Consider first an idealized case of a metal containing no sinks for vacancies other than loops (e.g. a single crystal infinite in extent and perfect except for loops and vacancies). Let the metal contain a uniform density of loops of various sizes given by a distribution function $g(r)$ such that there are $g(r)\,dr$ loops per unit volume with radii between r and $r + dr$. Up-quench the metal to a temperature

$T \sim 200°\text{C}$. The rate of emission of vacancies now depends on loop size and vacancy concentration c. Since there are no vacancy sinks the following continuity equation holds:

$$\sqrt{2\pi} z\nu_a \exp\left(-\frac{E}{kT}\right)\int_0^\infty g(r)\left[\alpha - \frac{\Delta c}{c_0}\cdot\frac{r}{b}\right]dr = \frac{dc}{dt}. \qquad (17)$$

Now for small supersaturations once the initial c has been established, both c and dc/dt are expected to be small in comparison with the two integrals subtracted on the left hand side of eqn. (17) at temperatures $\sim 170°\text{C}$ and $200°\text{C}$, as substitution of typical figures suggests. With this assumption the right-hand side of eqn. (17) can be replaced by zero, giving

$$\Delta c/c_0 = \frac{\alpha b \int_0^\infty g(r)\,dr}{\int_0^\infty r g(r)\,dr} = \alpha b/\bar{r} \quad . \quad . \quad . \quad . \quad . \quad . \qquad (18)$$

where $\bar{r}$ is the mean radius of the distribution $g(r)$. Electron micrographs suggest that $\bar{r} \sim 140$ Å in typical regions containing loops (see fig. 10). Putting $\alpha \sim 70$, c/c_0 is found to be $\sim 2{\cdot}4$ which confirms the assumption that c is small under near steady state conditions. For comparison the value of c/c_0 produced by quenching the metal from 600°C to room temperature is $\sim 10^9$.

Substitution of (18) in eqn. (16) gives

$$\frac{dr}{dt} = -\tfrac{1}{2} z\nu_a b^2 \alpha \exp\left(-\frac{E}{kT}\right)\left[\frac{1}{r} - \frac{1}{\bar{r}}\right]. \quad . \quad . \quad . \quad . \qquad (19)$$

Equation (19) shows that the rate of shrinking of a loop now depends on $r - \bar{r}$, i.e. $r_c = \bar{r}$. Loops of above average radius will grow at the expense of those below average radius which will gradually disappear. Thus $g(r)$ will change with time in such a way that $\bar{r}$ increases, i.e. $\Delta c/c_0$ decreases. Ultimately only a few very large loops will remain.

In this idealized case the effects of grain boundaries and dislocations as vacancy sinks have been neglected. If these are taken into account even these large loops would shrink and vanish, provided they are not ultimately incorporated in a dislocation network. While therefore the final state produced by annealing bulk material for a sufficiently long time should be the same as that of the annealed thin foils (i.e. no loops), the detailed behaviour of loops as they anneal out will be different and is expected to depend markedly on their proximity to vacancy sinks. For example loops near grain boundaries would be expected to anneal out as in thin foils, while those in the interior of grains should behave as outlined. In this last case since large loops are involved the annealing out time is expected to be longer.

§ 5. DISCUSSION

The agreement between observations and the theory of the previous section leaves little doubt that the disappearance of loops is due to climb. The time and temperature dependences of the annealing rates in thin foils are as predicted theoretically and are consistent with an activation energy of self diffusion of about 1·3 ev. Bulk material experiments have shown results expected from the growth of large loops.

It is of interest to consider the results in relation to the resistivity experiments of Panseri and Federighi (1958) and of Federighi (1959) on quenched aluminium. The first stage of their isochronal annealing curves (see fig. 2 of Panseri and Federighi) can be interpreted in terms of the removal of vacancies at dislocation loops (and possibly at small clusters of unspecified shape), and at fixed sinks such as network dislocations and grain boundaries. Now the temperature range in which the loops are observed to disappear is exactly the same as that found for stage II annealing by Panseri and Federighi. Thus stage II includes the annealing of resistivity due to the dislocation loops. It is therefore tempting to identify stage II with the annealing out of loops. It is not known with certainty at present whether very small clusters (other than loops) would be detected on transmission electron micrographs. No effects which can be attributed to very small clusters are observed. Even loops ~ 50 Å diameter would be expected to produce contrast in the form of a dark spot about equal in diameter to the theoretical width of the image of a dislocation (~ 100 Å), and such dark spots have been observed (see fig. 1 of Hirsch, Silcox, Smallman and Westmacott 1958). However there is no evidence that these spots are due to anything other than loops. With these facts in mind stage II annealing in the quenched aluminium is tentatively considered to be due to the observed loops. Panseri and Federighi (1958) and Federighi (1959) have shown that the decrease in resistivity of aluminium during stage II annealing is $\sim 3\,\mathrm{m}\mu\,\Omega\,\mathrm{cm}$ after quenching from 600°c. If this is produced by loops of average radius ~ 140 Å and density $\sim 10^{15}\,\mathrm{cm}^{-3}$, the average resistivity of dislocations in loops is about $3\times 10^{-19}\,\Omega\,\mathrm{cm}$ per centimetre length of dislocation. It is emphasized that this value is an order of magnitude estimate only. To make this type of estimate worthwhile electron microscope observations and resistivity measurements should be made on the same specimens. However it is worth noting that the value is comparable with estimates of dislocation resistivities in other metals. For example Seeger (1957) quotes figures leading to dislocation resistivities of $\sim 2{\cdot}5\times 10^{-19}$ and $\sim 10^{-18}\,\Omega\,\mathrm{cm}$ per centimetre length for copper and nickel respectively.

Federighi (1959) has also studied the shape of the isothermal annealing curve of stage II resistivity in aluminium. He found (see fig. 4 of Federighi) that the fraction of resistivity remaining after annealing for time t at temperature T could be fitted very well for all except large t by the function.

$$f=1-\left(\frac{t}{\tau_\rho}\right)^m$$

where $m\approx 0{\cdot}55$ and

$$\tau_\rho=\tau_{\rho 0}\exp\left(\frac{E}{kT}\right)$$

with $E=1{\cdot}32$ ev.

τ_ρ represents a decay time; more than 90% of the resistivity anneals out in time τ_ρ. $\tau_{\rho 0}$ was found to be $2{\cdot}6\times10^{-12}$ sec (see corrigendum to Federighi 1959).

Now if the resistivity of a loop is taken to be proportional to its perimeter (i.e. to its radius), the total resistivity of a distribution of loops $g(r, t)$ will be proportional to

$$\int_0^\infty rg(r,t)\,dr=\bar{r}(t)n(t),$$

where $\bar{r}(t)$ is the average radius of the distribution and $n(t)$ the total number of loops at time t. On this interpretation therefore the explanation of Federighi's empirical law should depend on the way in which the average radius and the total number of loops in the distribution changes with time. $g(r, t)$ will of course be determined by considerations such as those outlined in § 4.4 In the idealized case discussed there it is possible to formulate a differential-integral equation for $g(r, t)$; however the equation seems soluble only by numerical methods. In the absence of a complete solution it is only possible to speculate. It is thought that the initial rapid decrease in Federighi's annealing curve may be due to the initial rapid shrinking and disappearance of loops smaller than average radius and the growth of large ones. The subsequent slow decay would then be due to the slower shrinking of the large loops as vacancies are removed at network dislocations and grain boundaries at sinks. At present this problem is still unsolved and several other points are incompletely understood. It is not known for example what the contribution to the resistivity will be from heavily jogged dislocations. Furthermore examination of many specimens has shown that loops are not uniformly distributed over large regions. Loops tend to occur with high density in certain grains (usually free from isolated dislocations) and sometimes in patches in those grains. Other grains may show tangled networks of dislocation lines with lower loop density, e.g. fig. 5. These dislocations are probably produced by quenching stresses and are presumably heavily jogged by absorption of vacancies. During annealing these dislocations are observed to climb also; the jog density is thereby expected to decrease. This effect probably also contributes to resistivity although its magnitude is uncertain. Finally it must be pointed out that for small loops the contribution to electrical resistivity may not be proportional to r; for example it may be proportional to the loop area, i.e. to r^2. The shape of the isothermal annealing curve is therefore not determined by any simple considerations, but will depend on the complex annealing behaviour of loops in the bulk material.

However a plausible explanation of Federighi's τ_ρ and $\tau_{\rho 0}$ can be obtained by noting that τ_ρ depends on temperature in the same way as the theoretical quantity τ previously defined (eqns. (7), (8) and (9)), which refers to a loop of radius r_0 in a thin foil. Equating τ_0 and Federighi's value of $\tau_{\rho 0}$. it is found that $r_0 = 404$ Å. This is larger than the average loop size in material quenched from 600°C, as can be seen from the typical histogram of loop sizes in fig. 10. However this result is in accordance with the qualitative ideas of annealing of loops in bulk material, i.e. that loops of larger than average radius grow at the expense of smaller ones. The magnitude of the decay time of the resistivity is therefore expected to be determined by the simple theory of § 4.3 applied to a loop of larger than average radius. It must also be noted that τ_ρ is the time required for a large fraction of the resistivity to anneal out. It should therefore correspond to the lifetime of a large loop.

§ 6. CONCLUSIONS

Direct evidence for climb of dislocation loops has been obtained and the details confirm the theoretical predictions of the nature of the process, namely:

(*a*) The loops disappear by emitting vacancies.

(*b*) In thin foils the loops anneal out at an observable rate in the range of temperature $> \sim 170°$c and at a rate consistent with an activation energy of about 1·3 ev. The rate has been followed and within experimental error is found to be as predicted by theory. Supersaturation effects are not important in thin foils owing to the very effective vacancy sinks provided by the surfaces.

(*c*) In bulk material experiments the loops anneal out in the same temperature range, but the details are dependent on vacancy supersaturation effects. Large loops are found to grow at the expense of smaller ones.

(*d*) The work has shown that the loops disappear in the temperature range in which certain electrical resistivity effects produced by quenching also anneal out. The loops are therefore tentatively identified as the main cause of the increase in resistivity, although at present other effects such as small clusters of vacancies (not observed in the electron microscope) and effects due to joggy dislocations cannot be completely ruled out.

As regards the technique it appears that useful information can be obtained by high temperature examination of crystalline materials in the electron microscope. Thus it has been possible to study directly for the first time the annealing kinetics of individual dislocations. Similar experiments on alloys may yield useful information on precipitation effects.

Finally the fact that the annealing effects occur in about the same measured temperature range both in thin foils and in bulk material, is fairly convincing proof that under the conditions of operation used in this work the temperature rise of the thin foil due to heating by the electron beam is small (probably less than 15°c). This is also confirmed by the fact that loops usually disappear simultaneously both for regions inside and well away from the area exposed to the electron beam.

ACKNOWLEDGMENTS

The authors are indebted to Professor N. F. Mott, F.R.S., and to Dr. W. H. Taylor for their interest and encouragement, and to Dr. P. B.

Hirsch for much valuable advice and criticism. Thanks are due to Drs. J. Friedel, T. Federighi and J. Weertman for fruitful discussions, and to Mr. F. Marks for excellent workmanship in the construction of the high temperature stage. Acknowledgments for financial support are due to the A.E.R.E., Harwell (J.S.), and to the Department of Scientific and Industrial Research and to Gonville and Caius College, Cambridge for Research Fellowships (M.J.W.)

REFERENCES

BAUERLE, J. E., and KOEHLER, J. S., 1957, *Phys. Rev.*, **107,** 1493.
BRADSHAW, F. J., and PEARSON, S., 1957, *Phil. Mag.*, **2,** 570.
CABRERA, N., and VERMILYEA, D., 1958, *Report of the Cooperstown Conference on Growth and Perfection of Crystals* (New York : Wiley Sons), p. 393.
COTTRELL, A. H., 1957, *Institute of Metals Monograph and Report Series*, N.23, p. 1.
DESORBO, W., and TURNBULL, D., 1959, *Acta Met.*, **7,** 83.
FEDERIGHI, T., 1959, *Phil. Mag.*, **4,** 502.
FRANK, F. C., 1950, *Plastic Deformation of Crystalline Solids*, Office of Naval Research, p. 89 ; 1958, *Report of the Cooperstown Conference on Growth and Perfection of Crystals* (New York : Wiley and Sons), p. 411.
FRANZ, H., and KRÖNER, E., 1955, *Z. Metallkde.*, **46,** 639.
FRIEDEL, J., 1956, *Les Dislocations* (Paris : Gauthier-Villars), p. 72.
HIRSCH, P. B., HOWIE, A., and WHELAN, M. J., 1958, *Report of the Fourth International Conference on Electron Microscopy, Berlin* (in the press); 1959, *Phil. Trans. roy. Soc.* (in the press).
HIRSCH, P. B., SILCOX, J., SMALLMAN, R. E., and WESTMACOTT, K. H., 1958, *Phil. Mag.*, **3,** 897.
KIMURA, H., MADDIN, R., and KUHLMANN-WILSDORF, D., 1959 a, *Acta Met.*, **7,** 145 ; 1959 b, *Ibid.*, **7,** 154.
KOEHLER, J. S., SEITZ, F., and BAUERLE, J. E., 1957, *Phys. Rev.*, **107,** 1499.
MADDIN, R., and COTTRELL, A. H., 1955, *Phil. Mag.*, **46,** 735.
MESHII, M., and KAUFMANN, J. W., 1959, *Acta Met.*, **7,** 180.
PANSERI, C., and FEDERIGHI, T., 1958, *Phil. Mag.*, **3,** 1223.
SEEGER, A., 1957, *Dislocations and Mechanical Properties of Crystals* (New York : Wiley and Sons), p. 347.
TOMLINSON, H., 1958, *Phil. Mag.*, **3,** 867.
WHELAN, M. J., 1958, *Report of the Fourth International Conference on Electron Microscopy, Berlin* (in the press).
WHELAN, M. J., HIRSCH, P. B., HORNE, R. W., and BOLLMANN, W., 1957, *Proc. roy. Soc.* A, **240,** 524.
WINTENBERGER, M., 1957, *C. R., Acad. Sci. Paris*, **244,** 2800.

APPENDIX

ON THE QUESTION OF EMISSION VERSUS TRANSPORT OF VACANCIES AS THE RATE DETERMINING PROCESS OF THE CLIMB OF LOOPS IN THIN FOILS

Friedel (private communication) has pointed out to the authors that under certain circumstances climb might be determined by transport of vacancies by diffusion even in thin foils. He has considered two simple models—(*a*) diffusion of vacancies along a cylinder, (*b*) diffusion from the centre of a sphere.

(*a*) *Diffusion Along a Cylinder*

Consider a loop of radius r at a distance l from both surfaces of the foil. Imagine the vacancies to be transported to the surfaces through cylinders of radius r and length l. Then the vacancy flux obtained from eqns. (1) and (2) (assuming $c=c_0$ at the loop, i.e. no supersaturation) is

$$\phi_1 = -\frac{2\pi rb}{V2\pi r^2}\frac{dr}{dt} = \frac{z\nu_a b^2 \exp\left(-\frac{E}{kT}\right)}{Vr} c_c\left[\exp\left(\frac{F_c b^2}{kT}\right)-1\right]$$

$$= \frac{D}{Vr} c_c\left[\exp\left(\frac{F_c b^2}{kT}\right)-1\right] \quad . \quad . \quad . \quad . \quad . \quad . \quad (\mathrm{A}\ 1)$$

where $V(=b^3/\sqrt{2})$ is the vacancy volume, and where

$$D = z\nu_a b^2 \exp(-E/kT)$$

is the self diffusion coefficient. However if emission occurs more rapidly than transport, $c=c_0 \exp(F_c b^2/kT)$ at the loop and $c=c_0$ at the surface. The vacancy flux due to diffusion would then be

$$\phi_2 = -\frac{D}{Vc_0}\operatorname{grad} c = \frac{D}{Vl}\left[\exp\left(\frac{F_c b^2}{kT}\right)-1\right]. \quad . \quad . \quad . \quad (\mathrm{A}\ 2)$$

The climb rate is expected to be governed by transport of vacancies if $\phi_1 > \phi_2$, i.e. if $r/l < c_c$. Since $c_c \sim \frac{1}{2}$, r would have to be comparable with l for the climb to be determined by emission of vacancies.

(*b*) *Spherical Diffusion*

The above condition is however rather stringent and would be expected to apply to loops densely distributed in a plane at distance l from both surfaces. For randomly distributed loops in thin foils spherical diffusion is probably a closer approximation. In this case a loop of radius r is imagined to be at the centre of a sphere of radius $l(\gg r)$, i.e. for a very small loop in a thin foil. The vacancy flux at radius R for emission limited conditions (i.e. $c=c_0$ at the loop) is now

$$\phi_1 = \frac{Dr}{2VR^2} c_c\left[\exp\left(\frac{F_c b^2}{kT}\right)-1\right]. \quad . \quad . \quad . \quad . \quad (\mathrm{A}\ 3)$$

However if $c=c_0 \exp(F_c b^2/kT)$ over a sphere of radius r at the loop and $c=c_0$ at $R=l$ (transport limited conditions) then

$$c = c_0 + c_0\left[\exp\left(\frac{F_c b^2}{kT}\right)-1\right]\frac{r}{R},$$

and the vacancy flux due to diffusion is

$$\phi_2 = -\frac{D}{Vc_0}\operatorname{grad} c = \frac{Dr}{VR^2}\left[\exp\left(\frac{F_c b^2}{kT}\right)-1\right]. \quad . \quad . \quad . \quad (\mathrm{A}\ 4)$$

If the climb is determined by transport the condition $\phi_1 > \phi_2$ gives $c_c > 2$. In this case therefore vacancy emission from the loops appears to be the rate determining process since $c_c \sim \frac{1}{2}$. The actual case of loops in thin foils is expected to lie somewhere between these two cases but probably closer to case (*b*). Provided the loops are not too densely distributed and that the foil is not too thick, the approximation the authors have used in neglecting supersaturation effects in thin foils appears reasonable.

Finally, it must be remarked that the total flux of vacancies from the neighbourhood of the loop ($R \sim r$) under transport controlled conditions and assuming spherical symmetry is of the same order of magnitude as the total flux of vacancies emitted by the loop under emission controlled conditions. The form of eqns. (5) and (6) therefore remains similar. Essentially similar conclusions have been reached by Weertman (private communication) working on similar lines. It therefore appears that eqns. (5) and (6) are a valid description of the annealing process. However in the absence of more detailed observations on the rate of shrinking of loops it is not possible to decide by experiment whether the process is limited by emission or transport of vacancies. The considerations outlined above and in § 4.4 suggest that the rate would be determined by emission of vacancies.

On the Stability of the Dislocation Substructure in Quenched Aluminium†

By R. VANDERVOORT and J. WASHBURN
Minerals Research Laboratory, University of California, Berkeley, California

[Received August 14, 1959]

ABSTRACT

Dislocation loops formed by quenching thin aluminium specimens in iced brine were studied by the transmission electron microscope technique. As-quenched specimens contained loops 200 Å to 600 Å in diameter with a density of 10^{15} loops per cubic centimetre. Quenched-in loops were completely removed by heating to 200°c for ten minutes or by cold rolling to a 5% reduction in thickness. The disappearance of the loops was accompanied by an increase in the number of irregular kinked dislocation lines.

§ 1. INTRODUCTION

THE equilibrium concentration of vacant lattice sites in a crystal decreases with decreasing temperature according to the approximate relation:

$$C_v = \exp\left(-\frac{U_{fv}}{kT}\right)$$

where C_v is the fraction of the total number of lattice sites that are not occupied by an atom and U_{fv} is the energy of formation of a vacancy. Therefore, when a metal is cooled, vacant lattice sites must be eliminated. There are only three ways excess vacancies can be removed: (1) migration to an external surface, (2) precipitation on an edge dislocation line, or (3) clustering to form small voids or prismatic dislocation loops as proposed by Seitz 1950).

Resistivity measurements (Bauerle and Koehler 1957) suggest that when the cooling rate is rapid enough, the concentration of vacancies present at some higher temperature can be frozen in. As long as the temperature is then kept low enough to prevent migration no change in vacancy distribution can take place.

When an aluminium specimen which has been quenched from 600°c rapidly enough to retain the high temperature vacancy concentration is reheated to successively higher temperatures, the resistivity increment due to excess vacancies disappears in two distinct stages. The recent results of Panseri and Federighi (1958) are shown in fig. 1‡. The first stage of recovery which accounts for 80% of the total resistivity increment lies in the temperature range $-80°$c to just below room temperature. As pointed out by Panseri and Federighi it is probably due to disappearance of individual vacancies by formation of clusters. Direct electron microscope observations have shown that this thermal history does in fact produce vacancy clusters which collapse to form small dislocation loops 200 Å to 600 Å in diameter (Hirsch *et al.* 1958). A dislocation density as high as 10^{10} cm/cm^3 can be produced in this way. Therefore the resistivity increment remaining at room temperature may be due to the dislocations. The effect of the same thermal history on mechanical properties has been investigated by Maddin and Cottrell (1955). They observed a large increase in room temperature yield strength which must also be associated with the presence of prismatic dislocation loops.

---

† Communicated by the Authors.
‡ All figures except fig. 1 are as plates.

Fig. 1

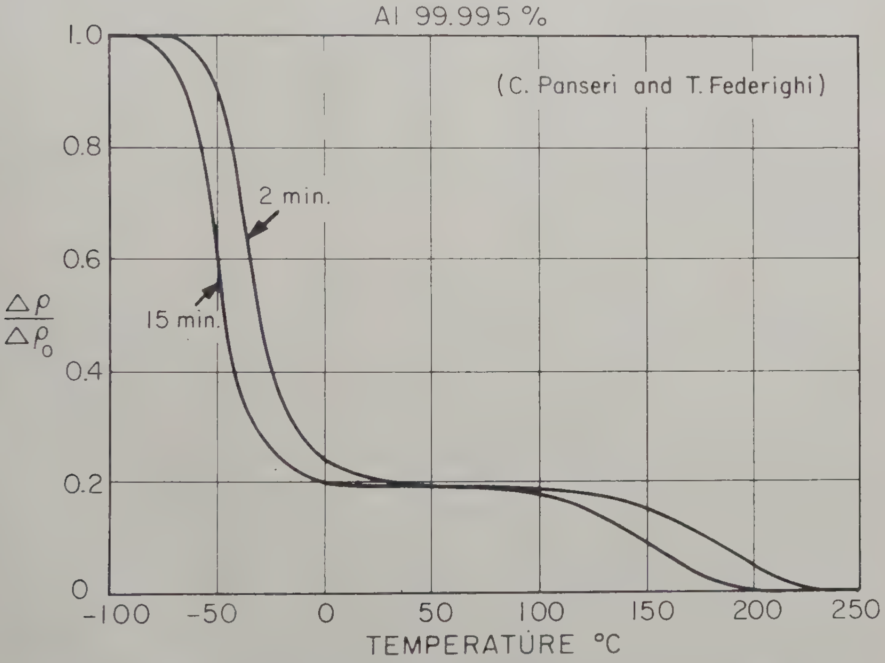

Resistivity decay for isochronal annealing of 2 or 15 min at each temperature after quenching from 600°c.

The second resistivity drop took place on heating into the temperature range between 100°c and 200°c. The activation energy for the process was found to be 1·33 ev (Federighi 1959). It seems likely that second-stage recovery may be associated with the disappearance of prismatic dislocation loops. Dislocation density could be greatly reduced by migration of vacant lattice sites from loops to other sinks or by growth of the largest loops at the expense of smaller ones. Small amounts of plastic deformation at room temperature also cause a decrease in resistivity

(Winterberger 1958). This suggests that loops can be swept out by moving dislocations even at room temperature. The present experiments were undertaken to obtain direct evidence concerning the mechanisms of this second stage resistivity decrease and of quench hardening. Changes in dislocation sub-structure in quenched aluminium specimens caused by reheating to successively higher temperatures or resulting from various amounts of cold work after quenching were observed by electron transmission microscopy.

§ 2. Experimental Procedure

Aluminium sheet specimens 0·005 cm thick of nominal purity 99·995% were quenched from 600°c into iced brine. The first series of specimens was then heated for ten minutes to either 100°c, 125°c, 150°c, 175°c, or 200°c. The second series was cold rolled at room temperature to $2\frac{1}{2}$%, 5%, 10%, 15%, or 45% reduction in thickness after quenching. A thicker specimen was cold rolled to 98% reduction in thickness. All specimens were then thinned by electropolishing in a solution of 20% perchloric acid 80% absolute alcohol to obtain fragments of about 1000 Å to 1500 Å in thickness. The thin foil fragments were examined in an RCA–2E electron microscope operating at 50 kv with either a 50 mil or a 25 mil aperture.

§ 3. Results and Discussion

As-quenched specimens which had not been heated above room temperature before electropolishing contained a dislocation sub-structure similar to that reported by Hirsch *et al.* (1958). Figure 2 shows a typical field. Nearly all areas of the foils that had convenient thickness for observation contained loops. They were absent only near occasional long dislocation lines or within about a micron from a grain boundary. Loops appeared to be nearly circular and apparently did not enclose a stacking fault. Therefore the Burgers vectors were probably of the type $(a/2)\langle 110 \rangle$. The loops appeared to belong to four sets; those in each family being quite accurately parallel to each other. This was particularly noticeable in foils oriented such that two sets were approximately at right angles to the plane of the foil because half of the loops then appeared as short straight lines. Foil orientation could not be determined because the instrument did not permit a diffraction pattern to be obtained. However, the observations were consistent with the hypothesis that most loops lay approximately on $\{111\}$ planes. Neighbouring loops lying on a given (111) plane often were revealed with vastly different contrast. This might be expected since the loops on any one plane should have three different Burgers vectors e.g. $(a/2)[1\bar{1}0]$, $(a/2)[10\bar{1}]$, $(a/2)[01\bar{1}]$, on (111). A few appeared to have a dark centre and an approximately hexagonal shape. Whether this different appearance could be caused by a particular relationship between the Burgers vector, the crystallographic orientation of the foil, and the direction of the electron beam, could not be determined because there was no provision for slightly tilting the specimen while under observation. An alternative explanation might be the presence of some loops enclosing a stacking fault. Most loops had the appearance shown at A in fig. 3. Hexagonal loops with uniform darkening across the entire area are shown at B. A few were revealed in double contrast as at C. The double contrast effect has been explained by Hirsch *et al.* (1960).

Little or no change in the loops was produced by heating for ten minutes at 100°C. Figures 4, 5 and 6 show typical fields after heating to 125°C. As a result of a large number of observations, it was estimated that loops were absent in about one-third of the specimen volume. The number of irregular dislocation lines appeared to be greater and a few larger loops were found. Heating to 150°C decreased the proportion of specimen volume containing loops to about 50%. In the regions still containing loops their density was reduced and their average size increased compared to the as-quenched specimens as shown in fig. 7. Still fewer were present after heating to 175°C and essentially none remained after the 200°C heat treatment. Figure 8 shows a field still containing a few loops after 175°C heating.

The results clearly showed that prismatic loops were eliminated by dislocation climb. Vacant lattice sites migrated from the smaller loops to the larger ones, causing growth of some at the expense of others or from loops to long dislocation lines. During this process there was a definite increase in the number of irregular kinked dislocation lines. Further heating caused disappearance of all loops and a straightening of the irregular kinked dislocations. The observed decrease in dislocation density took place in exactly the same temperature range as the second-stage resistivity recovery reported by Panseri and Federighi (1958). This supports the hypothesis that the decrease in dislocation density accounts for the resistivity decrease. The kinetics of the process is complicated by microscopic inhomogeneity of the specimens. Even in as-quenched specimens the density of loops apparently varied from one part of the specimen to another. The disappearance of loops did not appear to take place primarily by a homogeneous coarsening process. Loops were eliminated in different parts of the same specimen at widely different temperatures. The higher the annealing temperature in the range between 125°C and 200°C the greater was the percentage of specimen volume that was free of loops. In those parts of the specimen where loops remained longest, growth of the larger ones at the expense of the smaller ones did take place. The rapid disappearance of loops in some regions suggests that they may have been eliminated during the heating by a combination of glide and short distance climb of nearby long dislocation lines. By combination of elements of the three dimensional dislocation network with vacancy loops the irregular kinked lines that were observed may have been produced. The regions that retained loops to the highest temperatures presumably were those farthest from network dislocations.

Further support for this general mechanism was provided by cold working after quenching. Dislocation loops combined at room temperatures with moving dislocations to form irregular kinked dislocation lines. All loops were swept out after only 5% reduction in thickness by cold rolling. A resistivity drop produced by room temperature deformation can therefore be associated with a decrease in total dislocation density. Figure 9 shows some loops remaining and irregular kinked dislocations after a plastic strain of 2½% in tension. Figures 10 to 15 show the gradual change from tangles of kinked dislocation lines to a system of well-defined sub-grains as the amount of cold work was increased.

The stress strain curve for quenched aluminium (Maddin and Cottrell 1955) can be qualitatively understood on the basis of these results. The yield stress was high, because the first dislocations to move appreciable distances became heavily jogged almost immediately by combination with loops. The resulting irregular dislocation lines were relatively immobile. At small strains the hardening effect due to formation of groups of tangled irregular dislocations was approximately compensated by the softening effect due to elimination of vacancy loops; therefore there was little strain hardening. Dislocation density decreased during the first few percent plastic strain. At higher strains the rate of hardening and the changes in dislocation sub-structure appeared to be the same in quenched as in furnace-cooled specimens except that the hardness and dislocation structure reached at 5% strain in the former was approximately equivalent to that produced by 10% strain in the latter.

§ 4. CONCLUSIONS

1. Dislocation loops formed by condensation of excess vacancies in quenched 99·995% aluminium began to disappear on heating for 10 min to 125°C and were completely eliminated by heating for 10 min to 200°C.

2. The process was not homogeneous throughout the specimen. Clear areas began to grow at about 125° and the proportion of specimen volume that was free of loops increased with increasing temperature of treatment.

3. In the regions still containing loops after heating into the upper part of the range coarsening took place by growth of the larger loops at the expense of the smaller ones.

4. Elimination of the high dislocation density associated with quenched-in loops probably explains the second-stage resistivity drop observed by Panseri and Federighi (1958).

5. Irregular kinked dislocation lines appeared during the disappearance of loops and then tended to straighten out and disappear again after the loops had been eliminated.

6. Moving dislocations combined readily with the loops at room temperature. Irregular kinked dislocation lines were produced. A plastic deformation of 5% reduction in thickness by rolling was sufficient to sweep out all the loops—resulting in a decrease in total dislocation density.

ACKNOWLEDGMENTS

The authors would like to thank the U.S. Atomic Energy Commission for support of this work. The continuous encouragement of Dr. R. R. Nash and Dr. D. K. Stevens has been greatly appreciated.

REFERENCES

BAUERLE, J. E., and KOEHLER, J. S., 1957, *Phys. Rev.*, **107,** 1493.
FEDERIGHI, T., 1959, *Phil. Mag.*, **4,** 502.
HIRSCH, P. B., SILCOX, J., SMALLMAN, R. E., and WESTMACOTT, K. H., 1958, *Phil. Mag.*, **3,** 897.
HIRSCH, P. B., HOWIE, A., and WHELAN, M. J., 1960, *Proc. roy. Soc.* (in the press).
MADDIN, R., and COTTRELL, A. H., 1955, *Phil. Mag.*, **46,** 735.
PANSERI, C., and FEDERIGHI, T., 1958, *Phil. Mag.*, **3,** 1223.
SEITZ, F., 1950, *Phys. Rev.*, **79,** 890.
WINTERBERGER, M. M., 1958, *Vacancies and Other Point Defects in Alloys* (The Institute of Metals), p. 201.

Dislocation-locking by Carbon, Nitrogen and Boron in α-Iron†

By I. Codd and N. J. Petch
Metallurgy Department, University of Leeds

[Received August 14, 1959]

Abstract

It is shown experimentally that nitrogen-locking is appreciably stronger than carbon-locking. This is contrary to the customary assumption and it is suggested that there may be chemical as well as elastic interaction with the dislocations. Boron is found to produce even stronger locking than nitrogen. These variations in the locking strength alter the ductile-brittle transition temperature. The stronger the locking, the higher the transition temperature.

§ 1. Locking by Boron

The locking of dislocations in α-iron by carbon and nitrogen due to relief of elastic strain energy is now well known (Cottrell 1948, Cottrell and Bilby 1949).

The present work began with an examination of the possibility of dislocation-locking by boron. Some doubt exists about the nature of the boron solution in α-iron. However, the observation of an internal friction peak at about room temperature and of a diffusion rate for boron in iron comparable to that of nitrogen and carbon suggests interstitial solution (Hasiguti and Kamoshita 1954, Thomas and Leak 1955, Samsonov and Tseitina 1955). Because of this and the fact that boron is a larger atom than either nitrogen or carbon, very strong dislocation-locking by boron seems possible.

The approach adopted to obtain information about this possibility involved an examination of the effect of boron on the lower yield point $\sigma_{\mathrm{l.y.p.}}$ of a steel at 18°c and −196°c over a wide range of grain diameter l. This permitted a study of the effect of boron on the constants σ_0 and k in the equation

$$\sigma_{\mathrm{l.y.p.}} = \sigma_0 + kl^{-1/2}. \qquad (1)$$

The form of this equation is consistent with the propagation of a Lüders band from grain to grain at the lower yield point by the concentrated shear stress generated ahead of a slip band where it is held up by a grain boundary. The constant k is taken to be a measure of the shear stress τ_{d} required ahead of the slip band to unlock a dislocation. In the expression given in the Appendix,

---

† Communicated by the Authors.

$$k \sim 4r^{1/2}\tau_{\mathrm{d}}, \qquad \ldots\ldots\ldots \quad (2)$$

where r is the distance of the dislocation from the end of the slip band. The other constant σ_0 in (1) is the stress opposing the motion of an unlocked dislocation along the slip plane. At room temperature, σ_0 is largely due to the interaction of the dislocations with fine precipitates, lattice defects and random impurity atoms, but at low temperatures another, very temperature-dependent contribution becomes dominant and this is apparently associated with the body-centred cubic structure (Cracknell and Petch 1955, Heslop and Petch 1956).

To study the effect of boron, three steels were used, representing the addition of molybdenum and of boron and molybdenum to a 0·13% carbon base material. The compositions are given in table 1 (A, B and C). This molybdenum–boron composition was chosen because it is representative of the principal boron steel used industrially.

Table 1. Analysis, Weight %

	C	Mn	Si	S	P	Mo	Al	N	O	'Acid-soluble' B	'Acid-insol.' B
A	0·12	0·52	0·34	0·010	0·027	0·50	0·07	0·008	0·005	0·002	0·002
B	0·13	0·53	0·40	0·011	0·030	0·48	0·07	0·008	0·004	<0·0001	trace
C	0·13	0·47	0·30	0·010	0·031	0·11	0·08	0·008	0·005	<0·0001	trace
D	0·12	0·51	0·02	0·050	0·029	—	<0·01	0·008	—	<0·0001	nil
E	0·019	0·005	0·006	0·014	<0·002	<0·01	<0·005	0·007	—	nil	nil
F	0·045	0·47	0·02	0·035	0·018	—	0·01	0·006	—	nil	nil

Ni, Cr, V, Cu, Co, Ti and W were all <0·02%, except for 0·08% Ni and 0·05% Cr in D.

The general experimental procedure for the determination of the yield points followed that already described (Cracknell and Petch 1955). Specimens with 1 in. gauge length of 0·125 in. diameter were used and the strain rate was $2\times10^{-4}\,\mathrm{sec}^{-1}$. The specimens were machined, polished to 3/0 emery and, to vary the grain size, they were annealed *in vacuo* in the range 910°–1200°c, followed by cooling in the furnace at various rates. They were then tested. As commercially heat-treated, this boron steel is air-cooled and does not show a yield point probably because of the internal stresses arising from the low temperature of transformation from austenite. However, by using a cooling rate not exceeding 6°c min^{-1}, the yield point was retained.

The results of these measurements are shown in figs. 1 and 2, and the values of σ_0 and k obtained from them are in table 2. Throughout the present work, the least squares method was used for curve-fitting.

It is apparent that boron produces a substantial increase in the slope k both at 18° and −196°c. Thus, from (2), unless boron affects the distribution of the dislocations so that r alters, this increase in k must mean that boron increases τ_{d}, the dislocation-locking strength.

Fig. 1

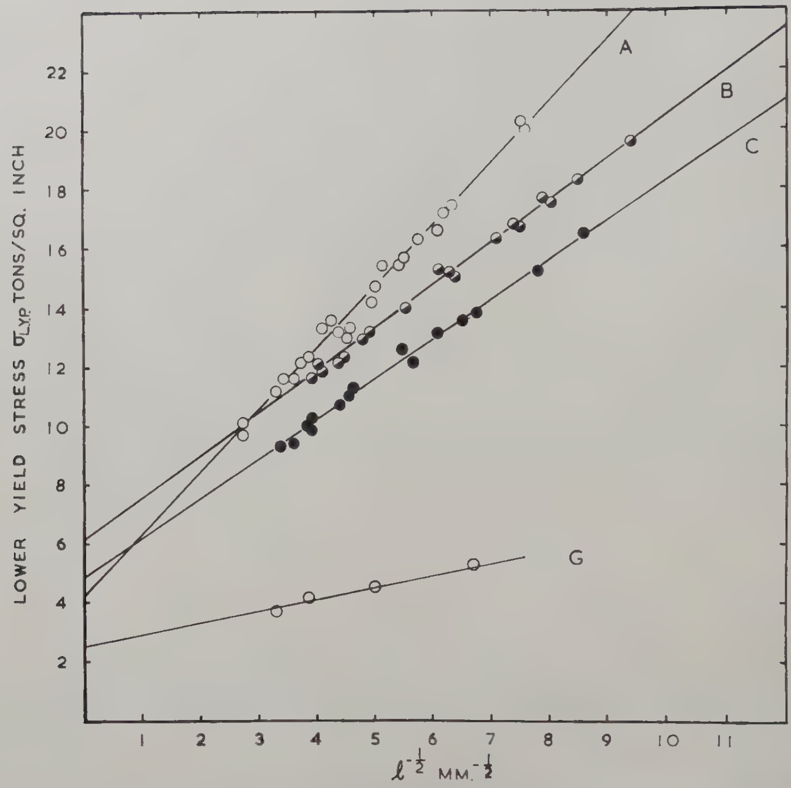

The lower yield point-grain size dependence at 18°c for steels A, B and C. G gives the limit of proportionality for the yield point-free material obtained from E.

Table 2. σ_0 and k Values

Steel	Temperature °c	σ_0 10^8 dynes cm^{-2}	k 10^8 cgs units
A (Mo–B)	18	6·5	1·02
B (Mo)	18	9·4	0·69
C (killed)	18	7·4	0·65
D (semi-killed)	18	7·1	0·74
A† (Mo–B)	18	6·6	0·66
A (Mo–B)	−196	40·1	1·94
B (Mo)	−196	45·0	1·28
C (killed)	−196	43·0	1·21
D (semi-killed)	−196	42·9	1·62
E′ (pure C)	−196	49·3	0·98
F′ (pure C)	−196	44·5	1·01
F″ (pure C–N)	−196	44·5	1·59

† Annealed 750–850°c.

Table 2 also shows that when the grain size range in the molybdenum–boron steel A was established by annealing at 750–850°c, instead of above 910°c, the effect of the boron on k disappeared. The solubility of boron in α-iron falls rapidly below 910°c to $<0{\cdot}0004\%$ at 710°c (McBride *et al.* 1954), so it seems that the amount of boron retained in solution in this annealing range was too small to affect the dislocation-locking. On cooling from the higher annealing temperatures, equilibrium was presumably not established and the boron was retained in solution.

Fig. 2

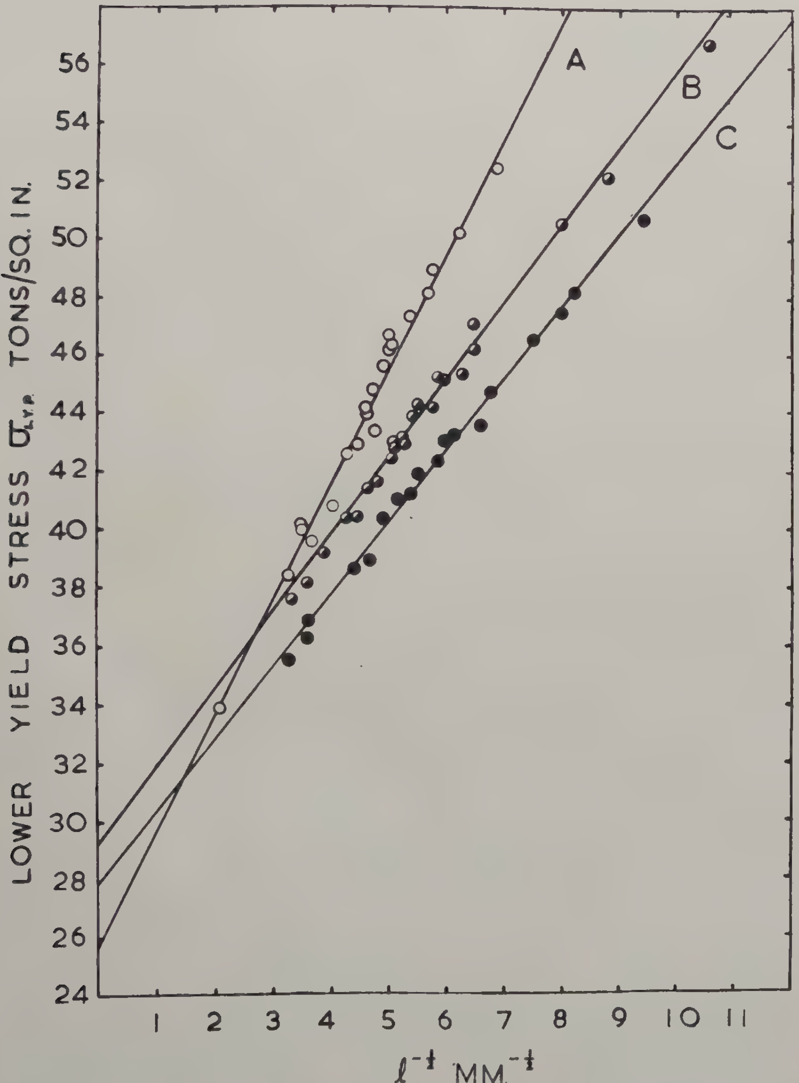

The lower yield point–grain size dependence at −196°c for steels A, B and C.

§ 2. Locking in Killed and Semi-killed Steels

The steels used in § 1 were fully killed (deoxidized) with Mn, Si and Al. Previously a semi-killed plain carbon steel had been examined (Cracknell and Petch 1955, Heslop and Petch 1956) and the σ_0 and k values for this steel D are included in table 2. The composition is in table 1. It is clear that the slope k is appreciably greater for the semi-killed D than for the fully-killed C, particularly at −196°c.

Fig. 3

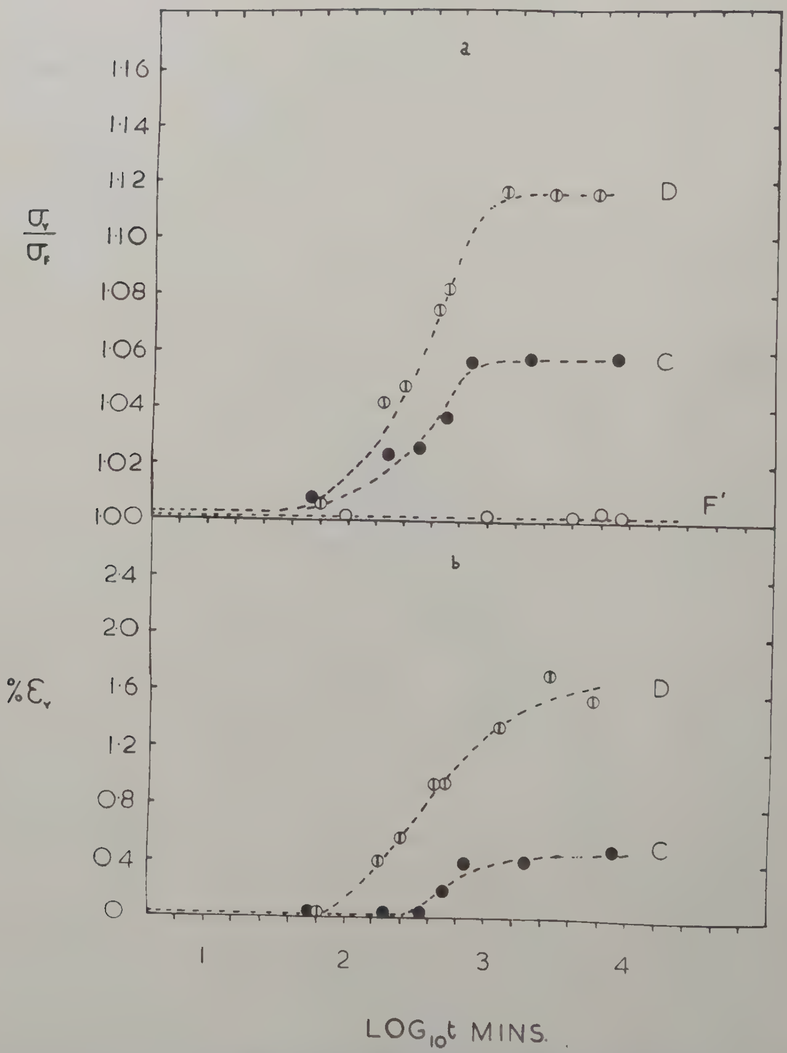

Strain-ageing at 35°c. Change with time of (*a*) the ratio of the yield point after ageing σ_r to the flow stress σ_F at the end of the initial 4% strain, (*b*) the yield elongation.

In an annealed semi-killed steel there is much more nitrogen than carbon in solution in the ferrite at room temperature and available for dislocation-locking. Fully-killing a steel, however, not only deoxidizes it, but in addition largely precipitates the nitrogen as AlN. Thus, this reduction in the slope k observed with the fully-killed steel suggests that removal of nitrogen from solution has weakened the dislocation-locking.

To get some idea of the extent of the nitrogen removal in these steels, their strain-ageing was examined. This was carried out at 35°C, since the temperature is then too low for any ageing due to carbon. Specimens annealed to the same grain size were used. Figure 3 shows the measurements for the fully-killed C and the semi-killed D after 4% strain. Also included is a nitrogen-free, iron–carbon alloy F′, described later. From the rate of ageing, it appears that the content of uncombined nitrogen in the killed steel C is about one-third of that in the semi-killed D. Figure 3 also shows that the yield point elongation after ageing was shorter for the fully-killed steel. Since this elongation measures the strain required in one crystal to unlock a dislocation in the next, it seems that the nitrogen available in the fully-killed steel was insufficient for the development of full nitrogen-locking on ageing.

A similar effect to that of full-killing upon k has been observed with high manganese additions (1–2%) to a semi-killed steel (Heslop and Petch 1957) and, although there is no precipitation of a nitride in that case, there is a 0·2 ev attraction between the manganese and nitrogen atoms in solution that may interfere with the supply of nitrogen atoms to the dislocations.

§ 3. PURE CARBON-LOCKING AND PURE NITROGEN-LOCKING

To examine further this effect of the availability of nitrogen on the dislocation-locking strength, pure carbon-locking and pure nitrogen-locking were prepared.

Carbon and nitrogen were removed by wet hydrogen from specimens of a fairly pure Swedish iron and of a 0·47% Mn steel (E and F in table 1) until the yield point was suppressed†. Carbon alone was then replaced as described in § 6. This gave two nitrogen-free steels, one with 0·20–0·26% C, the other with 0·09–0·12% C, 0·47% Mn. Their lower yield points at −196°C are shown in fig. 4 and the k values are in table 2 (E′ and F′).

It is clear that the pure carbon-locking gives a value of k only about two-thirds that of the semi-killed steel D at −196°C. This carbon k is even lower than k for the fully-killed steels B and C, which still contain some free nitrogen, and is close to the value reached in a high manganese (1·9%) steel (Heslop and Petch 1957).

Replacement of the nitrogen to 0·008% in the carburized specimens returned k to the value for the semi-killed steel D (F″ in fig. 4 and table 2).

---

† The limit of proportionality for the yield point-free iron obtained from E is included at G in fig. 1.

Direct nitriding (0·013% N_2) of the yield point-free material gave the same result with $k=1{\cdot}6\times10^8$ c.g.s. units at -196°c. (fig. 6).

Thus, it seems well established that carbon-locking is weaker than nitrogen-locking and that the locking in an annealed semi-killed steel is predominantly due to its nitrogen.

Fig. 4

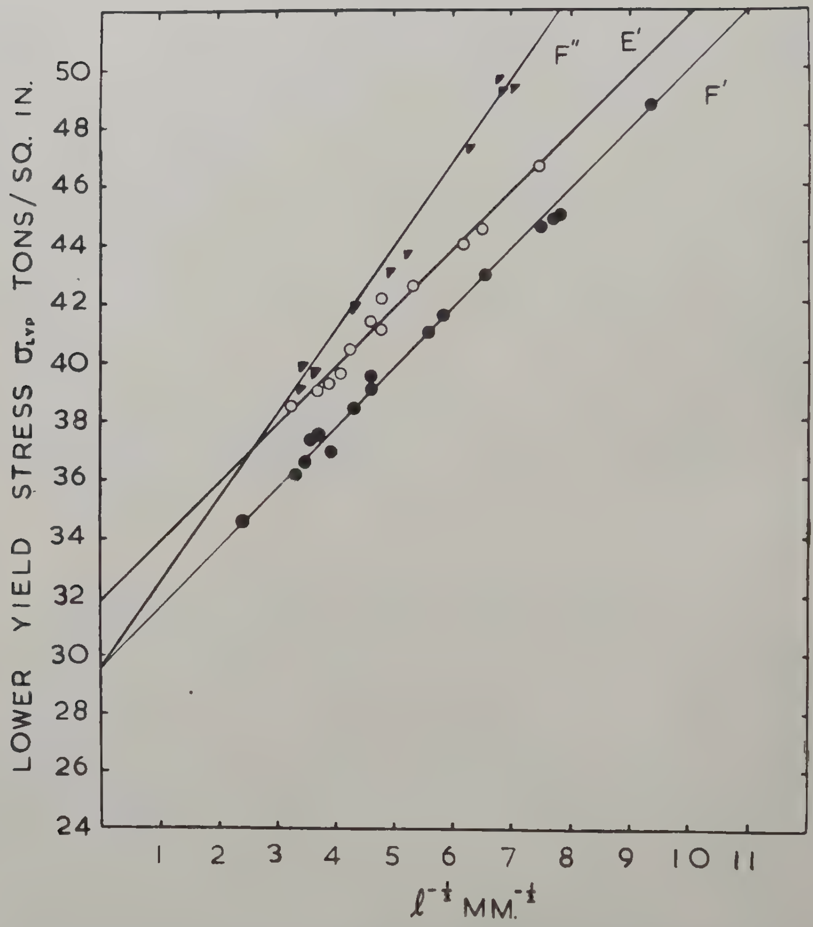

The lower yield point–grain size dependence at -196°c after treatment to give pure carbon-locking (E′ and F′) and after subsequent nitriding (F″).

Specimens of F treated to give pure boron-locking (0·004–0·006% 'soluble' B) have also been prepared (Codd, unpublished) and their k value at 18°c is very close to that for the molybdenum–boron steel A, so confirming that carbon–nitrogen-locking is replaced by boron-locking in this steel.

§ 4. THE RELATIVE STRENGTHS OF CARBON, NITROGEN AND BORON-LOCKING

In (2), a change in the slope k can arise from a change in the locking strength τ_d or from a change in the distance r between the end of the slip band and the dislocation that is unlocked in the propagation of yield from one grain to the next. Replacement of nitrogen-locking by carbon-locking changes not only k but also its temperature-dependence. An alteration in r would not have this effect. Also there seems no particular reason why r should change whenever the locking atoms change. On these grounds, the observed alterations in k have been interpreted as alterations in locking strength.

In the original Cottrell–Bilby theory, the dislocation-locking in α-iron was thought to be due to a condensed atmosphere consisting of a single line of carbon or nitrogen atoms at the dislocation. It now appears that the atmosphere is more extensive than this (Cottrell 1953 a, Dahl and Lücke 1954, Thompson 1958). Thus, one possible explanation of the greater strength of nitrogen-locking compared to carbon-locking is simply that the higher solubility of nitrogen in α-iron below about 580°C may give rise to a higher concentration of impurity atoms at the dislocations. Against this idea, there is the consideration that escape from a stronger-locking, more concentrated atmosphere would be expected to require a greater activation energy and this would make nitrogen-locking less temperature-dependent than carbon-locking, whereas the opposite is observed. Also, when the carbon-locked steel F′ was quenched from 650°C, its k value remained unchanged at the low value (F‴, fig. 5), and similarly on quenching the nitrogen-locked steel its k remained unchanged at the high value (fig. 6)†. Yet, in these treatments, the carbon concentration in the ferrite was greater than the nitrogen concentration. Thus, it does not seem possible to explain the difference between the carbon and nitrogen k values on the basis of a concentration effect.

It is now suggested that the observed difference in the k values shows that the interaction energy between a carbon atom and a dislocation is less than that between a nitrogen atom and a dislocation. This is, of course, contrary to the customary assumption based on the very nearly equal dilations produced by the two atoms and suggests that there must be some effect additional to the elastic interaction.

Recent theoretical work has emphasized the possible directional character of metallic bonding (Altman *et al.* 1957) and the observations of what may be an appreciable Peierls–Nabarro stress in α-iron also suggests directionality of bonding (Heslop and Petch 1957). Possibly, therefore, in the locking of a dislocation in α-iron, the important effect additional to the elastic interaction arises from a degree of residual chemical bonding at a dislocation to which the impurity atom becomes attached, as occurs in covalent silicon and germanium (Seitz 1952).

---

† There is an increase in the friction stress σ_0 on quenching the iron–carbon alloy (fig. 5) because of the increased concentration of carbon retained in solution in the ferrite, but there is little effect on σ_0 for the iron–nitrogen alloy (fig. 6) because most of the nitrogen is already in solution in the annealed specimens.

There is some evidence that such chemical bonding might be stronger for nitrogen than for carbon. The free energy of formation of the iron carbides and nitrides are about the same (Quill 1950) in spite of the greater stability of the bonding in elementary nitrogen (Pauling 1948), which suggests that the iron–nitrogen bond is stronger than the iron–carbon one.

Fig. 5

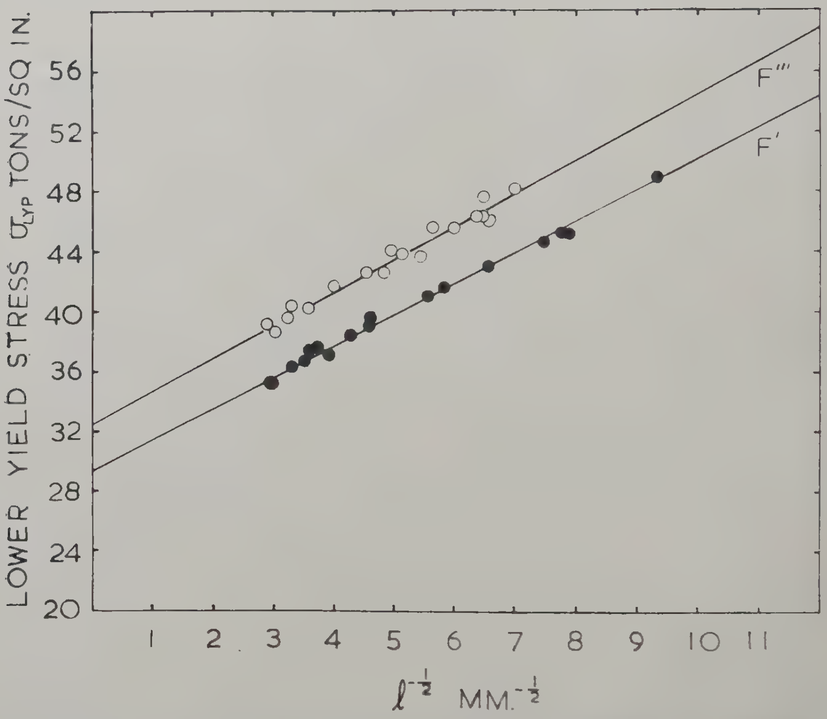

The effect of quenching from 650°C (F‴) on the strength of the pure carbon-locking at −196°C.

Now consider the boron-locking. That it is the strongest is consistent with the atomic size of boron. The boron radius in α-iron is uncertain, but taking the value 0·94 Å from Fe_2B, the tetragonal strain in α-iron should be ~0·53 and in the transverse directions the strain should be ~0·08. Using the expression due to Cochardt *et al.* (1955), these figures make the interaction energy with an atom situated directly below an edge dislocation ~2·0 times as great for boron as for carbon. The observed ratio of k for boron and carbon is 2·0 at −196°C and ~1·7 at room temperature. This agreement is probably fortuitous since the boron radius is uncertain and chemical interaction is neglected.

Fig. 6

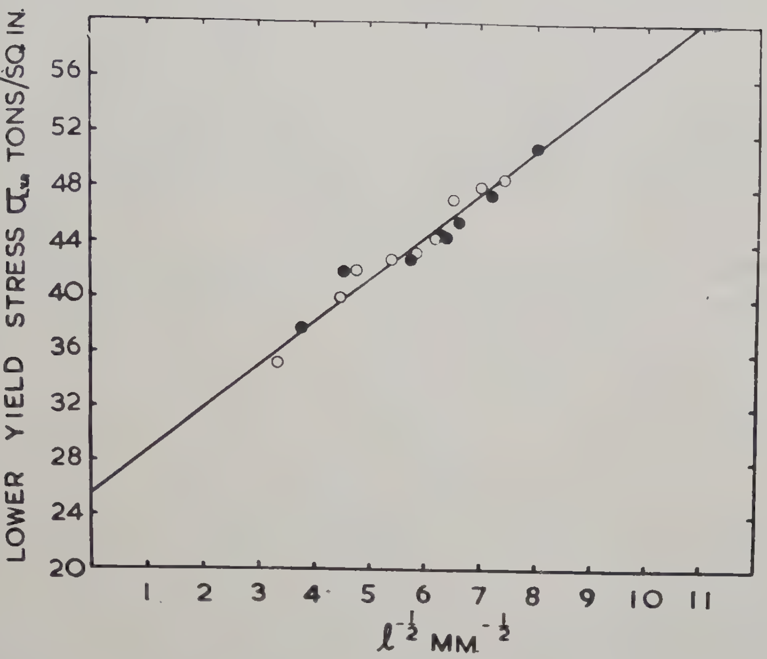

The lower yield point–grain size dependence at −196°c for pure nitrogen-locking; ○ annealed, ● quenched from 650°c.

§ 5. The Friction Stress and the Ductile–Brittle Transition

The value of σ_0 in (1) represents the friction opposing the movement of an unlocked dislocation along the slip plane. This is not a major concern in the present paper, so the observed values (table 2) will be discussed only briefly.

The friction σ_0 is due to the lattice itself and to interaction of the moving dislocation with precipitates, lattice defects and impurity atoms in solution. Between the semi-killed steel D and the fully-killed C there should be a fall in σ_0 due to the removal of nitrogen from solution, but this appears to be compensated for by the increased interaction with silicon. The addition of Mo in steel B makes a further contribution to σ_0. The subsequent fall on adding boron (steel A) presumably arises from further nitrogen fixation and possibly from some interaction of the boron and molybdenum atoms.

The variations in the dislocation-locking strength observed in the present measurements should be accompanied by variations in the ductile–brittle transition temperature (Heslop and Petch 1957, 1958, Cottrell 1958). The weaker the dislocation-locking, the easier is plastic deformation and the lower should be the transition temperature. This is confirmed for the present steels by fig. 7 in which the transition temperature is taken at

10 ft lb (~75% cleavage) for 5/16 in. V-notched specimens broken in a Charpy-type impact test.

The amount the transition temperature of the fully-killed C is below that of the semi-killed D agrees with previous measurements in which k was reduced by manganese (Heslop and Petch 1957).

The 1·3 ton in^{-2} increase in σ_0 between C and B (table 2) should give a 6°c rise in transition temperature (Heslop and Petch 1958).

Fig. 7

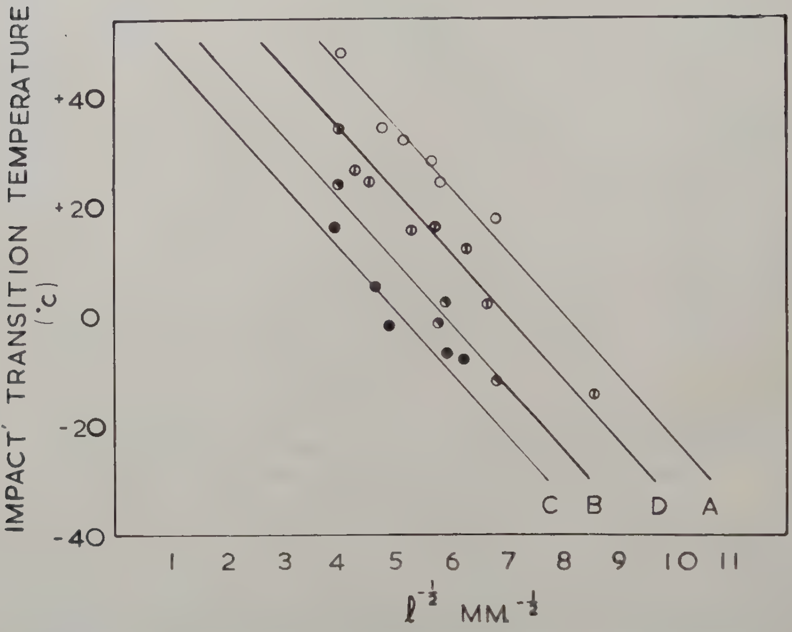

The ductile–brittle transition temperatures for boron-locked (A), killed (B and C) and semi-killed (D) steels.

§ 6. Exprimental Details

For the preparation of the pure carbon-locking, tensile specimens (1 in. gauge length of 0·125 in. diameter) were partly machined from the Swedish iron E and from a similar material F with 0·5% Mn added in the hope that it would help in the retention of a fine grain size. These specimens were heated in wet hydrogen at 850°c until samples showed that the carbon and nitrogen had been removed to such an extent that the yield point was suppressed (~600 hours). The treatment was continued for at least a further day and carbon only was then replaced by carburizing for a pre-determined time at 820°c in an atmosphere of purified hydrogen and hexane vapour.

To remove nitrogen and other gases from the hexane, it was previously refluxed at reduced pressure (2 mm) and temperature (0°c). After this treatment, the vacuum was released by purified hydrogen and, as an additional precaution, the hydrogen was bubbled slowly through the hexane for some time before passing the hydrogen–hexane mixture into the carburizing tube. Since there was very little carbon pick-up until the hexane decomposed at ~815°c, the hydrogen–hexane mixture was used to protect the specimens during heating and cooling and the time at 820°c gave a reasonable estimate of the carbon ingress. After homogenizing for eight days at 1050°c *in vacuo*, the specimens were machined to final size, polished and then heat-treated *in vacuo* to establish the desired grain size. Each specimen was analysed for carbon.

For the nitrogen-locking, nitriding was carried out at 580°c for ~100 hours in a stream of hydrogen bubbled through 3% ammonia in distilled water.

APPENDIX

CALCULATION OF THE SLOPE k

In Stroh's (1955) calculation, the distance r between the head of a slip band and the operated source (length s) in the next grain during the propagation of a Lüders band from one grain to the next at the lower yield point is taken to be at least equal to s. This is to allow sufficient room for the operation of the source. The shear stress ahead of a slip band depends upon $r^{-1/2}$, but the stress required for critical bowing of the source depends upon s^{-1}, so, with $s \sim r$ and no impurity-locking, the further the source is away from the slip band the longer it can be and the easier it is operated by the slip band. With a locked source, however, there will be a lower limit τ_d on the shear stress required for its working and the easiest source to bring into operation ahead of a slip band will then be the one for which the bowing stress and the locking stress are equal.

Stroh thus obtains

$$k \sim 2(2\tau_d \mu \mathbf{b})^{1/2}, \qquad (3)$$

where μ is the rigidity modulus and $\mathbf{b}$ is the Burgers vector.

This argument will however break down if the locking stress is greater than the bowing stress for all the sources present and it seems probable that this will be so in α-iron. At −196°c, τ_d is $\sim 1 \times 10^{10}$ dynes cm^{-2} and it is probably only a few times smaller at room temperature (Cottrell 1958). Thus, the locking stress is ~100 times greater than that required for the critical bowing of sources of the length (10^{-4} cm) normally expected in α-iron.

The argument for (3) in α-iron has been supported by showing that it gives the correct temperature-dependence of k from the temperature-dependence of τ_d. However, in this, τ_d was identified with the upper yield point, whereas it is now clear that the upper yield point is the stress required for the break-out of a plastic nucleus across the specimen (Cottrell 1953 b) and not the stress for unlocking a source. The upper yield point is influenced by the stress concentration ahead of slip bands in the plastic nucleus, so it depends on grain size in a similar way to the lower yield point (eqn. (1)). Thus the temperature-dependence of the upper yield point arises principally from the temperature-dependence of the friction stress σ_0 and it does not directly give the temperature-dependence of the locking strength τ_{d} in the way assumed in this support of (3).

In place of a value of r determined according to Stroh's suggestion, it may be that r is simply the average distance between the end of a slip band and the nearest source in the next grain. Then, from the equivalence of a crack and a slip band in the relaxation of shear stress

$$\tfrac{1}{2}(\sigma_{\mathrm{l.y.p.}}-\sigma_0)(l/4r)^{1/2}=\tau_{\mathrm{d}},$$

or

$$k=4r^{1/2}\tau_{\mathrm{d}}. \qquad \qquad (4)$$

At −196°c, with $\tau_{\mathrm{d}} \sim 1\times10^{10}$ dynes cm^{-2} and $k=1{\cdot}6\times10^{8}$ c.g.s. units, r is $\sim 0{\cdot}2\times10^{-4}$ cm.

The main difficulty with (4) is that r has to be constant, independent of grain size. It may be that the width of the grain boundary stress field imposes such a constancy.

Another possibility is that instead of operating a source in the next grain, the yield is propagated by forcing a length of dislocation out from the grain boundary.

References

Altman, S. L., Coulson, C. A., and Hume-Rothery, W. 1957, *Proc. roy. Soc.* A, **240,** 145.

Cochardt, A. W., Schoek, G., and Wiedersich, H., 1955, *Acta Met.*, **3,** 533.

Cottrell, A. H., 1948, *Rept. Conf. Strength of Solids* (London: The Physical Society), p. 30; 1953 a, *Relation of Properties to Microstructure* (Amer. Soc. Metals), p. 131; 1953 b, *Dislocations and Plastic Flow in Crystals* (Oxford: University Press), p. 147; 1958, *Trans. Amer. Inst. min. (metall.) Engrs*, **212,** 192.

Cottrell, A. H., and Bilby, B. A., 1949, *Proc. phys. Soc. Lond.*, A, **62,** 49.

Cracknell, A., and Petch, N. J., 1955, *Acta Met.*, **1,** 186.

Dahl, W., and Lücke, K., 1954, *Arch. Eisenhüttenw.*, **25,** 241.

Hasiguti, R. R., and Kamoshita, G., 1954, *J. phys. Soc. Japan*, **9,** 646.

Heslop, J., and Petch, N. J., 1956, *Phil. Mag.*, **1,** 866; 1957, *Ibid.*, **2,** 649; 1958, *Ibid*, **3,** 1128.

McBride, C. C., Spretnak, J. W., and Speiser, R., 1954, *Trans. Amer. Soc. Met.*, **46,** 499.

Pauling, L., 1948, *The Nature of the Chemical Bond* (Cornell University Press), p. 177.

Quill, L. L., (Editor), 1950, *The Chemistry and Metallurgy of Miscellaneous Materials, Thermodynamics* (New York: McGraw-Hill), p. 13.

Samsonov, G. V., and Tseitina, N.Ya., 1955, *Fizika Metallov i. Metallovedenie*, **2,** 303.

Seitz, F., 1952, *Phys. Rev.*, **88,** 722.

Stroh, A. N., 1955, *Phil. Mag.*, **46,** 968.

Thomas, W. R., and Leak, G. M., 1955, *J. Iron St. Inst.*, **180,** 155.

Thompson, R., 1958, *Acta Met.*, **6,** 23.

On Dislocation Formation by Vacancy Condensation[†]

By G. Schoeck[‡] and W. A. Tiller
Westinghouse Research Laboratories, Beulah Road, Churchill Borough.
Pittsburgh 35, Pennsylvania

[Received August 19, 1959]

Abstract

The mechanism of dislocation loop formation by vacancy condensation is examined in a quantitative manner. The critical vacancy supersaturation necessary for the growth of the loops and the climb rate of the dislocations are determined. It is shown that the mechanism proposed for lineage formation based upon loop growth (Frank, 1956 a) is inapplicable. The number of dislocation loops produced by collapsing vacancy discs is calculated as a function of the cooling rate, cooling range and dislocation density existing in the crystal before cooling.

§ 1. Introduction

Essentially five different mechanisms exist for the introduction of dislocations into freshly grown crystals: growth accidents (Frank 1950), vacancy condensation (Frank 1950, Seitz 1950, Kuhlmann-Wilsdorf 1958), segregation of solutes (Frank 1950, Friedel 1956, Goss *et al.* 1956, Tiller 1958), phase transformation and precipitation (Brooks 1952) and thermal and external stresses (Billig 1956, Wagner 1958). If one considers single phase crystals grown carefully from the melt so that both thermal and external stresses are absent we may neglect the last two mechanisms. In general, then, one needs to consider only the first three mechanisms in order to determine the total dislocation concentration either grown into the crystal at the solid–liquid interface or quenched-in during cooling of the crystal.

One would expect that not only the dislocation density but the dislocation arrangement in the crystal would differ depending on the mechanism by which they are introduced into the crystal. However, except in a few cases, little quantitative theoretical work has been carried out on the genesis of the original dislocations in metal crystals. Most theoretical investigations have been concerned with the somewhat simpler problem of the stable arrangements of dislocations either in two dimensional arrays (boundaries) or in three-dimensional networks.

Recently, Kuhlman-Wilsdorf (1958) has reconsidered the formation of dislocation rings from collapsed vacancy discs and proposed that these

---

[†] Communicated by the Authors.

[‡] Now at CNEA, Av. Lib. Gen San Martin 8250, Buenos Aires, Argentina.

dislocation rings are actually the main sources for the multiplication of dislocations during plastic deformation. From the kinetics of the electrical resistivity recovery and from quench hardening, it has been concluded by Kimura *et al.* (1959) that the dislocation rings can be formed from vacancy aggregation provided the crystal is quenched over a sufficiently large temperature range. More recently Hirsch *et al.* (1958) have actually observed such dislocation loops in quenched Al (Hirsch *et al.* 1958), and defects related to dislocation loops in the noble metals (Hirsch and Silcox 1958).

Fig. 1

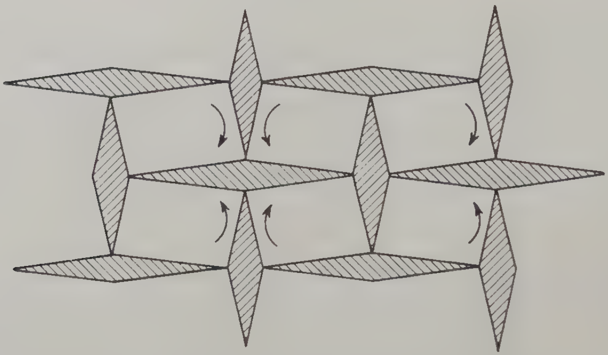

Striation-type dislocation array (after Frank).

The vacancy condensation model has also been used by Teghtsoonian and Chalmers (1951, 1952) and Atwater and Chalmers (1957) to account for a particular type of lineage structure called 'striations' observed to occur during the growth of crystals from the melt. This sub-structure consists of an assembly of low-angle grain boundaries which partitions the crystal into rod-like elements that are generally parallel to the crystal axis. The striations are often of the order of 1 sq. mm in cross-sectional area, the different rods being rotated with respect to each other about the growth axis by angles varying between a fraction of a degree and several degrees, as illustrated in fig. 1. In growing a single crystal without the use of a seed it is observed that the striations do not form immediately. They are observable only after a considerable length (approximately 1 cm) of solid has formed. After this incubation distance, the misorientations appear spontaneously and increase to a stable value with a little further solidification.

Frank (1956 a) has developed a detailed picture of the vacancy collapse mechanism to account for this 'striation' sub-structure giving a qualitative explanation of the origin, size and initial misorientation. It is very easy to show that the dislocations in the lineage array could not have been formed by the collapse of vacancy discs since the total vacancy concentration of the crystal is 2 to 3 orders of magnitude too small to provide the lineage size and misorientation. Therefore, Frank postulated the following.

The edge dislocation loops, formed by vacancy condensation at some distance behind the interface, grow in size to reduce the vacancy supersaturation. Those loops which lie in planes parallel to the growth axis will grow towards the interface and catch up to it. Once the dislocation has entered the interface it will contribute to the misorientation of the growing solid without further vacancy condensation. This is illustrated in fig. 2. He maintained that the elastic interaction between edge dislocations should cause them to assemble into parallel arrays as shown. A system of these arrays leads to the lineage type substructure (fig. 1). The ends of the loops in fig. 2 (*a*) are in an unstable position and are attracted into the interface with the liquid (fig. 2 (*b*)). The dislocations are then no longer effective for removing vacancies merely by lengthening and the vacancy excess will drive them apart. A new dislocation loop will then form preferentially in this central region (fig. 2 (*c*)) and the amount of rotation of the lineage boundaries will continually increase until the rate of production of new loops is balanced by the rate of annihilation of dislocations by the meeting of opposite pairs.

Fig. 2

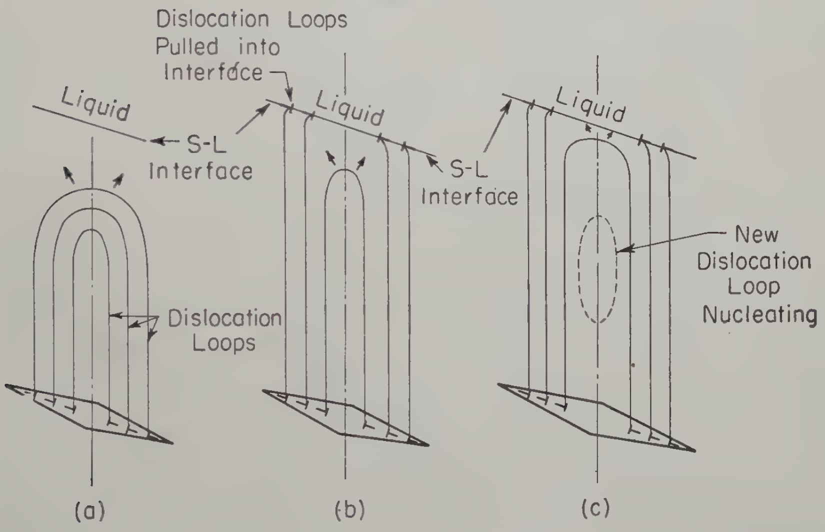
Dislocation Loops Pulled into Interface
Liquid
S-L Interface
Liquid
S-L Interface
Liquid
New Dislocation Loop Nucleating
Dislocation Loops
(a)
(b)
(c)

The climbing of dislocation loops into the solid–liquid interface.

The purpose of the present paper is to examine the vacancy condensation mechanism in a quantitative manner to determine (i) the critical vacancy supersaturation necessary for the formation and growth of dislocation loops by vacancy condensation and (ii) the climb rate of the dislocations as a function of the vacancy supersaturation. From these calculations and the experimental observations on striations it will be shown that Frank's model cannot account for the sub-structure. From the calculations it is also possible to determine the quenching rate and quenching range necessary for the formation of the dislocation loops by vacancy condensation. Finally, it is possible to estimate the density of dislocations introduced into the crystal by this mechanism during crystal growth.

§ 2. CONDENSATION OF VACANCIES

If the concentration of vacancies in a solid exceeds the thermal equilibrium value there is a tendency for the vacancies to anneal out by condensing into larger aggregates. The determination of the vacancy super-saturation necessary to nucleate this process is a very complex problem and has not yet been treated. It is very likely that the nucleation takes place heterogeneously in the neighbourhood of solute or impurity atoms rather than homogeneously, but it is not possible to state whether these aggregates will be preferentially pores or flat discs (Frank 1956 b). However, since we are interested in the formation of dislocations, we may assume that vacancy discs are formed which collapse into dislocation rings after they reach a critical size. After this has happened we can calculate the supersaturation necessary to keep the dislocation rings growing to a larger size by climbing. We thus know that the actual supersaturation must be at least this value. Since all dislocations formed by vacancy condensation must go through this early stage of growth we will obtain, in this way, a lower limit for the necessary vacancy supersaturation.

As has been discussed by various authors (Kuhlmann-Wilsdorf 1958, Kimura *et al.* 1959) the collapse of the disc will take place when the energy of the disc (which is essentially the surface energy) exceeds the energy of the dislocation ring (which is essentially strain energy). Usually the collapse of the disc will also form a stacking fault since the two lattice planes brought into contact with each other will generally have an incorrect stacking sequence. In very few cases the surface energy of this stacking fault is known. Since a coherency exists across the interface, the stacking-fault energy should be of the order of a coherent twin-boundary energy and it will not exceed, and in many cases be considerably less than, the energy of a large angle grain boundary. It seems therefore safe to assume that the stacking-fault energy γ_{st} is smaller than about $\frac{1}{3}$ or $\frac{1}{2}$ of the surface energy γ. To obtain an upper limit to the collapse radius in our calculations, we assume for numerical calculations $\gamma_{st}=\frac{1}{2}\gamma$ in all cases where γ_{st} is unknown.

If r is the radius of the vacancy disc, the energy of the disc E_d for not too small values of r, will be

$$E_d \approx 2\pi r^2 \gamma. \quad \ldots\ldots\ldots\ldots \quad (1)$$

The energy of a corresponding dislocation ring with the Burgers vector **b** perpendicular to the plane of the ring (Franz and Kroener 1955) and enclosing a stacking fault of surface energy γ_{st} will be

$$E_r = \frac{1}{2}\frac{G}{(1-\nu)}\mathbf{b}^2 r\left[\ln\frac{8r}{R_0}-1\right]+2\pi r\left[\pi\frac{R_0{}^2}{\mathbf{b}^2}L\right]+\pi r^2\gamma_{\mathrm{st}}, \quad . \quad (2a)$$

where G is the rigidity modulus, ν is Poisson's ratio, R_0 is the radius of the dislocation core and L is the average strain energy per atom of this core. For numerical purposes we use $\nu=\frac{1}{3}$.

We may determine the minimum core radius by noting that the free energy of the core cannot be greater than the free energy of a cylinder of liquid of radius R_0. If one determines the core radius using such an energy balance including a term which incorporates the solid–liquid interfacial energy it is found that $R_0 \sim \mathbf{b}/2$. However, for such a small cylinder of liquid the surface energy term should probably be excluded. If this term is neglected the core radius is given by

$$\frac{R_0}{\mathbf{b}} = \frac{1}{2\pi(1-\nu)}\left[\frac{G/\Delta H}{2\Delta T/T_{\mathrm{m}}}\right]^{1/2} \approx \left\{\frac{T_{\mathrm{m}}}{\Delta T}\right\}^{1/2}, \quad . \quad . \quad . \quad (2b)$$

where ΔH is the enthalpy difference between liquid and solid, T_{m} is the melting temperature and $\Delta T = T_{\mathrm{m}} - T$. For a typical value of

$$\Delta T/T_{\mathrm{m}} \sim 0{\cdot}25,\ R/\mathbf{b}=2$$

and eqn. (2 *a*) can be put in the form

$$E_r = \frac{1}{2}\frac{G}{(1-\nu)}\mathbf{b}^2 r\left[\ln\frac{r}{\mathbf{b}}+Z\right]+\pi r^2\gamma_{\mathrm{st}}. \quad . \quad . \quad . \quad . \quad (2c)$$

For $R_0/\mathbf{b}=2$, 1 and 0·5, $Z=1{\cdot}98$, 1·48 and 1·96 respectively. We will choose the value of $Z=1{\cdot}8$ in our calculations as a representative value.

The condition for collapsing, $E_r = E_{\mathrm{d}}$, gives the critical radius r_{c} from the equation

$$\frac{\mathbf{b}}{r_{\mathrm{c}}}\left[\log\left(\frac{r}{\mathbf{b}}\right)+1{\cdot}8\right]=\frac{4\pi(2\gamma-\gamma_{\mathrm{st}})}{3G\mathbf{b}}. \quad . \quad . \quad . \quad . \quad . \quad . \quad (3)$$

The critical radius r_{c} for several metals is given in table 1. In several cases r_{c} is astonishingly small and collapsing would occur according to eqn. (3) if the diameter of the disc is of the order of a few atomic distances. This estimate may not be quite realistic since the equation for the dislocation energy and the concept of surface energy may lose their significance for such small dimensions. Nevertheless it seems safe to assume that a disc with a radius of 10 atomic distances will have collapsed to form a dislocation ring. For some numerical estimates we will later assume that a vacancy disc exceeding a radius of 10 or 15 atomic distances will have formed a dislocation ring. Once the dislocation ring is formed, it is under the action of its own line tension and can grow or shrink by climbing. It will expand only if there is a sufficient supersaturation of vacancies. A vacancy condensing at the dislocation ring will increase its radius and hence its strain energy E_r. At the same time the free energy F_{v} of the crystal due to the vacancy supersaturation will decrease. If n is the number of vacancies, the critical supersaturation necessary to keep a dislocation ring of radius r from shrinking is obtained from the condition

$$\frac{\partial E_r}{\partial r}+\mu_V\frac{\partial n}{\partial r}\leqslant 0. \qquad (5)$$

where μ_V is the chemical potential of a vacancy which is given by

$$\mu_V=\frac{\partial F_V}{\partial n}=kT\ln\frac{c}{c_0}. \qquad (6)$$

Here c is the actual vacancy concentration and c_0 the concentration of vacancies in thermal equilibrium at temperature T.

Table 1

	G 10^{11} dyne/cm^2	b 10^{-8} cm	γ erg/cm^2	γ_{st} erg/cm^2	$\frac{4\pi(2\gamma-\gamma_{st})}{3Gb}$	$\frac{r_c}{b}$	Gb^3 ev
Sn	1·7	3·02	625†	$<\frac{1}{2}\gamma$	0·75	4·4	2·92
Pb	0·54	3·49	444†	$<\frac{1}{2}\gamma$	1·5	1·5	1·43
Zn	3·8	2·66	824	$<\frac{1}{2}\gamma$	0·52	7·5	4·5
Al	2·5	2·86	900	$\frac{2}{5}\gamma$(2)	0·83	3·75	3·66
Cu	4·1	2·55	1430‡	40(2)	1·1	2·5	4·25
Ag	2·6	2·88	1140‡	~40	1·2	2·1	3·86

† U.S. Atomic Energy Comm. Publ., (*Liquid Metals Handbook*, Wash. 1952).

‡ J. C. Fisher and C. G. Dunn, *Imperfections in Nearly Perfect Crystals* (John Wiley & Sons, Inc., New York 1950).

Since we want to obtain only a lower limit for the necessary supersaturation we are justified in neglecting the term in E_r in eqn. (2) which contains the energy γ_{st} of the stacking fault when we evaluate eqn. (5). The result then becomes somewhat simpler and we obtain from eqns. (2 c), (5) and (6)

$$\ln\frac{c}{c_0}=\frac{G\mathbf{b}^4}{4\pi(1-\nu)rkT}\left[\ln\left(\frac{r}{\mathbf{b}}\right)+2\cdot8\right]. \qquad (7)$$

In order to obtain an estimate of the temperature at which the dislocation ring will be stable we must know the actual concentration c of vacancies present. The concentration of vacancies in thermal equilibrium at temperature T is

$$c_0=\beta\exp(-U_f/kT), \qquad (8)$$

where U_f is the energy of formation of a vacancy and the constant β which is of the order of unity may contain an entropy term. Let us now assume that the equilibrium concentration of vacancies at the melting point, T_m, is frozen in at the advancing liquid–solid interface. Since the mobility of vacancies at T_m is extremely large it is very unlikely that any in excess of this number are frozen-in. Only if no sinks are present will this number be retained in the interior of the solid during cooling to a temperature T and hence we obtain as an upper limit for c

$$c=\beta \exp(-U_f/kT_m). \qquad (9)$$

If we call $\Delta T = T_m - T$ we obtain finally from eqn. (7) with eqns. (8) and (9)

$$\frac{\Delta T}{T_m}=\frac{3G\mathbf{b}^3}{8\pi U_f}\frac{\mathbf{b}}{r}\left[\ln\left(\frac{r}{\mathbf{b}}\right)+2{\cdot}8\right]\dagger. \qquad (10)$$

(The entropy term β drops out if it is temperature independent.) Equation (10) gives the relative undercooling $\Delta T/T_m$ necessary to keep a dislocation ring of radius r from shrinking. The magnitude of $\Delta T/T_m$ depends on the parameter $\alpha = 3G\mathbf{b}^3/8\pi U_f$, which is listed in table 2 for various metals. When measurements of U_f were available the correct value was used whereas otherwise the value of U_f was assumed to be half the activation energy for self-diffusion. Equation (10) is plotted in fig. 3 as $\Delta T/T_m$ *vs.* $r/\mathbf{b}$ for various values of α. The resulting supercooling for a dislocation loop radius of $r=10b$ and $r=15b$ is then also listed in table 2.

To obtain an estimate of the order of magnitude for $\Delta T/T_m$ we may note that U_f is of the order (Friedel 1956 b)

$$U_f \approx 5\,G\mathbf{b}^3. \qquad (11)$$

Using this estimate we obtain as a typical value, $\alpha = 0{\cdot}6$. For this value of α in fig. 3 we see that in order to keep a dislocation of radius $r=10b$ from shrinking, the relative temperature drop would have to be $\Delta T/T_m \approx 0{\cdot}35$. The corresponding value for a dislocation ring of radius $r=15b$ would be $\Delta T/T_m \approx 0{\cdot}21$. Assuming that a radius of $r=10b$ is realistic for a newly formed dislocation ring, the relative supercooling varies between 16% and 50% for the various metals (table 2). This means that the temperature at which these dislocation rings are stable is about 100°c to 400°c below the melting temperature if we are considering crystal growth or the temperature from which they are quenched if we are considering a quenching experiment. It must be remembered that these calculations assume the existence of no other vacancy sinks in the solid, otherwise the vacancy

---

† It has been pointed out by the referee that if the vacancies condense to form a ring of Frank sessile dislocation including a stacking fault, the Burgers vector of whole dislocations, $\mathbf{b}$, should not be used. Equation (10) and the tabulated values of $\Delta T/T_m$ refer, therefore, to the case of no stacking fault. However, if one wishes to treat the stacking-fault case, the right-hand side of eqn. (10) must be multiplied by two-thirds to take account of the reduced Burgers vector and a term $\mathbf{b}^2\gamma_{st}/U_f$ added to take account of the stacking-fault energy. For rings of $r=10b-15b$ the two changes tend to cancel for reasonable γ_{st} leaving $\Delta T/T_m$ negligibly changed.

Table 2

	U_d ev	D_0 cm²/sec	U_f ev	U_m ev	T_m °K	$\alpha \left(\frac{3Gb^3}{8\pi U_f}\right)$	Radius of Ring r/b	$\frac{\Delta T}{T_m}$	ΔT_c °K	T_c °K	$\frac{c}{c_0}$	D cm²/sec.	$D\left(\frac{c}{c_0}-1\right)$ cm²/sec	V_0 cm/sec
Sn	1·11†	4·35†	$\frac{U_d}{2}$	$\frac{U_d}{2}$	505	0·63	10	0·33	166	339	10^2	10^{-15}	10^{-13}	$1{\cdot}6\times10^{-6}$
							15	0·20	101	404	11	3×10^{-13}	3×10^{-12}	5×10^{-5}
Pb	1·08	0·5	$\frac{U_d}{2}$	$\frac{U_d}{2}$	600	0·31	10	0·16	96	504	7·2	10^{-11}	$6{\cdot}2\times10^{-11}$	8×10^{-4}
							15	0·10	60	540	3·2	5×10^{-11}	$1{\cdot}6\times10^{-10}$	2×10^{-3}
Zn	1·00	0·4	$\frac{U_d}{2}$	$\frac{U_d}{2}$	692	1·07	10	0·57	394	298	6×10^4	4×10^{-18}	$2{\cdot}4\times10^{-14}$	$4{\cdot}5\times10^{-7}$
							15	0·35	252	450	90	10^{-11}	9×10^{-10}	$1{\cdot}2\times10^{-2}$
Al	1·34		0·76‡	0·58‡	933	0·57	10	0·29	270	663	2×10^3			
							15	0·18	168	765	6·1			
Cu	2·05	0·2	0·9	1·15	1356	0·56	10	0·29	394	962	23	$3{\cdot}8\times10^{-12}$	8×10^{-11}	$1{\cdot}6\times10^{-3}$
							15	0·18	244	1112	5·3	$1{\cdot}4\times10^{-10}$	6×10^{-10}	$1{\cdot}2\times10^{-2}$
Ag	2·00	0·4	0·8	1·2	1233	0·58	10	0·30	380	853	26	$6{\cdot}4\times10^{-13}$	$1{\cdot}7\times10^{-11}$	3×10^{-4}
							15	0·19	233	1000	5·7	4×10^{-11}	$2{\cdot}3\times10^{-14}$	4×10^{-3}

† J. D. Meakan and Klokholm, Cleveland Meeting AIJE (1958).
‡ C. Panseri and T. Federighi, *Phil. Mag.*, **3**, 1223 (1958).

supersaturation at any temperature will be lowered and the $(\Delta T/T_{\rm m})$ required to keep a loop from shrinking must be increased.

Fig. 3

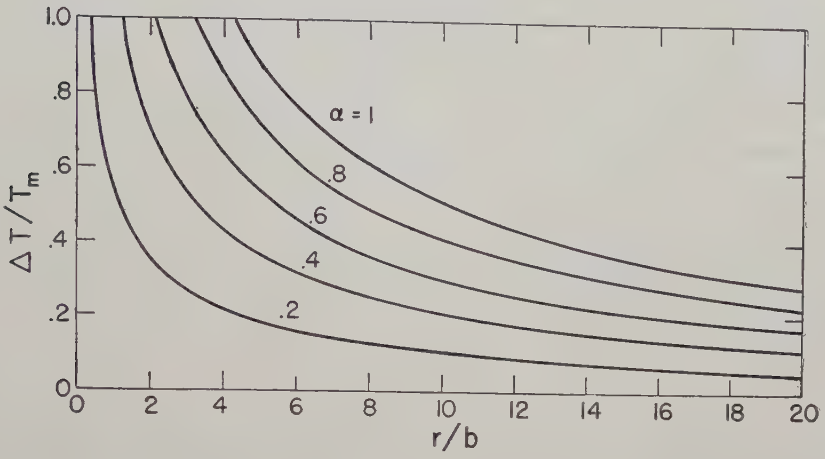

The relative undercooling, $\Delta T\ T_{\rm m}$, necessary to keep a dislocation ring of radius r atoms from shrinking ($T_{\rm m}$=melting temperature).

§ 3. RATE OF DISLOCATION CLIMBING

It was noted earlier that Frank's mechanism for striation formation (Frank 1956 a) requires that the dislocation loops, once formed behind the interface, must be able to climb towards the moving interface at such a rate that they can catch up with it. Therefore, we want now to consider the climb rate of the dislocations.

To simplify the problem we shall consider a crystal at a constant temperature, T, with a constant excess concentration, $c-c_0$, of vacancies present. In the crystal there may be a straight dislocation line which forms a perfect sink for vacancies. This last condition may perhaps not be satisfied for dislocations with high jog energies and hence a low concentration of thermal jogs. However, if the diffusion rate along the dislocation in its immediate neighbourhood is greatly enhanced, even a small number of jogs will be able to maintain the concentration of vacancies in thermal equilibrium all along the dislocation line. Furthermore, we are mainly interested in obtaining the fastest rate a dislocation could possibly climb; thus, we may neglect the problem of jog formation which could only slow down the climb process. We assume therefore that the concentration of vacancies at the dislocation will be kept in thermal equilibrium, c_0, and that the excess concentration will anneal out there. There are two reasons why vacancies diffuse to the dislocation line: (i) there is a chemical force due to the concentration gradient directed towards the line sink and (ii) the dislocation line attracts vacancies due to an elastic interaction (Friedel 1956 b). However, since the elastic interaction energy is proportional to

r^{-2}, the attractive force falls off rapidly with distance. As will be shown in Appendix I, in most cases the elastic interaction is too small to effect the steady-state climb rate.

From the formulation of the physical problem it is obvious that the dislocation will reach a steady state where it climbs with constant velocity. If we neglect the elastic attractive force an exact solution can be obtained (Jacob 1956) which is given in Appendix II. In order to gain a better understanding of how seriously our simplifying assumptions affect the final result we will derive the magnitude of this velocity by a simple physical argument, the result differing from the exact solution only by a numerical factor.

The dislocation will drain the surrounding region from its excess-vacancy concentration, $c-c_0$. After a radius r_0 has been drained, the number m of vacancies having arrived at the dislocation per atomic distance b are

$$m=\pi\frac{r_0^2}{\mathbf{b}^2}(c-c_0). \qquad (12)$$

After m vacancies have arrived per atomic distance b on the dislocation line the distance it has climbed will be

$$l=m\mathbf{b}. \qquad (13)$$

If $l=r_0$, the dislocation will essentially have climbed out of the region exhausted of vacancies and moved into a region which has not yet been drained. Hence from eqns. (12) and (13) we obtain as the radius of the drained region

$$r_0\approx\frac{\mathbf{b}}{\pi(c-c_0)}. \qquad (14)$$

The steady state velocity of climbing v_0 will now essentially be determined by the time t_0 it takes to drain an area of radius r_0 and will be of the order of $v_0=r_0/t_0$. If the dislocation tends to move much faster insufficient vacancies diffuse to it to maintain the higher rate, and if it tends to move much slower the vacancies which arrive would push it ahead faster. Now, in the time t a vacancy can move over a distance $x=(D_\mathrm{V}t)^{1/2}$, where D_V is the diffusion coefficient for vacancies. Hence the radius r_0 which is effectively drained of vacancies will be smaller but of the order of magnitude $r_0\approx(D_\mathrm{V}t_0)^{1/2}$. By use of eqn. (14) we obtained then

$$v_0\approx\frac{r_0}{t_0}=\frac{\pi D_\mathrm{V}(c-c_0)}{\mathbf{b}}. \qquad (15)$$

The exact solution in Appendix II shows that the right side of eqn. (15) must be multiplied by a numerical factor of $f=0{\cdot}2-0{\cdot}1$. If we further notice that the coefficient for self-diffusion is given by $D=c_0D_\mathrm{V}$ (assuming a vacancy mechanism for self-diffusion) we obtain finally

$$v_0\approx0{\cdot}5\frac{D}{\mathbf{b}}\left(\frac{c}{c_0}-1\right). \qquad (16)$$

We must keep in mind that eqn. (16) has been derived for straight dislocation lines. It will therefore give a reliable result only if the radius of curvature of the dislocation line is larger than the radius r_0 of the drained region of eqn. (14). It can be shown that the climbing rate of a dislocation ring with radius r much smaller than r_0 will be smaller than v_0 if we neglect the action of the attractive potential. However, for much smaller r, the attraction of vacancies to the dislocation line becomes important, but we would not expect v_0 to be very different from that already calculated. An exact solution for an expanding ring would be very complicated and no attempt has been made to calculate the climbing rate in this case.

If we use eqn. (16), we see that a dislocation ring of 10 atoms radius is generally climbing, at its equilibrium temperature, towards the interface at a rate slower than a typical rate of advance of the interface (10^{-2}–10^{-3} cm/sec). However, a dislocation of 15 atoms radius is climbing, at its equilibrium temperature, at a rate which is equivalent to the rate of advance of the interface.

§ 4. FORMATION OF STRIATIONS

1. A critical test of the origin of striations by vacancy collapse is to grow crystals under an ambient temperature so high that the critical supersaturation for the growth of dislocation rings is never reached. In this laboratory, crystals of Pb and Sn were grown in a horizontal crucible in an ambient temperature maintained at 20°C below the melting point. These crystals exhibited a fully developed striation type sub-structure. This sub-structure could be seen on the outer surfaces of etched crystals and on etched sections perpendicular to the growth axis. Since in these experiments $\Delta T/T_{\mathrm{m}} \leqslant 0{\cdot}04$, the radius of a ring which can expand by climbing would have to be at least $35\mathbf{b}$ in Pb and $85\mathbf{b}$ in Sn. It seems safe to say that rings of this size cannot be formed by spontaneous nucleation. Hence, we may conclude that collapsing vacancy discs are not responsible for striation formation.

Other objections to Frank's model (1956 a) can be made by considering the experiments of Teghtsoonian and Chalmers (1951, 1952). From the calculations of $\Delta T/T_{\mathrm{m}}$ necessary for a dislocation ring of 10 or 15 atoms radius to grow, we can see that the loops must nucleate several centimetres behind the solid–liquid interface. If we denote this value of $\Delta T/T_{\mathrm{m}}$ by $(\Delta T/T_{\mathrm{m}})_{\mathrm{c}}$ and the temperature gradient in the solid as G_{s}(°C/cm), then the distance, L, behind the interface at which the loops nucleate is given by $L \geqslant (\Delta T/T_{\mathrm{m}})_{\mathrm{c}}(T_{\mathrm{m}}/G_{\mathrm{s}})$. If we assume, for the moment, that Frank's (1956 a) model is correct and that all the vacancies collapse to form dislocations in lineage arrays, the angular misorientation, θ, between the striations at L cm from the beginning of the crystal (L is the incubation distance), is given by $tg\,\theta = c$. Thus, for reasonable values of $G_{\mathrm{s}} = 15$°C/cm and 30°C/cm for Pb and Cu respectively and for $c \approx 10^{-4}$ we see that the incubation distance for striation formation should be about 5–10 cm with a misorientation of about 10^{-2} degrees. However, the incubation distance is observed to be less than about 1 cm at high growth rates and the misorientation is observed to be about 1 degree.

2. We should now consider if a loop, once formed in the crystal, can catch up with the moving interface. As we see from table 2, a dislocation ring of 10 atoms radius will climb, at its equilibrium temperature, at a rate slower than the rate of advance of the interface and thus will be left behind.

However, a dislocation of 15 atoms radius is climbing at a rate which is equivalent to the rate of advance of the interface. If the initial loop size is 15 atoms radius there is some possibility that the loops will grow to a higher temperature if the interface is moving slowly. Whether it will climb close enough to the interface to be pulled into it by image forces must be decided.

If we write the diffusion coefficient in the form $D=D_0 \exp(-U_{\mathrm{d}}/Rt)$ the climbing velocity v_0 of eqn. (16) can be put in the form

$$v_0=\frac{0{\cdot}5D_0}{\mathbf{b}}\exp\left(-\frac{U_{\mathrm{d}}}{RT}\right)\left[\exp\left(\frac{U_{\mathrm{f}}}{R}\left(\frac{1}{T_{\mathrm{m}}}-\frac{1}{T}\right)\right)-1\right] \quad . \quad . \quad (17)$$

and using the empirical relations $U_{\mathrm{d}} \approx 39T_{\mathrm{m}}$, $U_{\mathrm{f}} \approx \frac{1}{2}U_{\mathrm{d}}$ (Birchendal 1951), the reduced velocity $V=v_0\mathbf{b}/D_0$ is plotted *vs.* T_{m}/T in fig. 4. We see that there is a maximum in V at $\Delta T/T_{\mathrm{m}} \approx 0{\cdot}1$. The climbing velocity vanishes for small T because there the vacancies become immobile and it also vanishes at the melting point, T_{m}, because there the supersaturation disappears. For $\Delta T/T_{\mathrm{m}} \leqslant 10^{-2}$ the velocity is practically linear with temperature.

Before a dislocation line can experience a significant influence of the image force at the solid–liquid interface it must move to, at least, a distance of 10^{-2} cm from the interface. Therefore, we are interested in v_0 at this point. With $G_{\mathrm{s}}=15$°c/cm and 30°c/cm for Pb and Cu respectively, $\Delta T/T_{\mathrm{m}}$ at this point is given by $\Delta T/T_{\mathrm{m}}=10^{-2}\,G_{\mathrm{s}}/T_{\mathrm{m}} \approx 2{\cdot}5\times10^{-4}$ for both these metals. Thus, at this point behind the interface the climb rate is of the order of 10^{-4}–10^{-5} cm sec and hence is about two orders of magnitude smaller than the conventional freezing rates. One must then conclude that the dislocations cannot catch up to the interface but can only trail behind it at a distance such that v_0 equals the freezing rate. From fig. 4, we see that this occurs at $\Delta T/T_{\mathrm{m}} \approx 10^{-2}$ which corresponds to a distance of about 0·5 cm from the interface. These calculations neglect any effect that thermal stresses may have upon the climb rate.

3. We have shown by various arguments that striations cannot be formed from collapsed vacancy discs. However, it is still possible that a number of independent dislocation loops may be produced by climb towards the interface in a manner similar to that suggested by Frank (1956 a). Let us consider this modified picture and calculate the upper limits to the number of dislocations introduced into the crystal in this manner. We will continue to assume that no other vacancy sinks are present in the crystal. Considering loops moving with the interface at a value of $\Delta T/T_{\mathrm{m}}=10^{-2}$, from eqn. (10) the minimum radius of the leading edge of the loop, r, may be determined to be about 10^4 atoms. From eqns. (8) and (9), the vacancy

excess is 10^{-5}; thus, the maximum number of elongated loops of width $2r$ in the crystal at the position corresponding to $\Delta T/T_m = 10^{-2}$, $\rho_{\max}$ is given by

$$\rho_{\max} = \frac{c - c_0}{2r\mathbf{b}} \quad . \quad . \quad . \quad . \quad . \quad . \quad . \quad . \quad . \qquad (18)$$

Fig. 4

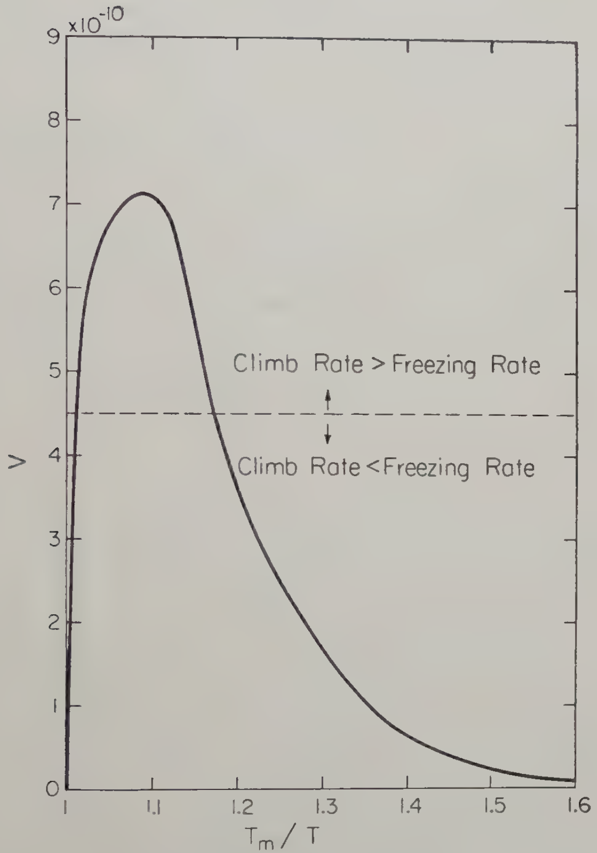

The reduced velocity of climb, V, as a function of T_m/T ($V = v_0 \mathbf{b}/D_0$ where v_0 = climb rate, $\mathbf{b}$ = Burgers vector and D_0 = diffusion constant).

which gives $\rho_{\max} \approx 10^6\,\mathrm{cm}^{-2}$. From this calculation we can see that, if no other vacancy sinks are present in the crystal and if the dislocation loops form at a value of $(\Delta T/T_m)_c$ where the climb rate is greater than the rate of interface advance, then a relatively large number of dislocation loops will form and trail the interface at a distance such that the climb rate is equal to the rate of interface advance. From Dash's (1958) work on dislocation-free Si crystals it would appear that $(\Delta T/T_m)_c$ is too large to allow the necessary climb rates.

4. It has been shown experimentally and theoretically that the 'vacancy disc mechanism' cannot account for the striation-type sub-structure, so the cause of striation formation is still unknown. It has been suggested that they most likely form from the dislocation lines grown into the crystal at microsegregation boundaries (Friedel 1956 a, Tiller 1958). The density of these dislocations is of the order of 10^5–10^8 lines/cm^2, which is sufficient to produce the striation arrays.

Evidence of these dislocation lines have been observed by etch pit techniques, in Zn (Bŏcek and Kratochvil 1959, Damiano private communication). Aggregation of these dislocations into micro-arrays occurs behind the solid-liquid interface, the arrays close to the interface being an order of magnitude smaller than striations and increase in size as the distance from the interface increases (Damiano, private communication).

A driving force for the growth of micro-arrays into striations is given by the strain energy of the system since the energy of the crystal containing a fixed number of dislocations arranged in small-angle cell boundaries decreases as the angle of the boundary increases. The limiting size of the striations would then be given by the distance a vacancy can diffuse to cause this rearrangement before the mobility drops to too low a value. This model gives the correct order of size for the striations (Frank 1956 a); however, a more detailed picture for striation formation is necessary before the model can be substantiated.

§ 5. The Influence of Other Dislocations

In the preceding sections we have always assumed that, except for the dislocations formed by vacancy condensation, there are no other sinks for vacancies. However, as just discussed, there will generally be other dislocations grown in either by growth accidents or by the micro-segregation of impurities. Since these dislocations will eat up part of the excess vacancy concentration, the number of vacancies frozen-in at the interface will never be available for dislocation ring formation. No attempt will be made to discuss the annealing of vacancies in general and its complicated kinetics (Kimura *et al.* 1959). We want only to estimate how many of the vacancies could possibly anneal out at the dislocations already present. For this purpose we assume again that a dislocation line forms a perfect sink for vacancies. This assumption may not be valid for metals in which the jog energy is high, i.e. in f.c.c. metals with low stacking fault energies. Specifically we wish to estimate how these grown-in dislocations affect the nucleation of dislocation rings in order to answer the following questions: (i) at what relative undercooling, $(\Delta T/T_{\mathrm{m}})_{\mathrm{c}}$, can dislocation rings grow as a function of the grown-in dislocation concentration and cooling rate, (ii) how many rings of a given area can be produced from the excess vacancies and what would be the resulting dislocation density from this source, (iii) if the rings should grow to form a network what would be the dislocation density?

It is possible to derive a differential equation for the actual vacancy concentration as a function of temperature, cooling rate, Q, and grown-in dislocation concentration, ρ_0, as parameters by considering the climb rate of these dislocations. However, if one wishes to study the solution as a function of these parameters, very tedious numerical integrations are necessary. Therefore, we calculate the excess vacancy concentration as a function of temperature by the following approximate method.

We consider the continuous cooling as being approximated by a series of sudden quenches over small temperature intervals, ΔT_{i}, with holding times of Δt_{i} at each temperature. The cooling rate will then be given by $Q=\Delta T_{\mathrm{i}}/\Delta t_{\mathrm{i}}$. In the time intervals Δt_{i} the area x_{i}^2 around a dislocation line drained of excess vacancies is of the order $x_{\mathrm{i}}^2=D_{\mathrm{v}}\Delta t_{\mathrm{i}}$. Let us now call the concentration of vacancies in thermal equilibrium after the ith quenching step c_{i} (c_{i} is identical with c_0 from eqn. 8) and the actual concentration p_{i}. Let us assume that the vacancies are uniformly distributed. If we have now ρ_0 grown-in dislocation lines/cm^2 they will drain an area $\rho_0 x_{\mathrm{i}}^2$ per unit area in the time Δt_{i} from the excess concentration $(p_{\mathrm{i}}-c_{\mathrm{i}})$. If we start with the equilibrium concentration c_0 at temperature T_0, then after the first quenching step the excess concentration will be

$$(p_1-c_1)=(c_0-c_1)(1-\rho_0 x_1^2) \quad . \quad . \quad . \qquad . \quad . \quad (19)$$

and for each successive step it follows that

$$(p_{\mathrm{i}}-c_{\mathrm{i}})=(p_{\mathrm{i}-1}-c_{\mathrm{i}})(1-\rho_0 x_{\mathrm{i}}^2). \quad . \quad . \quad . \quad . \quad . \quad . \quad (20)$$

By using the abbreviations $\xi_1=(1-\psi D_{\mathrm{v}}\Delta T_{\mathrm{i}}/T_{\mathrm{m}})$, $\psi=\rho_0 T_{\mathrm{m}}/Q$ and $\Delta c_{\mathrm{i}}=c_{\mathrm{i}-1}-c_{\mathrm{i}}$ it can be easily shown with the aid of the recursion relation (20) that

$$p_n-c_n=\sum_{m=1}^{n}\Delta C_{\mathrm{m}}\left[\prod_{i=m}^{n}\xi_{\mathrm{i}}\right] \quad . \quad . \quad . \quad . \quad . \quad . \quad . \quad (21)$$

after the cooling interval $\Delta T=\sum_{i=1}^{n}\Delta T_{\mathrm{i}}$.

The equilibrium vacancy concentration, c_n, and the vacancy excess, p_n-c_n, are plotted in fig. 5 as a function of $\Delta T/T_{\mathrm{m}}$ with ψ as a parameter assuming the activation energies used for eqn. (17). From these curves we see that the final vacancy concentration, in the absence of disc formation, depends strongly on the parameter ψ.

With the aid of fig. 5 we can now discuss the previously proposed questions:

(i) The growth of vacancy discs will take place when the supersaturation p_n/c_n reaches a critical value Z given in table 3. The undercooling $(\Delta T/T_{\mathrm{m}})_{\mathrm{c}}$ is easily found in fig. 5 by noting that $\log p_n$ has to exceed $\log c_n$ by a fixed amount $\log Z$. As it is readily seen $(\Delta T/T_{\mathrm{m}})_{\mathrm{c}}$ depends very weakly on the magnitude of Z except for very small values of ψ. We take therefore as a typical value $Z=10$, and have listed the resulting $(\Delta T/T_{\mathrm{m}})_{\mathrm{c}}$ in table 3 for the case $T_{\mathrm{m}}=1000$°K, $Q=0{\cdot}1$°C/sec and various values of ρ_0. This cooling rate is representative for careful crystal growth so we see that the presence of 10^5–10^6 grown-in dislocation lines per cm^2 more than doubles the necessary undercooling $(\Delta T/T_{\mathrm{m}})_{\mathrm{c}}$ for dislocation loop growth compared with a dislocation free crystal.

(ii) The maximum number, N/cm^3 of dislocation loops of area, A, which can grow after the crystal has been cooled below the critical ratio $(\Delta T/T_{\mathrm{m}})_{\mathrm{c}}$ is given by

$$N=(p_n-c_n)/\mathbf{b}A \quad . \quad . \quad . \quad . \quad . \quad . \quad . \quad . \quad . \quad . \quad (22)$$

Fig. 5

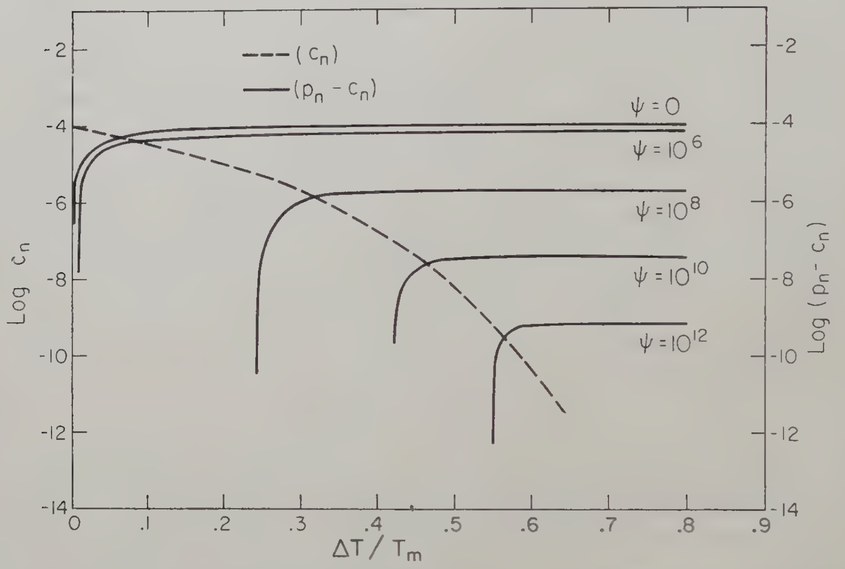

Plot used to determine the critical undercooling, $(\Delta T/T_{\mathrm{m}})_{\mathrm{c}}$ necessary to nucleate dislocation loops in the presence of ρ_0 grown-in dislocation lines/cm^2 as a function of the cooling rate, Q. (c_n = equilibrium vacancy concentration, $p_n - c_n$ = vacancy excess, $\psi = \rho_0 T_{\mathrm{m}}/Q$.)

where $\mathbf{b}$ is the Burgers vector. In order for these loops to act as Frank–Read sources during plastic deformation, the loops should be of the order of $1\,\mu$ in diameter. The number of rings for this radius $r=1\,\mu$ and also for $r=10\,\mu$ have been listed in table 3 and we see that an appreciable number of such sources could be produced during crystal growth over a wide range of grown-in dislocation densities. The resulting dislocation density ρ, is given by

$$\rho \approx (p_n-c_n)/\mathbf{b}r \quad . \quad . \quad . \quad . \quad . \quad . \quad . \quad . \quad . \quad . \quad (23)$$

and is also listed in table 3 (total dislocation density, $\rho^T=\rho_0+\rho$). Loops of radius $r=1\,\mu$ cannot be detected by etch-pit techniques, and for $r=10\,\mu$, ρ must be about $10^6\,\mathrm{cm}^{-2}$ to appear uniformly distributed by etch-pit observation. Thus, if ρ_0 is 10^4–$10^6\,\mathrm{cm}^{-2}$ a uniformly distributed array of dislocation etch-pits could not be due to dislocation loops formed by vacancy condensation.

Table 3

$T_{\mathrm{m}}=1000°\mathrm{K}$, $Q=0{\cdot}1°\mathrm{C/sec}$, $Z=10$

ρ_0 cm^{-2}	$\left(\frac{\Delta T}{T_{\mathrm{m}}}\right)_{\mathrm{c}}$	(ρ_n-c_n)	N cm^{-3}		ρ_{net} cm^{-2}	ρ		$X=(D_{\mathrm{v}}t)^{1/2}$		
			1 μ	10 μ		1 μ cm^{-2}	10 μ cm^{-2}	1 sec cm	10^2 sec cm	10^4 sec cm
0	0·20	10^{-4}	10^{11}	10^9	2×10^7	5×10^7	5×10^6	10^{-3}	10^{-2}	10^{-1}
10^2	0·22	8×10^{-5}	$6{\cdot}6\times10^{10}$	$6{\cdot}6\times10^8$	$1{\cdot}3\times10^7$	4×10^7	4×10^6	7×10^{-4}	7×10^{-3}	7×10^{-2}
10^4	0·40	$2{\cdot}5\times10^{-6}$	$2{\cdot}1\times10^9$	$2{\cdot}1\times10^7$	$1{\cdot}3\times10^4$	$1{\cdot}2\times10^6$	$1{\cdot}2\times10^5$	10^{-4}	10^{-3}	10^{-2}
10^6	0·52	5×10^{-8}	$4{\cdot}2\times10^7$	$4{\cdot}2\times10^5$	5	$2{\cdot}4\times10^4$	$2{\cdot}4\times10^3$	2×10^{-5}	2×10^{-4}	2×10^{-3}
10^8	0·60	8×10^{-10}	$6{\cdot}7\times10^5$	$6{\cdot}7\times10^3$	10^{-3}	$3{\cdot}8\times10^2$	38	$1{\cdot}7\times10^{-6}$	$1{\cdot}7\times10^{-5}$	$1{\cdot}7\times10^{-4}$

(iii) The loops can grow to a network, if their radius r grows to a size comparable with their spacing, i.e. if $N=1/r^3$. Thus the dislocation density, ρ_{net}, in a plane cut by the network is given by

$$\rho_{\mathrm{net}} \approx \frac{1}{r^2} \approx (p_n - c_n)^2/\mathbf{b}^2. \qquad (24)$$

For the particular case of $T_m = 1000°\mathrm{K}$ and $Q = 0{\cdot}1°\mathrm{C/sec}$, ρ_{net} is also tabulated in table 3 for various ρ_0.

From these considerations it is not possible to tell whether the dislocations found in crystals are due to vacancy condensation or due to other mechanisms. The only conclusion that can be reached is that if in slowly grown crystals, a dislocation density $\rho_0 \gtrsim 10^5\,\mathrm{cm}^{-2}$ of grown-in dislocations exists, then there are not enough vacancies left to form an appreciable network. However, with fast quenching rates from high temperatures the crystal can contain a large number of dislocation loops formed by vacancy collapse even when the crystal contains appreciable numbers of grown-in dislocations.

Finally, we want to discuss very briefly some experiments on highly perfect Si crystals. Dash (1958) has postulated that dislocation climb in the solid behind the advancing solid–liquid interface allows the dislocations to move to the outer surface of his crystals; thus leaving them dislocation free. However, as we have already shown, the climb rate is extremely slow relative to the rate of advance of the interface at small distances from the interface. Thus, this mechanism does not seem very likely to have produced the dislocation free crystals. It is much more likely that the dislocations were removed from his crystals due to the shape of the solid–liquid interface during a portion of the crystal growth (interface convex to liquid).

APPENDIX I

ATTRACTION OF VACANCIES TO DISLOCATIONS DUE TO ELASTIC INTERACTION

The interaction potential of vacancies with dislocations is (Friedel 1956 b)

$$U = W\frac{b^2}{r^2} \qquad (\mathrm{A}\,1)$$

where W is the interaction constant, b the interatomic distance and r the distance from the dislocation line. Thus, the drift velocity v of vacancies towards the dislocation due to the interaction potential is

$$v = \frac{D}{kT}\frac{\partial U}{\partial r} = -\frac{2WDb^2}{kTr^3}. \qquad (\mathrm{A}\,2)$$

The time t_0 it takes the vacancies within a radius r_0 to anneal out at the dislocation, due to the drift velocity in the energy gradient, is then easily shown to be

$$t_0 = \frac{kTr_0^4}{8WDb^2}. \qquad (\mathrm{A}\,3)$$

From eqn. (14) we use $r_0 = b/\pi\Delta C$ as the radius of the region which can be drained by the dislocation before it moves out of the drained region.

By the same argument as used in the text we obtain then as the climbing velocity

$$v_0' = \frac{r_0}{t_0} = 8\pi^3 \frac{WD\Delta C^3}{bkT} . \qquad (\text{A } 4)$$

This velocity v_0' would be obtained if vacancies would move towards the dislocation exclusively due to the action of the elastic attraction potential. With typical values $W \leqslant 0{\cdot}5$ ev, $T \sim 1000$°K and $\Delta C \leqslant 10^{-3}$ this velocity is always several orders of magnitude smaller than the steady-state velocity obtained from eqn. (15) due to chemical diffusion.

That we can neglect the elastic attraction of vacancies in the climbing process can also be seen by the following argument: The average chemical potential gradient during the steady state climbing at temperature T is of the order of μ/r_0 where μ is the chemical potential of vacancies quenched-in at the temperature T_{m}. If the sample is cooled by a temperature interval ΔT we obtain

$$\frac{\mu}{r_0} = \frac{\pi U_{\mathrm{f}} \Delta T \Delta C}{b T_{\mathrm{m}}} . \qquad (\text{A } 5)$$

(U_{f} = energy of vacancy formation, ΔC = excess concentration over thermal equilibrium value, b = atomic distance). The elastic energy gradient is however from eqn. (A 1)

$$\frac{\partial U}{\partial r} = -\frac{2Wb^2}{r^3} . \qquad (\text{A } 6)$$

By equating (A 5) and (A 6) we obtain the radius r_1 at which both gradients have the same value. It can be shown that in all cases r_1 is less than a few percent of r_0. Hence the attraction potential can be neglected over the greatest part of the diffusion path. In typical quenching experiments r_1 is of the order of $10b$ or less. The presence of the elastic attraction can then be accounted for by replacing the dislocation by a sink of effective radius $r_1 \approx 10b$.

APPENDIX II

DISLOCATION CLIMB RATE

We assume a straight dislocation line lying in the z-axis of a cartesian system (x, y, z). It acts as a sink for vacancies and may move with constant velocity v_0 in the x direction. We also assume that a steady state is reached in the coordinate system (ξ, y, z) moving with the dislocation.

If r is the distance from the dislocation line, D_{v} is the diffusion coefficient for vacancies and c_{m} the concentration of vacancies at infinity, the concentration of vacancies at the point (r, ξ) is given by Rosenthal (1946) to be

$$c_{\mathrm{m}} - c = A \exp\left(-\frac{v_0 \xi}{2D}\right) K_0\left(\frac{v_0 r}{2D_{\mathrm{v}}}\right), \qquad (\text{A } 7)$$

where K_0 is the modified Bessel function of second kind, zero order.

The constant A will be determined as follows: As discussed in Appendix I, we use $r_s = 10b$ as sink radius for the dislocation. The velocity v_0 of the dislocation line is proportional to the flux of vacancies over a cylinder of radius r_s around the dislocation line, or

$$-2\pi D_V r_s \left(\frac{\partial c}{\partial r}\right)_{r=r_s} = v_0 b. \quad . \quad . \quad . \quad . \quad . \quad . \quad . \quad (A\,8)$$

If $r_s \ll D_V/v_0$ we obtain then

$$c_m - c = \frac{v_0 b}{2\pi D_V} \exp\left(-\frac{v_0 \xi}{2D_V}\right) K_0\left(\frac{v_0 r}{2D_V}\right). \quad . \quad . \quad . \quad (A\,9)$$

Now we have the additional condition that at $r = r_s$ the concentration c has its thermal equilibrium value c_0. From eqn. (A 9) we obtain, then, an equation to determine the velocity v_0 as a function of c_m and c_0 which leads, for $r_s \ll D_V/v_0$ to

$$v_0 = \frac{2\pi}{\ln(4D_V/\vartheta v_0 r_s)} \cdot \frac{D_V(c_m - c_0)}{b}. \quad . \quad . \quad . \quad . \quad (A\,10)$$

If we compare the exact result (A 10) with the velocity given by eqn. (15) we find that eqn. (15) must be multiplied by a factor $f = 2/\ln(4D_V/\vartheta v_0 r_s)$, where ϑ is Euler's constant ($\vartheta = 1{\cdot}78$). Since all variables in f give only a logarithmic dependence we may take average values for D_V and v_0 ($D_V \approx 10^{-5}$ cm^2/sec, $r_s \approx 3 \times 10^{-7}$, $v_0 = 10^{-3}$ cm/sec) and obtain $f \approx 0{\cdot}2$ to $0{\cdot}1$.

REFERENCES

ATWATER, H., and CHALMERS, B., 1957, *Canad. J. Phys.*, **35,** 208.

BILLIG, E., 1956, *Proc. roy. Soc.* A, **235,** 37.

BIRCHENDAL, C. E., 1951, *Atom Movements* (Cleveland: American Society of Metals).

BŎCEK, M., and KRATOCHVIL, P., 1959, *Czech. J. Phys.* (to be published).

BROOKS, H., 1952, *Metal Interfaces* (Cleveland: American Society of Metals).

DASH, W. C., 1958, *Growth and Perfection of Crystals* (New York: John Wiley and Sons, Inc.).

FRANK, F. C., 1950, *Pittsburgh Symposium on the Plastic Deformation of Crystalline Solids* (O.N.R.), p. 150; 1956 a, *Deformation and Flow of Solids Madrid Conference* (Berlin: Springer-Verlag); 1956 b, *Dislocations and Mechanical Properties of Crystals* (New York: John Wiley and Sons, Inc.), p. 514.

FRANZ, H., and KROENER, E., 1955, *Z. Metallk.*, **46,** 639.

FRIEDEL, J., 1956 a, *Les Dislocation* (Paris: Gautheir-Villars), p. 130; 1956 b, *Dislocations and Mechanical Properties of Crystals* (J. Fisher, editor) (New York: John Wiley and Sons, Inc.).

GOSS, A. J., BENSON, K. E., and PFANN, W. G., 1956, *Acta Met.*, **4,** 332.

HIRSCH, P. B., SILCOX, J., SMALLMAN, R. E., and WESTMACOTT, K. H., 1958, *Phil. Mag.*, **3,** 897.

HIRSCH, P. B., and SILCOX, J., 1958, *Growth and Perfection of Crystals* (New York: John Wiley and Sons, Inc.).

JACOB, M., 1956, *Heat Transfer*, **1** (New York: John Wiley and Sons; Inc.), p. 348.

Kimura, H., Maddin, R., and Kuhlmann-Wilsdorf, D., 1959, *Acta Met.*, **7,** 154.

Kuhlmann-Wilsdorf, D., 1958, *Phil. Mag.*, **3,** 125.

Rosenthal, D., 1946, *Trans. Amer. Soc. mech. Engrs*, **68,** 849.

Seitz, F., 1950, *Phys. Rev.*, **79,** 890.

Teghtsoonian, E., and Chalmers, B., 1951, *Canad. J. Phys.*, **29,** 370; 1952, *Ibid.*, **30,** 388.

Tiller, W. A., 1958, *J. appl. Phys.*, **29,** 611.

Wagner, R. S., 1958, *J. appl. Phys.*, **29,** 1679.

An Approximate Correlation between the Electron Fermi Energy and Work Function of a Metal†

By J. H. O. Varley
Atomic Energy Research Establishment, Harwell, Didcot, Berks.

[Received August 17, 1959]

Abstract

The object of this paper is to estimate, semi-empirically, the Fermi energy of the free electrons in a metal and to indicate why a simple correlation may be expected between this quantity and the electronic work function. Such a straightforward correlation is found to hold approximately for most metals in Groups I to IV of the periodic table.

§ 1. Introduction

The theoretical considerations of Wigner and Seitz (1933, 1934) on the cohesive energies of the alkali metals suggest that the energies of the electrons in the metal may be described to a fair approximation in the following manner. The valence electrons move under the influence of the periodic electrostatic field of the ion cores and also under their mutual interactions. In accordance with Fermi–Dirac statistics the electrons occupy a band of energy levels, based on a ground state energy, E_0, up to a maximum energy, $(E_0+\zeta_0)$, at absolute zero. E_0 is the lowest energy, potential plus minimum kinetic energy, which a valence electron can have in the field of a single positive ion core within the metal lattice, with the appropriate boundary conditions. ζ_0 is the *additional* kinetic energy of the most energetic electrons, since, by the requirement of Pauli's exclusion principle, all electrons cannot occupy the same quantum state. ζ_0 may be assumed to have the same value as for free electrons moving in a bounded region of constant potential V_0, outside which V is zero and within which the electron density is the same as in the metal under consideration.

In this wave mechanical treatment the mutual electron interactions give a further large positive contribution to the total energy not already accounted for in E_0. This is offset by a negative contribution arising from the exchange interactions between electrons with like spin and different wave numbers. Wigner and Seitz (1933, 1934) calculated the positive term on the assumption of a uniform distribution of negative charge and this was corrected to allow for the correlated motion of the electrons (Wigner 1934). The effect of this correlation and also of the exchange energy is to tend to keep the electrons away from each other and thus to reduce the mutual electrostatic interactions of a uniform electron distribution. The calculations indicate that together, for free electrons, these three contributions almost cancel one another, leaving only a small net interaction energy, Q_i, of the order of 10% of the average energy of an electron in the metal relative to an electron at rest in free space as the energy zero.

---

† Communicated by the Author.

The mean energy of an electron in the metal is thus approximately

$$E = E_0 + \tfrac{3}{5}\zeta_0$$

where the factor $\frac{3}{5}$ is the averaging factor relating the mean additional kinetic energy of a free electron distribution to the maximum additional kinetic energy, ζ_0.

In the absence of any double layer at the metal surface least work is required to remove an electron from inside the metal to rest at infinity if an electron of maximum energy is ejected. This will require an amount of work of the order $-(E_0+\zeta_0)$ at absolute zero if there is no relaxation of the electronic charge distribution remaining within the metal. There will in fact be some relaxation of the electrons within the metal when one is ejected and therefore the energy required to remove one electron will be less than $-(E_0+\zeta_0)$ by the amount of this relaxation energy $(-\Delta Q_i)$ say.

Consider a ring of metal which is cut to create fresh surface. At the instant of separation of the two surfaces the electrons associated with the new surface ions have their potential energy increased (less negative) to approximately half the numerical value which was obtained before separation. This is because the electrons instantaneously associated with the surface ions are no longer completely surrounded by positive ions. The kinetic energy of the electrons in these surface states will, by the virial theorem, be reduced by a factor of approximately one half also, so that the numerical magnitude of the total mean energy of an electron in a surface state will be of the order of one half that of the mean energy of an electron in the interior of the metal. Similarly, the magnitudes of the maximum electron energies in the interior $(E_0+\zeta_0)$ and in the surface $(E_0+\zeta_0)_s$ will be in the approximate ratio of two to one.

Electrons will therefore move from the surface atomic cells towards the interior of the metal setting up a double layer of charge, with the positive layer on the outside. Equilibrium will be established when the work done to move an electron against the double layer field from the surface to the interior of the metal is equal and opposite to the decrease in energy $(E_0+\zeta_0)-(E_0+\zeta_0)_s$. The work, χ, required to remove an electron from anywhere in the system, interior or surface, to infinity is now the same. Thus to remove an electron from the interior requires an amount of work

$$\chi = -(E_0+\zeta_0) - 4\pi ne^2x \quad . \quad . \quad . \quad . \quad . \quad . \quad . \quad . \quad (1)$$

where $4\pi ne^2x$ is the work gained in passing through the double layer of strength n electrons/sq. cm and thickness x. But

$$4\pi ne^2x + (E_0+\zeta_0) - (E_0+\zeta_0)_s = 0. \quad . \quad . \quad . \quad . \quad . \quad . \quad (2)$$

Therefore χ in (1) also equals $(E_0+\zeta_0)_s$ which is the work required to remove an electron from the surface layer.

The work required to remove an electron at constant temperature and pressure from the system is a measure of the change in the free energy of the system per electron removed, which is the negative of the thermodynamic potential of the electrons. At equilibrium therefore the thermodynamic potential of the electrons in the metal is everywhere the same, as indeed it must be. For other and further discussions of electronic work functions reference may be made to the review article by Herring and Nichols (1949) and also the book by Seitz (1940).

The foregoing argument suggests that the work function χ should be of the order of $-\frac{1}{2}(E_0+\zeta_0)$, if the mutual interaction terms within the electron distribution of the metal can be neglected.

In the next section semi-empirical calculations of the Fermi energy $\zeta=(E_0+\zeta_0)$, are made using as many experimental facts as possible, and assuming that the resultant electron–electron interaction energy can in fact be neglected within the metal, but not between valence electrons in polyvalent atoms. The arguments used in computing ζ for elements with more than one valence electron have been set down before by the author (Varley 1954) but are reproduced here for completeness.

§ 2. EXPRESSIONS FOR THE FERMI ENERGY OF ELECTRONS IN METALS

2.1. *Monovalent Metals*

The average energy of an electron in the metal, relative to the energy zero of an electron at rest in free space, is taken to be $(E_0+\frac{3}{5}\zeta_0)$. The electrons within the metal can be brought to this zero energy state by vaporizing the solid and then ionizing the atoms. It follows that

$$E_0+\tfrac{3}{5}\zeta_0=-(\Lambda+I_1) \quad . \quad . \quad . \quad . \quad . \quad . \quad . \quad (3)$$

where Λ is the latent heat of vaporization per atom at absolute zero and I_1 is the first ionization energy of the free atom.

Thus $E_0=-(\Lambda+I_1+\frac{3}{5}\zeta_0)$,

$$\zeta_0=\frac{h^2}{8m}\left(\frac{3n}{\pi}\right)^{2/3},$$

where n is the number of free electrons per unit volume, h is Planck's constant and m is the electronic mass. The Fermi energy for monovalent metals is thus:

$$\zeta=(E_0+\zeta_0)=-\left[\Lambda+I_1-\frac{h^2}{20m}\left(\frac{3n}{\pi}\right)^{2/3}\right]. \quad . \quad . \quad . \quad (4)$$

2.2. *Polyvalent Metals of Groups II, III and IV*

In a polyvalent metal the exchange interactions between electrons of like spin approximately cancel out the repulsive, correlated Coulomb interactions. This effect of the exchange forces is lost when the metal is vaporized into free atoms and in the latter the repulsive electrostatic forces predominate. The exchange forces tend to keep electrons of like spin apart so that most of the exchange energy may be regarded as arising between electrons which are in different atomic cells. Therefore the energy per atom required to vaporize a polyvalent metal into free atoms may be considered to result from (*a*) changing the energy of the Z valency electrons associated with the ion core of each atom and (*b*) overcoming the exchange forces which produce an effective attraction between adjacent atomic cells.

The mean energy of an electron in the metal is $(E_0+\frac{3}{5}\zeta_0)$; its energy in the free atom is

$$-\frac{1}{Z}\sum_{i=1}^{Z} I_i$$

where I_i is the ionization energy of the ith valency electron and the sum is over the Z valency electrons. The change in energy on evaporation is thus:

$$-\frac{1}{Z}\sum_{i=1}^{Z} I_i-(E_0+\tfrac{3}{5}\zeta_0).$$

The exchange interaction energy between electrons of like spin in different atomic cells of the metal is approximately the difference between the total interaction energy per electron in the metal and that in the free atom. The total mutual interaction energy per electron in the metal is taken to be zero. That in the free atom is

$$\left\{I_Z-\frac{1}{Z}\sum_{i=1}^{Z} I_i-\frac{Z-2}{Z}I_T\right\},$$

where I_Z is the ionization potential of the last valence electron and I_T is the energy to promote an electron from the s to the p state in the ionization spectrum M^{Z+}. The last term only occurs in elements of valency greater than 2.

The energy of vaporization per electron is Λ/Z, where Λ is the experimental heat of vaporization per atom, and this is therefore equal to

$$I_Z-\frac{Z-2}{Z}I_T-\frac{2}{Z}\sum_{i=1}^{Z} I_i-(E_0+\tfrac{3}{5}\zeta_0). \quad . \quad . \quad . \quad . \quad . \quad (5)$$

It follows that

$$\zeta=(E_0+\zeta_0)=-\frac{2}{Z}\sum_{i=1}^{Z} I_i+I_Z-\frac{Z-2}{Z}I_T-\frac{\Lambda}{Z}+\frac{h^2}{20m}\left(\frac{3n}{\pi}\right)^{2/3} \qquad (6)$$

for an element with Z free electrons per atom.

§ 3. Numerical Computations

Using data from standard references and published papers (*Handbook of Chemistry and Physics* 1957–8, Kubaschewski and Evans 1951) on ionization spectra and heats of vaporization, calculations of the Fermi energy, ζ, have been made for several metals in the first four groups of the periodic table. These calculated values, together with experimental values of the work function, χ (*Handbook of Chemistry and Physics* 1957–8) are set out in the table together with the ratio $(-\chi/\zeta)$ in the last column. It will be seen that in most cases this ratio is not too different from the value 0·5 suggested in the text.

Element	$-\zeta$	χ	$-\chi/\zeta$
Li	5·08	2·49	0·49
Na	5·01	2·28	0·46
K	4·45	2·24	0·50
Rb	4·34	2·09	0·48
Cs	4·06	1·81	0·45
Cu	8·38	4·5	0·54
Ag	8·33	4·73	0·57
Au	10·89	4·82	0·44
Be	6·88	3·9	0·57
Mg	5·50	3·68	0·67
Sr	5·78	2·74	0·47
Ba	5·72	2·5	0·44
Zn	6·22	4·0	0·64
Cd	6·54	4·07	0·62
Hg	7·85	4·5	0·57
Al	5·64	4·0	0·71
Ga	6·75	4·1	0·61
Tl	7·96	3·68	0·46
Ge	7·99	4·5	0·56
Sn	7·77	4·38	0·56
Pb	8·13	4·0	0·49

§ 4. CONCLUDING REMARKS

An exact ratio of 0·5 for $(-\chi/\zeta)$ is, of course, not to be expected for several reasons. There are many approximations in the calculations for the Fermi energy. For instance, it has been assumed that the energy to ionize an electron in a free monovalent atom gives a measure of the energy of that electron alone, whereas the electrons in the ion core will relax and their energies will be reduced when the valence electron leaves the atom.

Again, using the free electron value of ζ_0 is only approximately true, although soft x-ray spectra indicate that the true energy band widths are not very different from the free electron widths in several cases. However, differences are to be expected, especially in the case of the polyvalent elements in which the details of the energy bands are influenced by the periodic lattice potential (Brillouin zones) at the top of the Fermi distribution. Nevertheless, an approximate correlation between Fermi energy and work function seems to be indicated on the basis of these calculations and may possibly serve as a rough guide for other elements, such as the transition elements, in the periodic table.

References

Handbook of Chemistry and Physics, 1957–8 (Ohio: Chemical Rubber Publishing Co.).

Herring, C., and Nichols, M. H., 1949, *Rev. mod. Phys.*, **21,** 185.

Kubaschewski, O., and Evans, E. Ll., 1951, *Metallurgical Thermochemistry* (London: Butterworth-Springer).

Seitz, F., 1940, *The Modern Theory of Solids* (New York: McGraw-Hill Book Co. Inc.), p. 395.

Varley, J. H. O., 1954, *Phil. Mag.*, **45,** 887.

Wigner, E., 1934, *Phys. Rev.*, **46,** 1002.

Wigner, E., and Seitz, F., 1933, *Phys. Rev.*, **43,** 804; 1934, *Ibid.*, **46,** 507.

The Density of States in Lead†

By A. V. Gold‡
Division of Pure Physics, National Research Council, Ottawa, Canada

[Received August 11, 1959]

Abstract

Refinements of the curve of density of states $n(E)$ in lead, as deduced from the de Haas–van Alphen effect, are inferred from existing superconductivity and transport data on pure lead and on Pb–Tl and Pb–Bi alloys when these data are interpreted in terms of a simple 'inverse transition metal' model. $n(E)$ is found to have a maximum just below the Fermi level. It is suggested that the maximum might be accounted for by supposing the multiply-connected portion of the Fermi surface to split up into separate portions as the electron concentration is reduced; however, this particular interpretation does not seem to be compatible with a model of rigid bands.

A highly schematic curve of density of electronic states $n(E)$ *versus* energy E for lead has been inferred recently from an interpretation of the de Haas–van Alphen effect (Gold 1958; hereinafter referred to as I) and is shown in fig. 1. Also shown are the contributions from the various Brillouin zones; the curves have been drawn in a more or less parabolic fashion from the computed values of $n(E_0)$ at the Fermi level such that their areas give the number of electronic states within the various parts of the Fermi surface. In order to obtain a more detailed $n(E)$ curve for pure lead we shall examine first of all the effects of varying the electron concentration as inferred from existing data on alloys of lead with thallium and bismuth. Since thallium and bismuth occur on either side of lead in the same row of the periodic table, alloying with these particular metals should produce the least distortions in the band structure of pure lead.

The variation of the density of states $n(E_0)$ at the Fermi level with decreasing electron concentration can be obtained from the superconducting critical-field curves of Pb–Tl alloys; no suitable data are available for the Pb–Bi system. $n(E_0)$ is related to the electronic specific heat constant γ_{el} by

$$n(E_0)=1{\cdot}59\times10^{-12}(a^3/4)(3/2\pi^2k^2)\gamma_{\mathrm{el}} \text{ per ev per atom} \qquad (1)$$

(cf. Mott and Jones 1936, p. 179), where a is the lattice constant in cm and γ_{el} is given by

$$\gamma_{\mathrm{el}} \doteq 1/2\pi(H_0/T_c)^2 \text{ erg cm}^{-3}\text{ deg}^{-2}, \quad . \quad . \quad . \quad . \qquad (2)$$

---

† Communicated by the Author.

‡ National Research Laboratories Postdoctorate Fellow.

assuming the critical-field curves to be parabolic (Shoenberg 1952, Ch. III). The mean zero-field transition temperatures T_c have been interpolated from the results of Meissner *et al.* (1932) and the critical fields H_0 at the absolute zero have been extrapolated from the data of Schubnikow *et al.* (1936), taking the critical field to be the value at which magnetic flux begins to enter the specimen rapidly as the field is increased. The dependence of a on Tl concentration has been given by Tang and Pauling (1952) and the resulting variation of $n(E_0)$ deduced from (1) and (2) is shown in fig. 2 (a). Also shown is the value of $n(E_0)$ obtained by Decker *et al.* (1958) from the actual non-parabolic critical-field curve of pure lead; however, the data of Schubnikow *et al.* are insufficient to show up any significant departures from parabolicity for the alloys.

Fig. 1

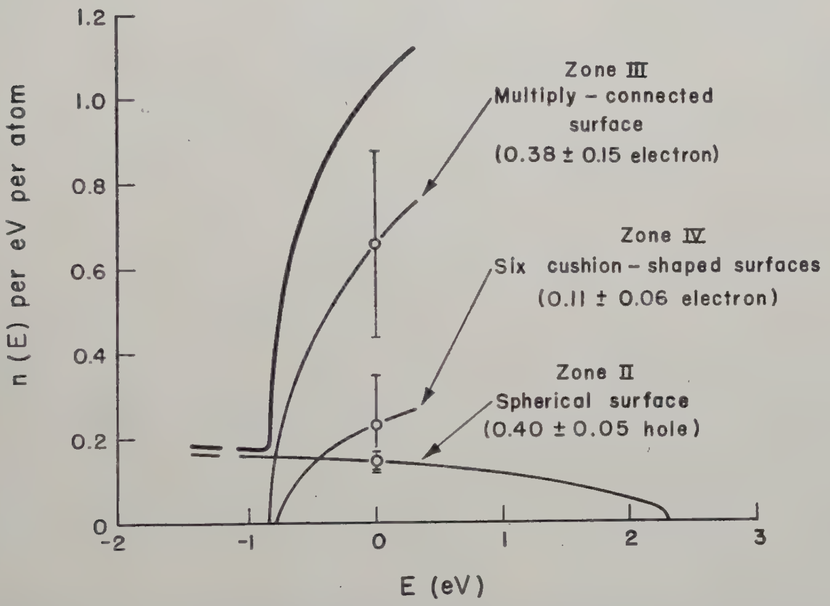

Schematic curve of density of states near the Fermi level as inferred from the de Haas–van Alphen effect (I). The energy is measured relative to the Fermi level.

While this interpretation of the superconductivity data is likely to be too naïve on account of the lack of a Meissner effect in the alloys, the curve of fig. 2 (a) nevertheless suggests that $n(E_0)$ drops rapidly from its value for pure lead, reaching some fairly constant value at about 15% Tl. It is worth noting that the γ_{el} values obtained by Stout and Guttman (1952) from the critical-field data on alloys of *tin* with up to 20% thallium show no such rapid variation, thus suggesting that the decrease found in the Pb–Tl system is indeed an electronic structure effect.

We can obtain further information about the variation of $n(E_0)$ on alloying from the temperature dependence of the resistivity, $\partial\rho/\partial T$, and from the absolute thermoelectric power S. In interpreting such data it is convenient to think of lead as a kind of 'inverse transition metal' since

Fig. 2

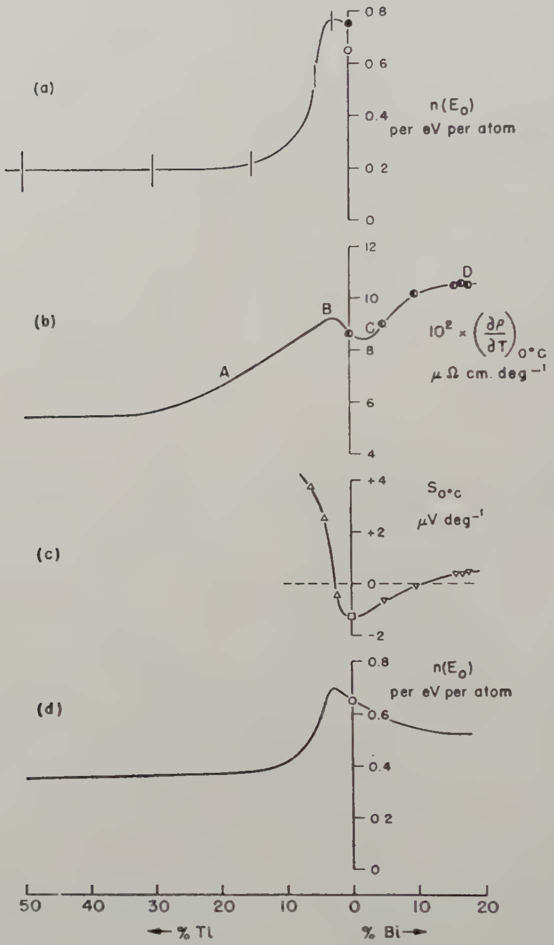

Variation with Tl and Bi concentration of (*a*) $n(E_0)$ from critical-field data, (*b*) $\partial\rho/\partial T$ at 0°C, (*c*) S at 0°C and (*d*) $n(E_0)$ as inferred from (*a*), (*b*) and (*c*). Curve (*a*) is from Meissner *et al.* (1932) and Schubnikow *et al.* (1936); the Pb–Tl portion of curve (*b*) is from Guertler and Schulze (1923) and Tammann and Rüdiger (1930) and is estimated to be reliable to about 2%. ●, Decker *et al.* (1958), assuming parabolic H_c vs. T curve; ○, Decker *et al.*, from actual non-parabolic H_c vs. T curve; ◐, ▽, Thomas and Evans (1933); △, Rolla (1915); □, Christian *et al.* (1958). The α-phase boundaries lie at 80% Tl and 18% Bi (cf. Hansen 1958), with ordering taking place at $PbTl_3$ (i.e. 75% Tl; Tang and Pauling 1952).

we see from fig. 1 that the rapidly varying contribution from the electrons to $n(E)$ is much greater than the slowly varying contribution from the holes. On the basis of such a model we should expect the major part of the conductivity to be due to the holes (cf. Mott and Jones 1936, p. 267); this has been confirmed experimentally by Borovik (1954) who has shown, on the basis of a two-band analysis of the galvanomagnetic effects, that the holes in fact account for between 85% and 90% of the total conductivity in pure lead. Thus, assuming the validity of the Mathiessen rule, we may write for the temperature dependence of resistivity (cf. Mott and Jones 1936, p. 301)

$$\frac{\partial\rho}{\partial T}=\frac{\partial\rho_T}{\partial T}=\frac{\partial}{\partial T}(m_{\mathrm{h}}^*/\mathcal{N}_{\mathrm{h}}e^2\tau_T)\propto\frac{n(E_0)}{\mathcal{N}_{\mathrm{h}}} \qquad . \quad . \quad . \quad . \quad (3)$$

where $\mathcal{N}_{\mathrm{h}}$ is the number of holes per cc; we have taken $1/\tau_T\propto Tn(E_0)$ and have assumed that the effective mass of the holes is not appreciably altered on alloying ($m_{\mathrm{h}}^*(\mathrm{Pb})=1{\cdot}0m_0$ from I). Turning now to the thermoelectric power, we have rather generally

$$S=-\frac{\pi^2k^2T}{3e}\left\{\frac{\partial\log\rho(E)}{\partial E}\right\}_0; \qquad . \quad . \quad . \quad . \quad . \quad (4)$$

for our model this reduces to (cf. Mott and Jones 1936, p. 313)

$$\begin{aligned}S&=-\frac{\pi^2k^2T}{3e}\frac{1}{n(E_0)}\left(\frac{\partial n(E)}{\partial E}\right)_0\\&=+2{\cdot}45T\frac{1}{n(E_0)}\left(\frac{\partial n(E)}{\partial E}\right)_0\mu\mathrm{v\,deg}^{-1}, \qquad . \quad . \quad . \quad (5)\end{aligned}$$

the energy being measured in ev.

The variation of $\partial\rho/\partial T$ at 0°c is given in fig. 2 (*b*); the Pb–Bi results are from Thomas and Evans (1933) while the Pb–Tl curve has been drawn from values of the temperature coefficient of resistance given by Guertler and Schulze (1923) and of the absolute resistivity given by Tammann and Rüdiger (1930) (the absolute resistivity measurements of Guertler and Schulze are fraught with systematic errors). As we move from left to right in fig. 2 (*b*) the number of holes in the second zone will be progressively reduced so that we should expect from (3) a smooth increase in $\partial\rho/\partial T$, modulated by $n(E_0)$. We therefore infer that $n(E_0)$ begins to increase from a roughly constant value near A, reaches a maximum near B and then falls through its value for pure lead, this decrease being offset near C by the effect of diminishing $\mathcal{N}_{\mathrm{h}}$; the flattening-off of the curve at D is probably due to an increasing contribution to the conductivity from the electrons so that (3) is no longer valid. Thus the behaviour of $\partial\rho/\partial T$ for the Pb–Tl series confirms qualitatively the scheme of fig. 2 (*a*) but it is difficult to draw any definite conclusions from the Pb–Bi results.

In fig. 2 (*c*) we show the variation of S at 0°c from Rolla (1915) and Thomas and Evans (1933), the relative values given by these authors having been converted into absolute values using the absolute value of S for pure lead given by Christian *et al.* (1958). Although the variation of

S with T for *pure* lead is approximately linear above about 100°K (Christian *et al.*), it is not exactly in accordance with (5) since the high-temperature results do not extrapolate to $S=0$ at $T=0$; this matter will be discussed later but for the present we shall take (5) to be approximately valid for our discussion of the alloys. While the effect of impurity scattering on S is not well understood we shall nevertheless suppose it to be small by comparison with the rapid rise in S with increasing Tl concentration. Assuming then a quasi rigid-band model for the alloys it seems reasonable from (5) to associate the large positive S at 6% Tl with a sharply rising $n(E_0)$ and the value $S=0$ at about 2·5% Tl with a maximum in $n(E_0)$; both inferences are in qualitative agreement with fig. 2 (*a*). The negative S near pure lead implies a falling $n(E_0)$ while the subsequent slow rise in S with increasing Bi concentration suggests that $n(E_0)$ begins to flatten-off somewhat; in view of the inapplicability of our model when the electronic contribution to the conductivity becomes appreciable, the rising $n(E_0)$ beyond 11% Bi as suggested by (4) must be viewed with some scepticism.

We are now in a position to give, in fig. 2 (*d*), an approximate curve of the variation of $n(E_0)$ with Tl and Bi concentration. For pure lead we have taken the value from Decker *et al.* as being the most reliable. Although the curve of fig. 2 (*a*) suggests a total drop in $n(E_0)$ of roughly 60% with the addition of about 15% Tl we shall take this drop to be nearer 30% as being more in keeping with the results of fig. 2 (*b*). Assuming then that any departures from the rigid-band model are not too large, so that changes in $n(E_0)$ on alloying can be related to the $n(E)$ curve for pure lead solely by a shift in the Fermi level, we give in fig. 3 a more realistic density of states curve for pure lead than that given in fig. 1, changes in area under the $n(E)$ curve being related to the corresponding changes in electron concentration in fig. 2 (*d*). The peak in the $n(E)$ curve is then found to lie at about 0·02 ev below the Fermi level. The contributions from the holes and overspill electrons are also indicated; as is required for a metal of even valency, these have been drawn in with equal area, this corresponding to a weighted mean of the number per atom of holes and electrons given in fig. 1, viz. $0{\cdot}41 \pm 0{\cdot}06$ per atom.

We shall now give a discussion of the temperature dependence of the thermoelectric power of pure lead (Christian *et al.* 1958) in relation to the $n(E)$ curve. The low-temperature values of S below about 6°K lie on a straight line with $S=0$ at $T=0$ (results of Steele; see fig. 3 of Christian *et al.*) and we have used these results and (5) to infer the slope of the $n(E)$ curve at the Fermi level (broken line in fig. 3); in this connection we note that the variation of S with addition of small amounts of impurities is in no sense 'anomalous' (Jan *et al.* 1958). As we have already mentioned, S also varies linearly with T above 100°K, but the variation is much slower than that below 6°K and, moreover, the high-temperature results do *not* extrapolate to $S=0$ at $T=0$ in accordance with (5). These features may be accounted for qualitatively in terms of the rapid change in $\partial n(E)/\partial E$

near the Fermi level from positive to negative values within an energy range comparable with kT. We can make a crude estimate of this effect by considering the $n(E)$ curve near the peak to consist of two intersecting straight lines and by supposing that we can replace $(\partial n(E)/\partial E)_0$ in (5) by a straightforward average of $\partial n(E)/\partial E$ over an energy range of $2kT$ on either side of the Fermi level. This results in the modification of (5) by the factor $((C+1)\epsilon/2kT-C+1)/2$, where C is the magnitude of the ratio of $\partial n(E)/\partial E$ below the peak to that above the peak and ϵ is the energy between the peak and the Fermi level $(2kT>\epsilon)$. The modified linear expression for S can be fitted to the high-temperature results by choosing $C\sim 0{\cdot}8$ and $\epsilon \sim 0{\cdot}01$ ev. This crude argument thus suggests that the slopes of the $n(E)$ curve on either side of the peak are comparable in magnitude and the value of ϵ turns out to be comparable with that suggested by our rigid-band interpretation of the alloy results†.

Fig. 3

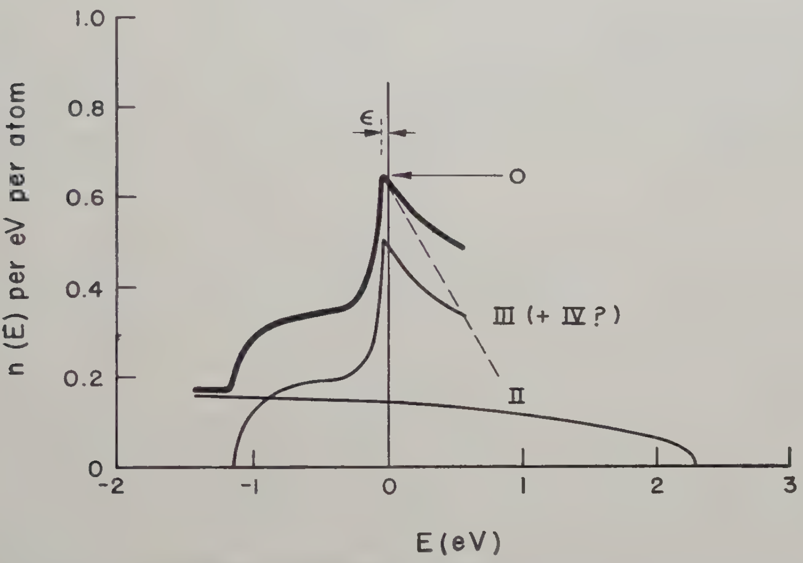

Proposed curve of density of states. The energy is measured relative to the Fermi level; – – –, slope at the Fermi level from absolute thermoelectric power below 6°K ; O, Decker *et al.* (1958).

It is tempting, at first sight, to account for the peak in the $n(E)$ curve at roughly 0·02 ev below the Fermi level in terms of the multiply-connected Fermi surface in the third Brillouin zone, a portion of which is illustrated diagrammatically in fig. 4 (*a*); a drawing showing the three-dimensional character of this surface is given in I. When the electron concentration has been sufficiently reduced (e.g. by alloying with Tl), this surface will break up into separate portions centred about either the zone corners W

---

† We should also expect the electronic contribution to the specific heat for $T>\sim 100$°K to be much less than that deduced from low-temperature measurements.

(fig. 4 (*b*)) or the mid-points K of the lines joining adjacent corners (fig. 4 (*c*)), depending on whether the energy is lowest at W or at K respectively. When the separate portions are nearly in contact, $\text{grad}_k E$ along zone lines will be particularly low, resulting in a peak in $n(E)$ when contact has just taken place. However, if this is the correct explanation, it is indeed surprising that the peak should lie so close to the Fermi level. The 'limbs' of the multiply-connected surface are, in fact, quite thick

Fig. 4

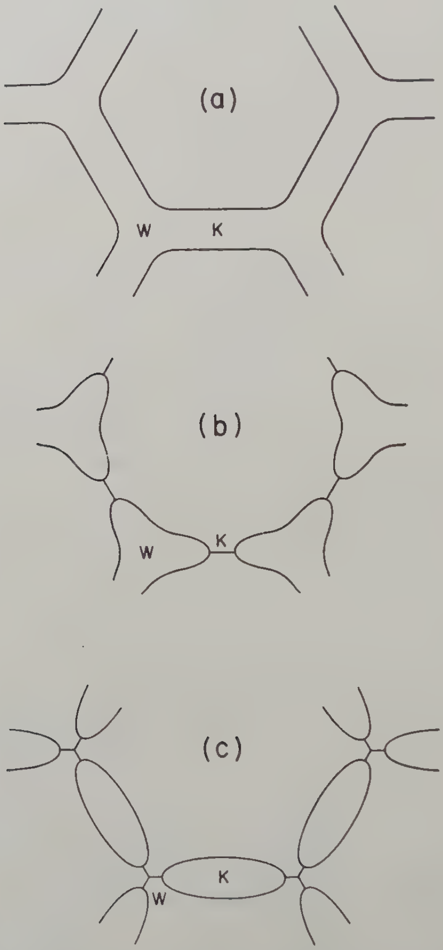

Diagrammatic illustration of the breaking-up of the multiply-connected third-zone Fermi surface.

so that one would expect the breaking-up of the surface to occur at an energy comparable with that associated with complete disappearance of the surface, i.e. at roughly 1 ev below the Fermi level; thus the above interpretation of the peak does not seem to be compatible with a model of rigid bands. In order to assess the extent of shifts in the band structure, low-temperature heat-capacity measurements on isoelectronic Pb–Tl–Bi alloys would be very desirable (cf. Guthrie 1959).

In conclusion we wish to point out that there is some doubt as to the existence of the cushion-shaped pieces of Fermi surface in the fourth zone. From the detailed reasoning given in I we can state that *either* there are electrons in this zone giving a reasonably large contribution, with the lowest energies in zones three and four being nearly equal (fig. 1), *or* the fourth zone is completely empty; the evidence from the de Haas–van Alphen effect alone is insufficient to distinguish unambiguously between these two possibilities. However, the values of the electronic specific heat and of the total area of the Fermi surface as deduced from the de Haas–van Alphen data can be brought into considerably better agreement with the results of other experiments by taking the fourth zone to be empty; this supposition also makes the numbers of electrons and holes more nearly equal. Since in drawing fig. 3 the data in fig. 1 for the holes have been more heavily weighted than that for the electrons, it makes little difference to the areas under the curves whether a contribution from the fourth zone is included or not.

ACKNOWLEDGMENTS

It is a pleasure to thank Drs. J. S. Dugdale, W. A. Harrison and D. K. C. MacDonald for helpful discussions and criticism.

REFERENCES

BOROVIK, E. S., 1954, *J. exp. theor. Phys.*, **27,** 355.

CHRISTIAN, J. W., JAN, J.-P., PEARSON, W. B., and TEMPLETON, I. M., 1958, *Proc. roy. Soc.* A, **245,** 213.

DECKER, D. L., MAPOTHER, D. E., and SHAW, R. W., 1958, *Phys. Rev.*, **112,** 1888.

GOLD, A. V., 1958, *Phil. Trans.* A, **251,** 85.

GUERTLER, W., and SCHULZE, A., 1923, *Z. phys. Chem.*, **104,** 269.

GUTHRIE, G. L., 1959, *Phys. Rev.*, **113,** 793.

HANSEN, M., 1958, *Constitution of Binary Alloys* (New York: McGraw-Hill Book Company).

JAN, J.-P., PEARSON, W. B., and TEMPLETON, I. M., 1958, *Canad. J. Phys.*, **36,** 627.

MEISSNER, W., FRANZ, H., and WESTERHOFF, H., 1932, *Ann. Phys., Lpz.*, **13,** 967.

MOTT, N. F., and JONES, H., 1936, *Theory of the Properties of Metals and Alloys* (Oxford: Clarendon Press).

ROLLA, L., 1915, *Gazz. chim. ital.*, **45,** 185.

SCHUBNIKOW, L. W., CHOTKEWITSCH, W. I., SCHEPELEW, J. D., and RJABININ, J. N., 1936, *Phys. Z. Sowjet.*, **10,** 165.

SHOENBERG, D., 1952, *Superconductivity* (Cambridge: University Press).

STOUT, J. W., and GUTTMAN, L., 1952, *Phys. Rev.*, **88,** 703.

TAMMANN, G., and RÜDIGER, H., 1930, *Z. anorg. Chem.*, **192,** 35.

TANG, Y.-C., and PAULING, L., 1952, *Acta Cryst.*, **5,** 39.

THOMAS, W. R., and EVANS, E. J., 1933, *Phil. Mag.*, **16,** 329.

The Fine Structure of Films of Rubber and other Polymers†

By M. Seal

Research Laboratory for the Physics and Chemistry of Solids,
Department of Physics, University of Cambridge

[Received September 10, 1959]

Abstract

High resolution electron microscopy has been used to examine thin films of natural rubber and other polymers. Dispersions of various materials (in particular neoprene and chlorinated natural rubber) in natural rubber have been studied. Structures which are believed to be the individual curled-up molecules of the dispersed polymer have been photographed. Stretched rubber films have also been examined and some information about the mode of deformation obtained.

§ 1. Introduction

Films of various plastic materials have been commonly employed in electron microscopy—for the most part as supports for other specimens and as replicas of solid surfaces from which they have been stripped. They have not, however, been used very much as specimens in their own right to provide information about the properties of the plastic material itself (a notable exception is the work of Agar *et al.* 1959, on polyethylene). In the present paper an account will be given of an electron microscope study of rubber films from which information about the rubber has been deduced. In particular, structures which are thought to be individual rubber molecules have been found.

§ 2. Materials and Technique

2.1. *Materials*

Films of four materials were examined. These were natural rubber and three related polymers—neoprene, guttapercha, and Alloprene. Natural rubber is mainly cis-polyisoprene $(\text{—CH}_2\text{—C}.\text{CH}_3=\text{CH—CH}_2\text{—})_n$, neoprene is polychloroprene $(\text{—CH}_2\text{—C}.\text{Cl}=\text{CH—CH}_2\text{—})_n$, guttapercha is mainly trans-polyisoprene, and Alloprene is a chlorinated natural rubber made by Imperial Chemical Industries Limited (approximate composition $C_{10}H_{13}Cl_7$). A purified natural rubber was also used. This was rubber from which the small amounts of proteins, etc. which commonly occur in the natural product had been removed. None of these materials had been vulcanized. Thus, there was little cross-linking of the molecular chains and the polymers were soluble in suitable organic solvents. All the samples were obtained from the British Rubber Producers' Research Association.

---

† Communicated by Dr. F. P. Bowden, F.R.S.

2.2. *Specimen Preparation*

A solution in 'Analar' benzene of the material to be examined was made. A drop of this was allowed to fall on a clean water surface where it spread and, after evaporation of the benzene, left a floating film. Part of this was then picked up on a specimen grid and subsequently examined in the electron microscope—Siemens Elmiskop I. The film thickness was found to be critical. The concentration of the solution was therefore adjusted to give films of the correct thickness judged by the interference colour—low order white with veining of yellow. Such films (of the order of 1000 Å thick) were over most of their area too thick for high resolution electron microscopy, but they did show thin patches where the local thickness was probably less than 100 Å. These were the regions studied. Films of lower mean thickness could not be used since they formed networks of thin threads rather than continuous sheets.

Stretched rubber films were also examined. The technique of stretching them was as follows. The film while floating on the water surface was touched with two pieces of filter paper. Unvulcanized rubber being sticky, it adhered to them. The pieces of filter paper were then drawn apart and parts of the stretched film in between picked up on specimen grids. Once on a grid the film remained stretched since it adhered to the bars of the grid.

§ 3. RESULTS

3.1. *Changes Produced in Specimens by the Electron Beam*

Polymers suffer changes when irradiated with electrons (see, for example, Little 1954, Charlesby and Pinner 1959). Consequently, it was thought advisable to investigate the effect on a specimen of its irradiation during examination in the electron microscope. No visible changes occurred in rubber films as the electron beam intensity was increased from a low value, but a rubber film after examination in the electron microscope was found to be insoluble in benzene. This change was studied further by placing glass plates coated with a film of rubber in the camera of the electron microscope instead of the normal photographic plates, and exposing them to the much less intense beam of this part of the instrument. It was found that exposure for about 2 min to a fairly intense beam rendered the rubber insoluble in benzene. This suggested that, even if examined at low magnification (say 5000 ×) and low intensity, a rubber film in the normal specimen position would be rendered insoluble within a few milliseconds. Consequently, if a rubber specimen is examined in the electron microscope one cannot avoid altering it by the action of the electron beam.

However, sharp spotty diffraction patterns were obtained from crystalline polymers (polyethylene, guttapercha) provided that a reasonably low intensity beam was used. Thus the changes in these polymers caused by a weak electron beam were not too drastic. It seems likely that the first effect of the electron beam is a cross-linking of the molecular chains, followed after much greater irradiation by a complete disruption of the structure. The rubber specimens if examined at low intensity probably remained as rubber (albeit vulcanized rubber), but even if an intense beam was used the changes in structure produced no visible alteration of the specimen.

3.2. *Appearance of Rubber Films*

An electron micrograph of a purified natural rubber specimen is reproduced in fig. 1†. Such micrographs show little structure apart from gross features such as holes, wrinkles, thick and thin patches, etc. There is a granular structure on a scale of about 20 Å visible at high magnification, but this may well be due to electron-induced contamination. Films of ordinary natural rubber, neoprene, Alloprene, and guttapercha have a similar appearance.

Filled rubbers have also been examined and the dispersion of filler particles photographed (fig. 2). These are important since carbon black and other materials are commonly incorporated in rubber to improve its mechanical properties. A micrograph of a stretched filled rubber is shown in fig. 3. The thin patches (which occur sparsely in unstretched rubber) are more extensive and seem to have developed at the expense of the thicker regions. This would be expected for unvulcanized rubber will flow plastically but the sharpness of the boundary between thick and thin regions is perhaps surprising.

3.3. *Mixed Films*

The most interesting results were obtained from films made from a solution containing a mixture of polymers. Mixtures of purified natural rubber and neoprene, and purified natural rubber and Alloprene were used. The neoprene and Alloprene which contain a high percentage of chlorine might be expected to scatter electrons more strongly than the natural rubber which apart from impurities is entirely made up of carbon and hydrogen. Thus the neoprene or Alloprene should appear darker than the natural rubber in a bright field image. Films of natural rubber containing a few per cent of neoprene show numerous dark patches (fig. 4): these presumably are the neoprene. Furthermore films of neoprene containing a few per cent of natural rubber also have the expected appearance of light patches on a dark background (fig. 5), but it is difficult to distinguish these from the occasional thin patches which these films show.

A more detailed study was made of the Alloprene/natural rubber system. Figure 6 shows the appearance of a film containing equal parts by weight of the two materials. The contrast system is difficult to interpret, but the film is obviously not homogeneous. One would not expect it to be, for chemically different polymers are, in the absence of a solvent, generally immiscible or only slightly miscible (Dobry and Boyer-Kawenoki 1947, Scott 1949).

---

† With the exception of fig. 10, all figures are as plates.

Figure 7 was obtained from a film containing 20% of Alloprene. The dark spots presumably represent globules of the Alloprene. The profiles of these globules could be seen in regions where the edge of a film had curled over. They were thicker than the surrounding film and appeared to be flattened spheres. Thus at least part of the contrast is here due to the greater thickness of these globules. Again one would not expect miscibility of the polymers in these proportions. Similar pictures were obtained from films containing 10% of Alloprene. A micrograph of a stretched film having this composition is shown in fig. 8. It can be seen that the film has torn at the Alloprene globules indicating that the adhesion between the natural rubber and the Alloprene was weak.

When the proportion of Alloprene was reduced to about 5% it was found that the dark spots were smaller and of lower contrast (fig. 9). The proportions are similar to those of the neoprene/natural rubber system of fig. 4, and it may well be that in both cases the proportion of the minor constituent was sufficiently small to render the polymers completely miscible. In such a case the Alloprene or neoprene molecules would be randomly kinked and interwoven with the molecules of the natural rubber as are the molecules in the bulk of a pure rubber (see Treloar 1958). The contrast would then be due to the greater local concentration of chlorine and would be low, and the edges of the darker regions would be expected to be diffuse. Experimentally, it was found that the contrast was very low and that the darker patches which often had diffuse edges could only be seen in regions where the specimen was very thin. The contrast could be increased by operating the electron microscope at 40 kv instead of the usual 80 kv but was still low.

However, whether or not the polymers are miscible, there is one point of particular interest. The smaller dark patches are less than 100 Å in diameter and are of the order of size of the individual polymer molecules. It may well be that the smaller patches contain only one more or less tightly curled molecule. Information on this point was obtained by using a fractionated Alloprene, having a narrow range of molecular weights which was prepared for the author by the British Rubber Producers' Research Association. Films of purified natural rubber containing 5% of this material were prepared and examined and the size distribution of the dark spots measured. A histogram showing the size distribution of over 1000 spots is shown in fig. 10. Spots greater than 180 Å in diameter were not measured since they are outside the range of interest, nor were spots less than 40 Å in diameter since they become indistinguishable from the granular fine structure of the films. This fractionated Alloprene was stated to have a mean molecular weight of 70 000 ± 10 000 (determined by viscosity measurements). This would correspond to a sphere having the bulk density of Alloprene (1·6) of diameter 50 ± 10 Å. Thus the peak in the histogram at 80 Å probably corresponds to the diameter of a single molecule of the Alloprene, the slightly greater size being due either to it having a non-spherical envelope or to it being interwoven with the surrounding rubber molecules. The smaller spots presumably correspond to the tail of the molecular weight distribution.

Fig. 10

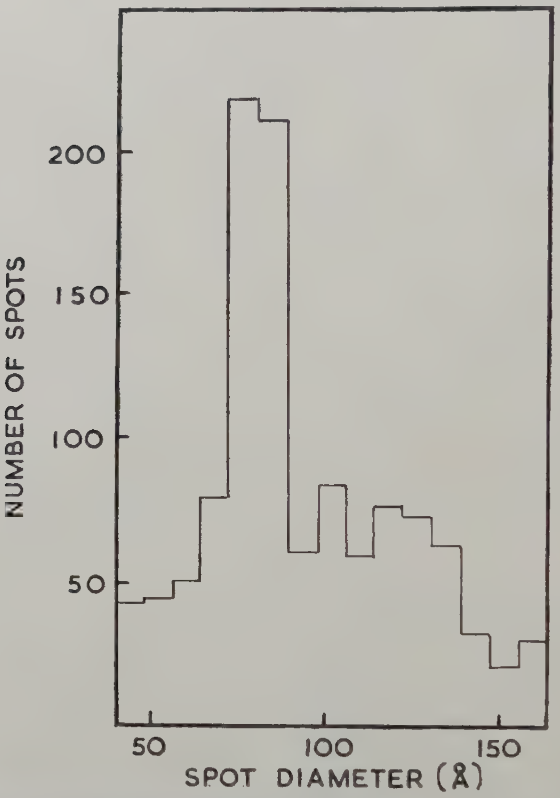

Histogram showing the distribution of spot size in natural rubber films containing about 5% Alloprene.

It would be interesting to study the appearance and distribution of the spots in stretched films and an attempt to do this has been made. Unfortunately the results were not reproducible. The film often stretched by thinning similar to that shown in fig. 3, but a few micrographs show evidence of the spots themselves. Figure 5 is an example. This film was not stretched deliberately but was deformed slightly by the stresses set up on drying and the spots appear elongated.

ACKNOWLEDGMENTS

The author thanks Dr. F. P. Bowden, F.R.S., for his interest and advice; Drs. L. C. Bateman, L. Mullins, and A. G. Thomas of the British Rubber Producers' Research Association for valuable discussions and for supplying the materials used in this work; and the British Rubber Producers' Research Association for a Fellowship.

REFERENCES

AGAR, A. W., FRANK, F. C., and KELLER, A., 1959, *Phil. Mag.*, **4**, 32.
CHARLESBY, A., and PINNER, S. H., 1959, *Proc. roy. Soc.* A, **249**, 367.
DOBRY, A., and BOYER-KAWENOKI, F., 1947, *J. polymer Sci.*, **2**, 90.
LITTLE, K., 1954, *Proc. 3rd International Conf. Electron Microscopy* (London: Royal Microscopical Society), p. 165.
SCOTT, R. L., 1949, *J. chem. Phys.*, **17**, 279.
TRELOAR, L. R. G., 1958, *The Physics of Rubber Elasticity*, 2nd edition (Oxford: The Clarendon Press).

The Thermal Conductivity of Germanium, Silicon and Indium Arsenide from 40°C to 425°C†

By Audrey D. Stuckes
Metropolitan-Vickers Electrical Co. Ltd., Trafford Park, Manchester, 17

[Received May 6, 1959 ; and in revised form August 24, 1959]

Abstract

Measurements have been made of the thermal conductivity of germanium, silicon, pure ($n=3\times10^{16}$) indium arsenide and impure ($n=10^{19}$) indium arsenide. In each case the electronic contribution κ_e to thermal conductivity has been calculated and the phonon contribution κ_L estimated by subtraction of κ_e from the experimental values. The thermal resistance of the lattice has not generally been found to be proportional to the absolute temperature as expected for three-phonon processes but the trend is towards a higher power relationship. The lattice resistance of heavily doped indium arsenide has been found to be greater than that of the pure material.

§ 1. Introduction

There have been few measurements of the thermal conductivity of semiconductors above room temperature. The possible application of semiconducting materials to the thermoelectric generation of electrical power makes thermal conductivity a factor of increasing importance. At the same time it is of interest theoretically since if one also has knowledge of the electrical properties of the semiconductor the lattice component of the thermal conductivity can be deduced near and above the Debye temperature.

§ 2. Method of Measurement

Earlier experiments on indium antimonide (Stuckes 1957) indicated the need for increased accuracy. Although the same comparative method (Stuckes and Chasmar 1956) has been used, certain modifications in thermometry and in thermal contacts have been found necessary to improve the accuracy to ±5% up to 450°c.

2.1. *Thermometry*

Many precautions must be taken to avoid errors in thermocouple measurements due to work hardening and temperature ageing effects.

---

† Communicated by the Author.

Continuous 0·005 in. diameter thermocouples of T_1-advance (nickel–chromium and copper–nickel alloys) have been found to give the least trouble amongst the more sensitive thermoelectric materials although it is necessary to have two sets of apparatus in use so that one can be kept for room temperature experiments only.

Temperature measurements in a vacuum furnace were found to be inconsistent when the thermocouple junctions were electrically insulated from the copper blocks because the presence of exchange gas was essential to bring the thermocouples into temperature equilibrium. Rather than discard the differential method of measurement (which necessitates electrical insulation between thermocouples) experiments were carried out in an inert atmosphere. Calculation of the sideways heat loss from the column was made assuming a uniform temperature surround. This was achieved by placing a cylindrical copper shield between the column and the cylindrical container; the temperature variation down the copper shield was found to be less than half a degree at 450°c.

2.2. *Thermal Contacts*

High accuracy in this method depends on there being virtually no contact resistance between any member of the stack and its thermocouple blocks. Since a good electrical contact is an indication of a good thermal contact, voltage probe measurements were taken along the column with a constant current flowing. A graph of voltage against distance should be a series of straight lines with sharp changes of slope at each contact—a step in the graph at the interface would indicate a high resistance at the contact. Precautions were necessary to eliminate thermoelectric e.m.f.'s when probing the surface of the semiconductor.

Indium–mercury and indium–gallium alloys, which are both liquid at room temperature, were found to be unsatisfactory as intermediate contact layers above 200°c. The stack was therefore assembled by a soldering technique using pure indium after copper or nickel plating the semiconductors. Very good permanent contacts between the standards and the copper blocks were made by a silver–copper eutectic alloying process.

2.3. *The Comparative Standards*

In all experiments FH stainless steel has been used as a standard. The material was supplied by the Brown–Firth Research Laboratory and had a composition and heat treatment very similar to that investigated by Powell in 1936 and his values of thermal conductivity have been used throughout.

As a subsidiary experiment the FH standards were compared with some Armco iron, which was part of a batch extensively measured by Powell (1934) and found to agree with Powell's results to ±3% up to 425°c.

§ 3. Experimental Results

3.1. *Germanium*

Only one sample of germanium was available at the time of these experiments and this was n-type and had a resistivity of about 5 ohm cm at 300°K. Unfortunately, electrical probe measurements indicated that it was very inhomogeneous, having a high resistance or barrier region near the centre; this may not matter since the electronic component of thermal conductivity is found to be very small. The results of two sets of thermal measurements are given in fig. 1.

Fig. 1

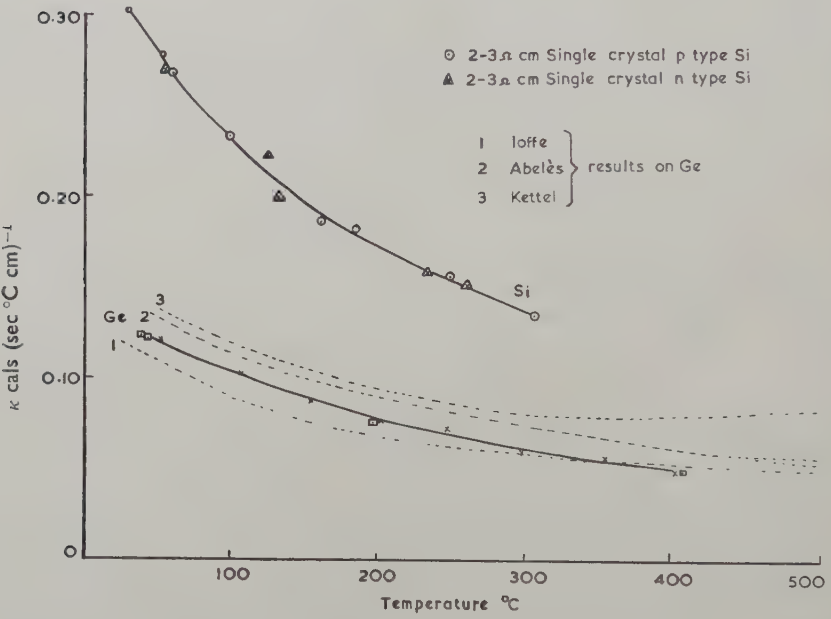

Thermal conductivity of germanium and silicon.

Four samples of germanium ranging in resistivity from 3 ohm cm to 0·001 ohm cm have been measured by Abelès (1958). Although there was a wide spread in his experimental points, up to 700°K, the thermal conductivity of all four samples can be represented by the line shown in fig. 1. Above 700°K the very impure sample deviates from the others and has a lower thermal conductivity. The results of Ioffe and Ioffe (1954) and those of Kettel (1959) are also shown in this figure.

3.2. *Silicon*

Two samples of single crystal silicon have been measured, one 'n' type and one 'p' type, both having a room temperature resistivity of about 3 ohm cm. Great difficulty was experienced in plating the silicon before soldering. A nickel layer was deposited by an electroless plating method (Sullivan and Eigler 1957); from this good ohmic contacts were obtained so long as great care was taken. The results of thermal measurements are given in fig. 1. As the contacts deteriorated rapidly above 300°C no useful measurements have been made above that temperature.

As far as it is known no other measurements on silicon at high temperature have been published. The value of 0·30 cals (cm°C sec)$^{-1}$ is in the middle of some rather divergent room temperature values. The *American Metals Handbook* (1948) quotes 0·20 cals (cm°C sec)$^{-1}$, Ioffe and Ioffe (1954) give 0·26 cals (cm°C sec)$^{-1}$ whilst 0·35 cals (cm°C sec)$^{-1}$ has recently been reported by Steele and Rosi (1958).

3.3. *Indium Arsenide*

One pure sample ($n \sim 3 \times 10^{16}$) and one sulphur-doped sample ($n \sim 10^{19}$) of polycrystalline indium arsenide have been measured. Electrical conductivity and Hall coefficient up to 500°C (fig. 2) were measured on a specimen from each ingot cut immediately adjacent to that used in the thermal measurements.

Fig. 2

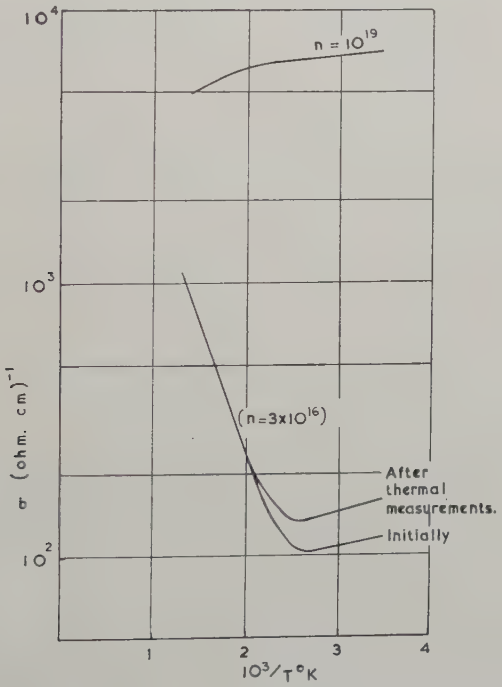

Electrical conductivity of two samples of indium arsenide.

From the ingot of pure material a piece 1·5 cm long was initially used (much larger than the usual samples). After one set of thermal measurements this specimen was cut into two further pieces 1 cm and 0·5 cm long and the experiment repeated on each. The results are given in fig. 3.

Only one sample of impure material was used but three sets of measurements, each on a freshly assembled stack, were made and the results shown in fig. 3.

Bowers *et al.* (1959) investigated two samples of indium arsenide, one similarly pure ($n \sim 5 \times 10^{16}$) and one rather less heavily doped ($n \sim 10^{18}$) than that measured in these experiments; their results are indicated in fig. 3.

Fig. 3

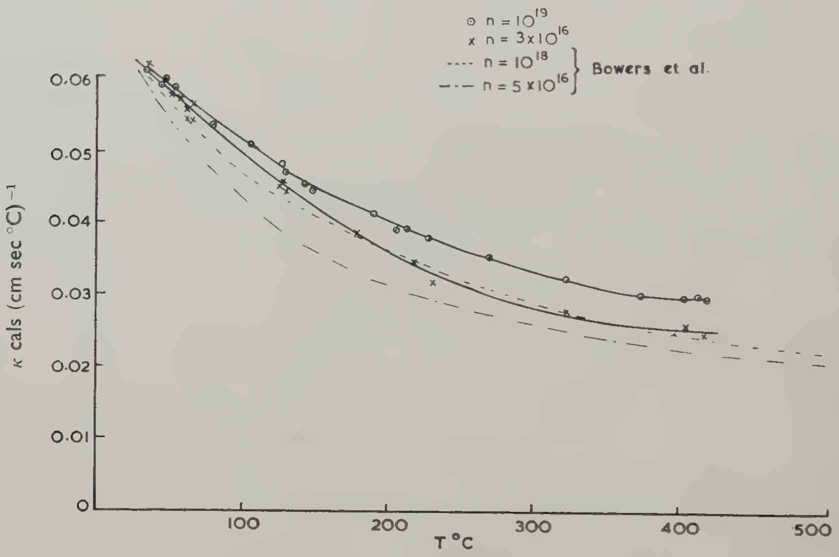

Thermal conductivity of pure ($n = 3 \times 10^{16}$) and impure ($n = 10^{19}$) indium arsenide.

§ 4. Electron Contribution to Thermal Conductivity

4.1. *Theoretical Discussion*

In the presence of a temperature gradient electrons and holes in a semiconductor will diffuse down the temperature gradient transporting kinetic energy from the hot to the cold end of the semiconductor. If on their way, an electron and a hole meet and recombine, they may give up their potential energy to the crystal lattice. This may be large compared to their kinetic energy and in some circumstances may be a very important mechanism of heat transfer; the terms 'ambipolar diffusion' or 'ionization energy transport' are sometimes applied to it. A further possible mechanism of heat conduction that has been postulated, but not so far definitely established, is exciton transport. An exciton is a related electron-hole pair with a weak binding energy; diffusing excitons could clearly carry thermal energy in a manner similar to free electron-hole pairs.

In addition to this electron contribution, heat is conducted through the semiconductor by vibrations of the crystal lattice (phonons) so that the thermal conductivity is given by

$$\kappa = \kappa_{\text{electronic}} + \kappa_{\text{lattice}}.$$

Neglecting any contribution from excitons, the electronic thermal conductivity κ_e may be expressed in the form

$$\kappa_e = \left(\frac{k}{e}\right)^2 T\sigma\Delta \quad . \quad . \quad . \quad . \quad . \quad . \quad . \quad . \quad (1)$$

where $\sigma = \sigma_n + \sigma_p$ is the electrical conductivity at temperature T°K and is the sum of the contributions from electrons and holes. The factor Δ may be expressed as a sum of terms

$$\Delta = \Delta_n + \Delta_p + \Delta_{np} \quad . \quad . \quad . \quad . \quad . \quad . \quad . \quad . \quad (2)$$

where the suffixes n, p and np refer to electrons, holes and electron-hole pairs respectively. The various terms involve Fermi–Dirac integrals whose form is related to the scattering mechanism in the semiconductor, while Δ_{np} also includes a term involving the energy gap.

This subject has been discussed by Price (1955), Ioffe (1956) and Madelung (1957).

In the particular case where the relaxation times for electron and hole scattering are given by $\tau \propto E^{\nu_n}$ and $\tau \propto E^{\nu_p}$ respectively, assuming that classical statistics apply, that the scattering is elastic and that the states distribution in valence and conduction bands is parabolic, it can be shown that

$$\Delta_n = (\nu_n + \tfrac{5}{2})\frac{\sigma_n}{\sigma}, \quad \Delta_p = (\nu_p + \tfrac{5}{2})\frac{\sigma_p}{\sigma}, \quad . \quad . \quad . \quad . \quad . \quad . \quad (3)$$

$$\Delta_{np} = \frac{\sigma_n\sigma_p}{\sigma^2}\left\{\frac{E_g}{kT} + \delta_n + \delta_p\right\}^2. \quad . \quad . \quad . \quad . \quad . \quad . \quad . \quad . \quad (4)$$

where $$\delta_n = \nu_n + \tfrac{5}{2}, \quad \delta_p = \nu_p + \tfrac{5}{2};$$

E_g is the forbidden gap width at T°K and

$$\sigma_n = n\mu_n e, \quad \sigma_p = p\mu_p e.$$

The value of ν depends on the particular mechanism of scattering of electrons; for example, it can range from $-\frac{1}{2}$ for acoustic scattering to $+\frac{1}{2}$ for polar scattering above the optical mode temperature and to $+\frac{3}{2}$ for either impurity scattering or electron-hole scattering.

The ambipolar contribution Δ_{np} will be most important when $\sigma_n \simeq \sigma_p$ that is for essentially intrinsic samples with comparable electron and hole mobilities. The value of E_g/kT is usually very much greater than $\nu_n + \nu_p + 5$ and is dominant in this term.

For partial degeneracy the Δ's may be evaluated in terms of Fermi–Dirac integrals (see Madelung). In the limit of complete degeneracy the results are again simple. For example, if the electron system is completely degenerate while the hole system is non-degenerate (classical) then for all forms of electron scattering

$$\Delta_n = \frac{\pi^2}{3}\frac{\sigma_n}{\sigma}, \quad \Delta_p = (\nu_p + \tfrac{5}{2})\frac{\sigma_p}{\sigma}, \quad \ldots\ldots \quad (5)$$

$$\Delta_{np} = \frac{\sigma_n \sigma_p}{\sigma^2}\left\{\frac{E_g}{kT} + \frac{\xi_n}{kT} + \nu_p + \tfrac{5}{2}\right\}^2 \quad \ldots\ldots \quad (6)$$

where ξ_n is the Fermi energy. In general, degeneracy tends to increase the term in brackets but the effect is small until the electrons become highly degenerate.

With sufficient knowledge of the electrical properties of a semiconductor κ_e can, therefore, be calculated. So long as κ_e is not too large compared to the measured value of thermal conductivity, the lattice component κ_L can then be deduced with reasonable accuracy.

4.2. κ_e *for Germanium and Silicon*

The germanium sample used in the experiments was fairly pure and by comparison with some results of Dunlap (1957) would be intrinsic by 500°K and the silicon by 600°K. Electrical data from Morin and Maita (1954 a, b) have, therefore, been used to calculate κ_e for intrinsic germanium and silicon. The ratio of electron to hole mobility has been taken from the extrapolated high temperature curves. The temperature dependence of mobility in germanium is found to be $T^{-1\cdot66}$ for electrons and $T^{-2\cdot33}$ for holes and in silicon is $T^{-2\cdot6}$ for electrons and $T^{-2\cdot3}$ for holes. Although acoustic mode scattering would lead to a $T^{-1\cdot5}$ dependence, nevertheless this has been assumed as a first approximation taking $\nu = -\frac{1}{2}$.

The results are given in fig. 4. Ambipolar diffusion is dominant in both materials there being virtually no kinetic energy transport in silicon up to 1000°K. By comparison with fig. 1 it can be seen that the electronic component in silicon is negligible and the experimental results represent the lattice conductivity.

The predominance of ambipolar diffusion in germanium is confirmed by the results of Abelès. He finds that the thermal conductivity of his pure sample starts to increase above 700°K (the temperature at which it becomes intrinsic) while that of his impure sample continues to decrease until about 900°K (where it becomes intrinsic). At this temperature κ for the pure material is 0·008 cals (cm°c sec)$^{-1}$ greater than that of the impure; this is equal to the calculated value for ambipolar diffusion in intrinsic germanium at 900°K.

Ioffe (1956) has also calculated the ambipolar contribution in germanium; he does not state what assumptions he has made but his results shown by the dotted line in fig. 4 seem somewhat high.

4.3. κ_e *for Indium Arsenide*

The calculation of κ_e in indium arsenide is extremely complex, for not only has it been shown to be weakly degenerate but it also has a non-parabolic conduction band so that the simple formulae given in § 4.1 do not apply. Moreover the scattering mechanism has not been established. Ehrenreich (1957) has considered the problem of electron scattering in the analogous compound InSb and finds that in the temperature range 200–500°K polar lattice scattering is predominant whereas at higher temperatures electron-hole scattering may become important.

Fig. 4

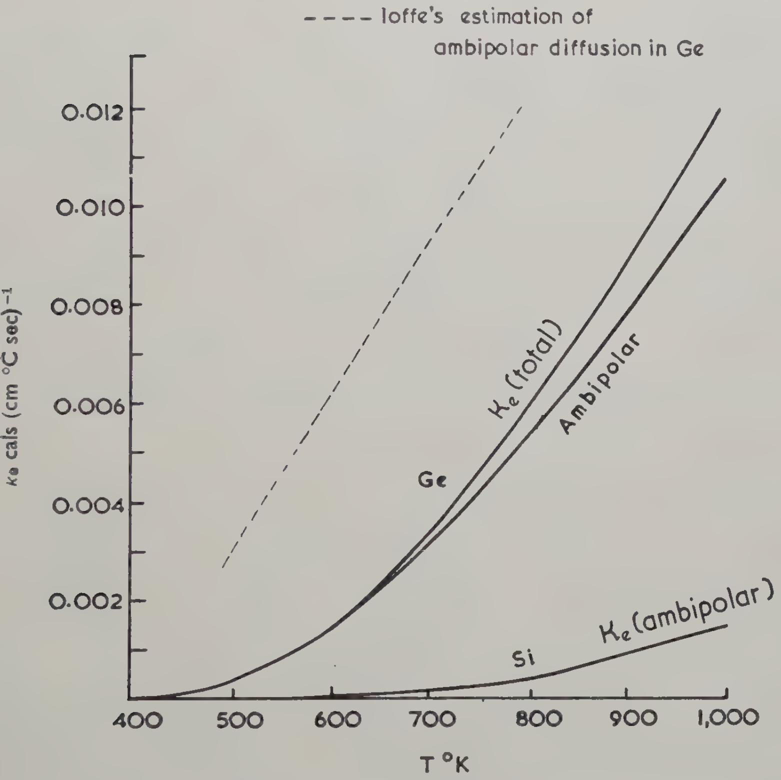

Calculated electronic component κ_e of thermal conductivity for intrinsic germanium and silicon.

In view of these facts no attempt has been made to use Ehrenreich's analysis for the ambipolar transport term (denoted as A by him). The simple formulae (§ 4.1) have been used, assuming classical statistics and polar scattering that is $\nu = \frac{1}{2}$.

In the calculation of Δ_{np} a value for the gap width E_g equal to $0{\cdot}5\,\text{ev} - 3{\cdot}5 \times 10^{-4} T$ has been used. The value of E_0 (E_g at 0°K) of 0·5 ev was obtained from thermoelectric measurements by Antell *et al.* (1956) while the temperature dependence was found from optical measurements by Oswald (1955). From a survey of the literature an average value for the ratio μ_p/μ_n of 1/64 at 300°K has been obtained, this being only slightly dependent upon impurity concentration. Owing to a lack of reliable information on the temperature variation of both electron and hole mobility the value of 1/64 has been taken as constant over the whole temperature range.

The kinetic energy and ambipolar contributions are shown in fig. 5 (*a*) while the total electronic component is given in fig. 5 (*b*). It can be seen that in indium arsenide the ambipolar diffusion is less than the kinetic energy transport.

An attempt has been made to estimate the effect of variations in the assumptions used in the above calculations. For example κ_e for two alternative scattering mechanisms is indicated by the dotted lines in fig. 5 (*b*). If, as seems likely by comparison with InSb, electron hole scattering dominates at the higher temperatures then κ_e will be increased to the values shown by the upper curve; should however, acoustic scattering predominate, κ_e would follow the lower curve.

From Oswald's optical measurements a value for the gap width $E_0 = 0{\cdot}43$ ev was obtained, surprisingly smaller than the value of 0·5 ev from thermoelectric measurements. This would lead to a reduction in κ_e of about 6%.

Components of κ_e for Various Scattering Mechanisms Allowing for Weak Degeneracy

Scattering mechanism	Kinetic energy transport $(\sigma/\sigma_n)\Delta_n$				Ambipolar transport δ_n			
	$\eta^* \to -\infty$	$\eta^* - 0$	$\eta^* = 1$	$\eta^* = 2$	$\eta^* \to -\infty$	$\eta^* = 0$	$\eta^* = 1$	$\eta^* = 2$
$\nu = -\frac{1}{2}$	2·0	2·17			2·0	2·37		
$\nu = \frac{1}{2}$	3·0		3·05		3·0		3·60	
$\nu = \frac{3}{2}$	4·0			3·73	4·0			4·81

It might be expected that the assumption of classical statistics in a material known to be weakly degenerate, would lead to an underestimate of κ_e. It has been shown by Antell *et al.* that for a similar sample measured over the same temperature range, the value of η^* (the Fermi energy in units of kT) will at no temperature exceed 0, 1 or 2, according to whether acoustic, polar or electron scattering predominates. Both components of κ_e (see table) have, therefore, been evaluated for these degrees of degeneracy using formulae given by Madelung (1957) in terms of Fermi–Dirac integrals, while the classical case ($\eta^* \to -\infty$) has been evaluated from equations 3 and 4.

From these figures, the maximum effect on the kinetic energy transport is an increase of about 8·5% which occurs for acoustic scattering. The effect on the ambipolar contribution is an increase of about 12% at 700°K where ξ_n/kT, E_g/kT and $\nu_p + \frac{5}{2}$ are all of the same order of magnitude —it will be less at lower temperatures and more at higher temperatures.

The assumption of a constant mobility ratio has almost certainly led to an overestimate of the ambipolar contribution, since this ratio probably decreases as the temperature increases. If the mobility is a function of temperature of the form $\mu \propto T^{-\alpha}$ then α (extrapolated from Folberth

Fig. 5

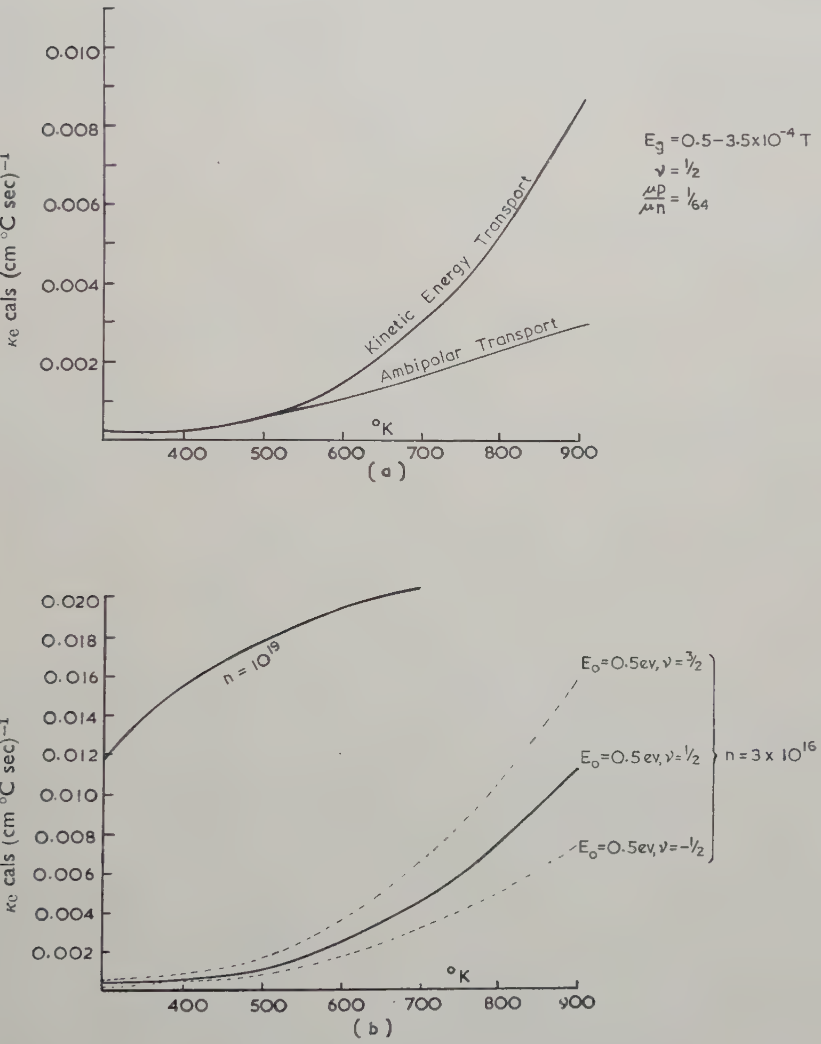

(*a*) Estimates of the kinetic energy and ambipolar transport in pure indium arsenide ($n = 3 \times 10^{16}$). (*b*) Estimated κ_e for pure ($n = 3 \times 10^{16}$) and impure ($n = 10^{19}$) indium arsenide.

et al. (1954) and Antell *et al.*) would be 2·3 for holes and between 1 and 1·5 for electrons, leading to a value for μ_p/μ_n at 750°K of about 40% of that at 300°K. Taking this into account and the effect of the lower value for the gap width, the lower estimate of the ambipolar diffusion would be about 10% of the kinetic energy contribution for all scattering mechanisms. This contrasts with the statement of Bowers *et al.* that up to 750°K the ambipolar term is less than 6% of the kinetic energy contribution. Unfortunately, they do not state what assumptions were made in their calculation.

Estimation of the electronic transport in the impure sample is less complex. The ambipolar contribution will be negligible owing to the small number of intrinsic holes. At the same time the electrons are highly degenerate so that the electronic component is given by

$$\kappa_e = \frac{\pi^2}{3}\left(\frac{k}{e}\right)^2 \sigma T.$$

The results are given in fig. 5 (*b*).

§ 5. LATTICE THERMAL CONDUCTIVITY

5.1. *Theoretical*

The theory of lattice conduction is somewhat complex and has not yet been completely formulated (cf. Berman (1953), Peierls (1955), Klemens (1956)).

Above the Debye temperature Θ phonon–phonon U-processes predominate and the following laws should be obeyed

$$W_L \propto T \quad \text{three-phonon processes}$$

$$W_L \propto T^2 \quad \text{four-phonon processes}$$

where W_L $(1/\kappa_L)$ is the thermal resistance. The first equation applies where the major phonon interaction is one involving three phonons, either two phonons combine to form a third or one phonon splits up into two. The second equation holds where either one, two or three phonons interact to produce three, two or one phonon respectively.

Well below Θ, the resistance due to U-processes should decrease exponentially as the temperature is lowered until additional components of thermal resistance (such as phonon collisions with crystal imperfections, impurities, or crystal boundaries) swamp that due to interphonon collisions causing a rapid rise in W_L.

Even at high temperatures if there is a sufficiently large impurity concentration, there may be a contribution to the thermal resistance, due to phonon collisions with the impurities, which is comparable to the resistance arising from interphonon collisions. According to Peierls, above the Debye temperature, the impurities will contribute an additional thermal resistance which is independent of temperature: this depends on their number remaining constant and on their scattering cross section for a given phonon energy being constant, since ($T > \Theta$) the average phonon energy will be independent of temperature.

5.2. *Germanium and Silicon*

Since κ_e is found to be negligible in silicon up to 600°K the experimental results represent the lattice conductivity. κ_L has been deduced for germanium by subtraction of κ_e from the measured values. The lattice resistance for each material is shown in fig. 6. There is a linear relation between W_L and T up to 600°K for silicon (the full range of the experiment) but only up to 500°K for germanium. From 500°K to 700°K there is a marked increase in the temperature dependence. In neither case does the linear portion extrapolate through the origin.

Fig. 6

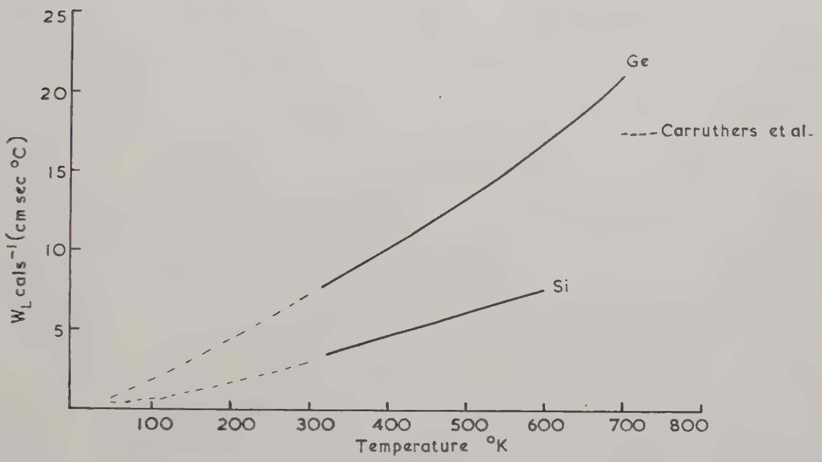

Estimated lattice resistance of germanium and silicon.

Low-temperature measurements by White and Woods (1956) and by Carruthers *et al.* (1957) have shown that the exponential dependence expected for U-process is not obtained in germanium or silicon but the thermal resistance in each case is approximately proportional to the temperature. This has been explained (cf. Berman *et al.* (1956)) by the presence of isotopes which scatter the phonons. As the temperature is increased the thermal resistance due to U-processes will increase and ultimately become dominant. It is not clear at what stage this will happen (Θ for germanium is 360°K and for silicon is 658°K) and it is perhaps not surprising that over the linear part W_L is found to be proportional to the absolute temperature minus a constant. The results of Carruthers up to 300°K, which agree closely with those of White and Woods, are shown by the dotted lines in fig. 6 where they can be seen to be mutually consistent with the high-temperature results: the merging of the two curves is particularly good in the case of germanium.

The logarithmic plot (fig. 9) indicates that as the temperature is increased, the thermal resistance in germanium is tending to the square law dependence expected for four phonon processes. Since κ_e is only 6% of the measured value at 700°K it seems unlikely that a false assumption in calculating it would account for the departure of W_L from linearity. Silicon does not show this effect; in this case measurements were not made above the Debye temperature.

5.3. *Indium Arsenide*

The lattice conductivity for both samples of indium arsenide has been deduced using values of κ_e calculated in § 4.3 and the results are given in fig. 7; the deduced values of Bowers are indicated by the dotted lines. The most striking feature is the much lower lattice conductivity of the impure sample ($n = 10^{19}$) compared to that of the pure sample ($n = 3 \times 10^{16}$), contrasting with the fairly close agreement obtained by Bowers for both his samples ($n = 5 \times 10^{16}$ and $n = 10^{18}$). However, the two impure samples are not identical and there may be increased scattering of the phonons by impurities in the more heavily doped material.

Fig. 7

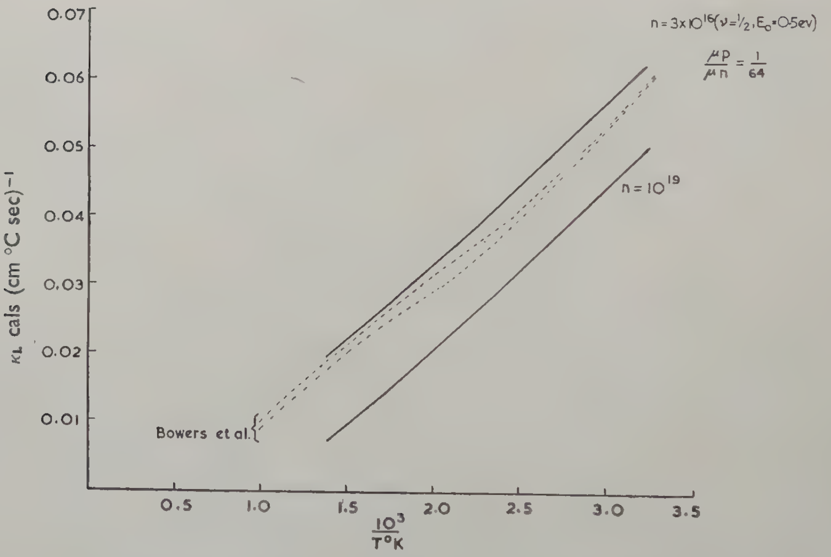

Estimated lattice conductivity of indium arsenide.

The full lines in fig. 8 represent the thermal resistance of the two samples assuming that the impure is completely degenerate and that for the pure material, classical statistics apply, polar scattering predominates and the mobility ratio is constant. The part shaded between the dotted lines on either side of the lower full line represents the range of values for W_L ($n = 3 \times 10^{16}$) taking into account the uncertainty of electrical properties discussed in § 4.3. The maximum values of W_L are obtained for electron-hole scattering, $E_0 = 0{\cdot}5$ ev, a constant mobility ratio and weak degeneracy. The minimum values correspond to $E_0 = 0{\cdot}43$ ev, a temperature dependent mobility ratio, acoustic scattering and no degeneracy.

The lattice resistance of the impure material could be reduced if κ_e has been overestimated by the assumption of complete degeneracy to the extent shown by the shaded curve, the lower limit representing acoustic scattering and classical statistics. This limit is extremely unlikely since even if there is only partial degeneracy, polar, electron-hole or impurity scattering is the more probable scattering mechanism to which the upper limit is a better approximation.

Fig. 8

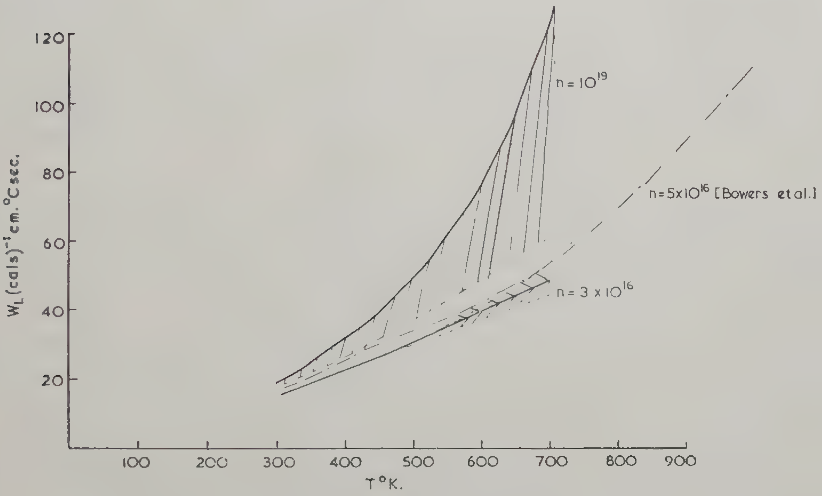

Estimated lattice resistance of indium arsenide.

It would, therefore, appear that the thermal resistance of the impure sample is greater than that of the pure and the additional component increases as the temperature increases.

Dr. J. M. Ziman and Mr. F. W. Sheard (private communication), however, have estimated that the sulphur-doped sample should have an additional component due to scattering of phonons by impurities of only about 0·5 cals^{-1} (cm °c sec) and this should be independent of temperature. They have suggested that the calculated value of κ_e may be too large (and hence too large a value for W_L) when there is scattering of electrons by optical modes instead of acoustic modes.

It is interesting to note that again the thermal resistance does not show a linear relationship with temperature over the whole range and the extrapolation of the lower part of the curves in neither case passes through the origin. Bowers' results between 700°K and 1000°K also indicate a more rapid dependence on temperature. From the logarithmic plot (fig. 9) the lattice resistance of the heavily doped sample can be seen to be approaching a square law dependence.

§ 6. CONCLUSIONS

Taking into account the accuracy obtained in measurements on stainless steel samples of known thermal conductivity and the reproducibility of repeated measurements on semiconductors the experimental accuracy of measurement using the techniques described here is estimated as ±5% up to 450°c.

Fig. 9

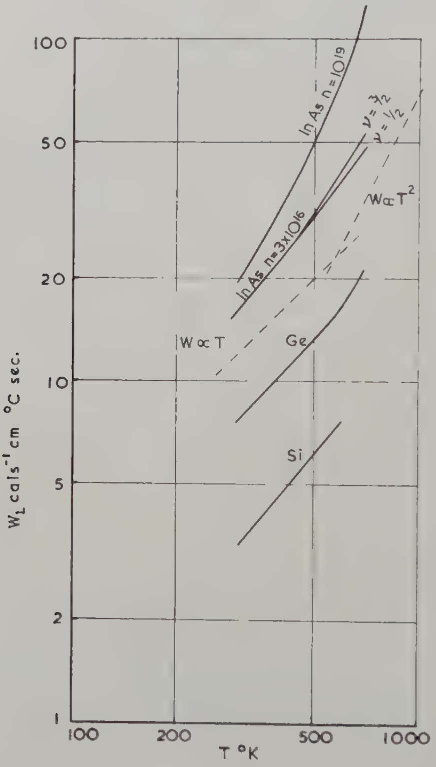

Lattice resistance against temperature for germanium, silicon and indium arsenide.

From fig. 9 it can be seen that in no case is the thermal resistance directly proportional to temperature over the whole range as expected for three-phonon processes, although germanium approximates to this at the lower temperatures. The trend in other materials is to a higher power relationship as found for indium antimonide (Stuckes 1957). Since a T^2 dependence would be expected for four-phonon processes it may be concluded that higher order phonon processes are operative in these materials.

An observation of particular interest is that the estimated lattice resistance of the highly impure InAs specimen is greater than that for the pure specimen, the difference being more marked at the higher temperatures. As a simple theoretical picture would suggest that impurity scattering should yield an additional thermal resistance independent of temperature, this result may be of both theoretical interest and also of practical importance in thermoelectric applications.

ACKNOWLEDGMENTS

The author wishes to thank the British Thomson-Houston Co. Ltd., the Brown Firth Research Laboratories and the National Physical Laboratory for providing some of the specimens used in this work. It is a pleasure to acknowledge the invaluable assistance in the measurements from Mrs. B. Brooks and the many helpful and stimulating discussions with Mr. R. P. Chasmar and Dr. R. Stratton. The author also wishes to thank Sir Willis Jackson, F.R.S., Director of Research and Education, Metropolitan-Vickers Electrical Company Limited, for permission to publish this paper.

REFERENCES

ABELÈS, B., 1958, *J. Phys. Chem. Solids*, **8,** 340.

Metals Handbook, 1948 (Cleveland : American Society for Metals).

ANTELL, G. R., CHASMAR, R. P., CHAMPNESS, C. H., and COHEN, E., 1956, *Report of the Meeting on Semiconductors* (London : The Physical Society), p. 99.

BERMAN, R., 1953, *Advanc. Phys.*, **2,** 103.

BERMAN, R., FOSTER, E. L., and ZIMAN, J. M., 1956, *Proc. roy. Soc.* A, **237,** 344.

BOWERS, R., URE, R. W., BAUERLE, J. E., and CORNISH, A. J., 1959, *J. appl. Phys.*, **30,** 930.

CARRUTHERS, J. A., GEBALLE, T. H., ROSENBERG, H. M., and ZIMAN, J. M., 1957, *Proc. roy. Soc.* A, **238,** 502.

DUNLAP, W. CRAWFORD, 1957, *An Introduction to Semiconductors* (New York : John Wiley and Sons), p. 230.

EHRENREICH, H., 1957, *J. Phys. Chem. Solids*, **2,** 21.

FOLBERTH, O. G., MADELUNG, O., and WEISS, H., 1954, *Z. Naturf.* A, **9,** 954.

IOFFE, A. F., 1956, *Canad. J. Phys.*, **34,** 1342.

IOFFE, A. V., and IOFFE, A. F., 1954, *Zhurn. Tekh. Fiz.*, **24,** 1910.

KETTEL, F., 1959, *J. Phys. Chem. Solids*, **10,** 52.

KLEMENS, P. G., 1956, *Handb. Phys.*, **14** (Berlin : Springer-Verlag), p. 198.

MADELUNG, O., 1957, *Encyclopaedia of Physics*, Vol. XX (Berlin : Springer-Verlag), p. 87.

MORIN, F. J., and MAITA, J. P., 1954 a, *Phys. Rev.*, **94,** 1525 ; 1954 b, *Ibid.*, **96,** 1528.

OSWALD, F., 1955, *Z. Naturf.* A, **10,** 927.

PEIERLS, R. E., 1955, *Quantum Theory of Solids* (Oxford: Clarendon Press), p. 52.

POWELL, R. W., 1934, *Proc. phys. Soc., Lond.*, **46,** 659 ; 1936, *Ibid.*, **48,** 351.

PRICE, P. J., 1955, *Phil. Mag.*, **46,** 1252.

STEELE, M. C., and ROSI, F. D., 1958, *J. appl. Phys.*, **29,** 1517.

STUCKES, A. D., 1957, *Phys. Rev.*, **107,** 427.

STUCKES, A. D., and CHASMAR, R. P., 1956, *Report of the Meeting on Semiconductors* (London : The Physical Society), p. 119.

SULLIVAN, M. V., and EIGLER, J. H., 1957, *J. electrochem. Soc.*, **104,** 226.

WHITE, G. K., and WOODS, S. B., 1956, *Phys. Rev*,, **103,** 569.

CORRESPONDENCE

Hall Effect in Liquid and Solid Mercury

By P. W. Kendall and N. E. Cusack
Department of Physics, Birkbeck College, University of London

[Received December 21, 1959]

Until about 1930 there was some doubt as to whether liquid metals showed Hall effects. In 1914, Fenninger failed to find Hall voltages in liquid Hg, but he also found a zero effect in solid Hg and the latter result has been contradicted in at least two subsequent experiments. In 1931, Kikoin and Fakidow showed that a liquid Na–K alloy possessed a Hall coefficient approximately equal to the free electron value of $-1/nec$, where n is the number of conduction electrons per unit volume. Nevertheless they too concluded that liquid Hg has zero Hall effect. Taken in conjunction with later results for solid Hg (e.g. those of Serduke and Fisher 1932), this would mean that the Hall coefficient, R, changes considerably on melting. It seemed desirable to check this result in the course of developing apparatus for investigating the Hall coefficient of liquid metals generally.

The measurement was by conventional d.c. techniques much as described by Lindberg (1952), the specimens being confined between flat glass plates whose separation was measured by an optical interference method. A Hall voltage, of the order 1 μV, was detected and was found to be proportional to the magnetic field for constant current through the specimen, and vice versa. The Hall coefficient was the same for three specimens of thicknesses 4·17, 2·03 and $5{\cdot}51 \times 10^{-3}$ cm. These facts indicate that a true Hall voltage was being measured, not seriously influenced by any magnetohydrodynamic effects. The mean of a large number of values of R was $-74{\cdot}6\times10^{-5} \pm 4\%$ e.m.u. and this was independent of temperature between room temperature and the M.P. ($-38{\cdot}9$°c).

The best way of describing electron states in liquid metals is not yet clear. Using the terminology normal in solid state theory, the conditions that R should have the free electron value are, according to Cooper and Raimes, (i) the Fermi surface should be spherical and (ii) the relaxation time should be isotropic. It seems plausible to assume that both these conditions should hold in a liquid devoid of long-range order. On this view the Hall coefficient of liquid mercury should be $-77{\cdot}4\times10^{-5}$ e.m.u. assuming two valence electrons per atom. This agrees quite well with the observed value. The results of Schulz (1957) on the optical properties of liquid Hg also fit very well with the free electron theory but the optical properties are not perfectly well established because the measurements of Hodgson (1959) do not confirm those of Schulz.

The values of R for solid Hg varied somewhat from specimen to specimen as did those of Serduke and Fisher (1932). It is possible that this is due to the different ways in which the mercury crystallized each time it was frozen, for the specimens may have contained fairly large oriented regions and the Hall coefficient is probably anisotropic. The values of R, which were independent of temperature between -39 and -71°c, ranged from -87 to -101×10^{-5} e.m.u.; those of Serduke and Fisher from -72 to -88×10^{-5} e.m.u. There is, of course, no reason to believe that either of Cooper and Raimes's conditions are fulfilled in the solid. It is interesting that R is negative in the solid Hg while it is positive in Zn and Cd. This is a possible point against Wallace's (1955) theory of bonding in these metals which treats them all on the same footing and entails the positive R in Zn and Cd.

The present results for liquid Hg disagree with those of Kikoin and Fakidow. If the value of R now reported is correct, then, other things being equal, the Hall voltage from Hg will be about 17% of that from the Na–K alloy used by Kikoin and Fakidow. Since the error reported in their value of R(Na–K) is ±10%, it is possible that their method was not sensitive enough to detect reliably the effect with Hg. Nevertheless it would be desirable to repeat the measurement with an entirely different technique, as well as to extend it to other metals, and such work is in progress.

REFERENCES

COOPER, J. R. A., and RAIMES, S., 1959, *Phil. Mag.*, **4,** 145.
FENNINGER, W. N., 1914, *Phil. Mag.*, **27,** 109.
HODGSON, J. N., 1959, *Phil. Mag.*, **4,** 183.
KIKOIN, J., and FAKIDOW, I., 1931, *Z. Phys.*, **71,** 393.
LINDBERG, O., 1952, *Proc. Inst. Radio Engrs, N.Y.*, **40,** 1414.
SCHULZ, L. G., 1957, *Advanc. Phys.*, **6,** 102.
SERDUKE, J. T., and FISHER, T. F., 1932, **39,** 831.
WALLACE, W. E., 1955, *J. chem. Phys.*, **23,** 2281.

The Effect of Electropolishing on the Retention of Vacancies During Quenching in Al and Al Alloys[†]

By E. J. FREISE[‡], M. E. FINE and A. KELLY[‡]
Department of Materials Science,
Northwestern University, Evanston, Illinois, U.S.A.

[Received December 28, 1959]

RECENTLY Smallman and Westmacott (1959) observed diffuse scattering of x-rays at small angles in quenched pure metal foils. They attributed the effect to double Bragg scattering caused by distortion due to dislocations formed by condensation of vacancies during quenching. Doherty

---

[†] This research was supported by the United States Air Force under Contract No. AF 49(638)–524 monitored by the A.F. Office of Scientific Research and Development Command.

[‡] Present address: Department of Metallurgy, Cambridge University.

Fig. 1

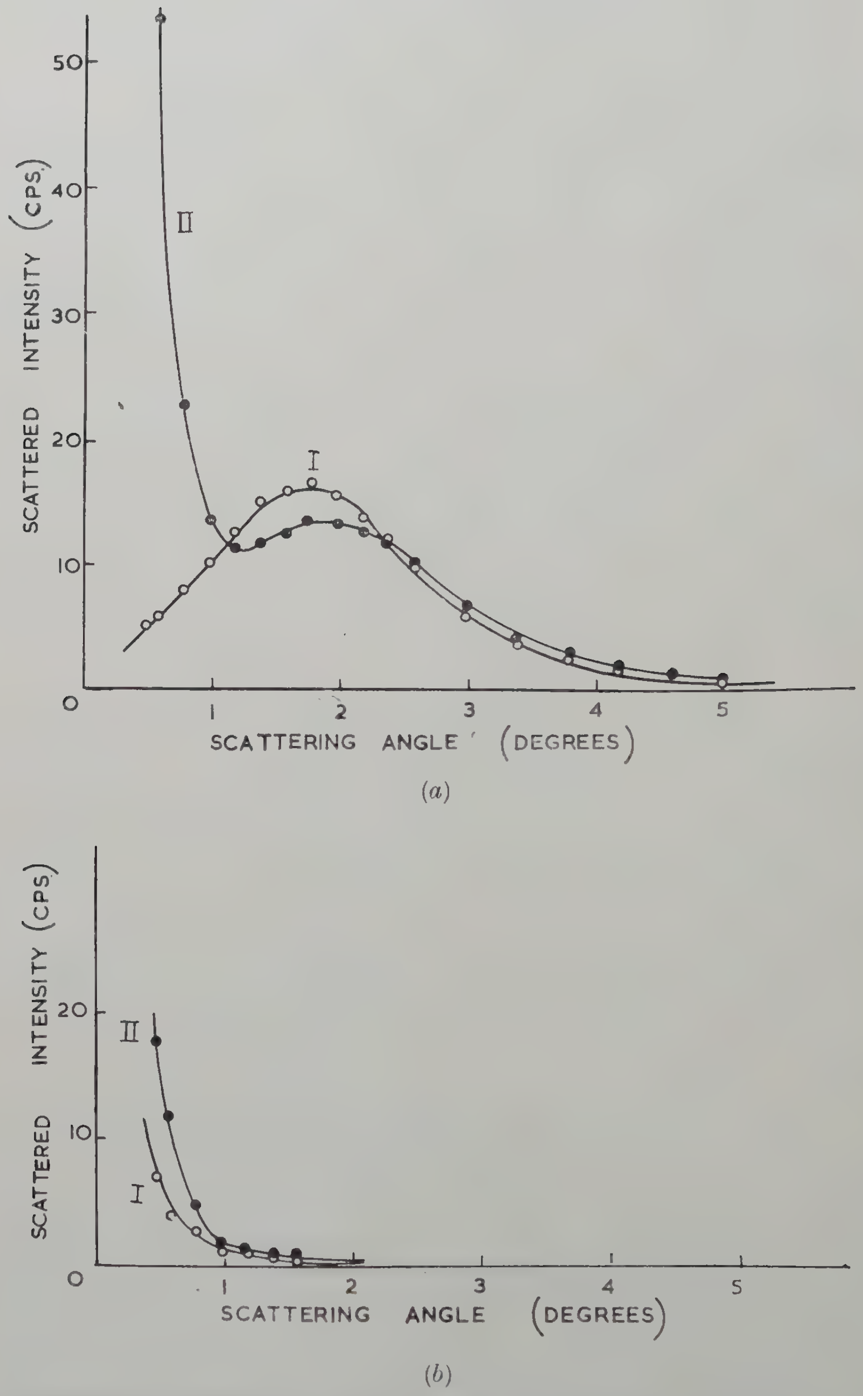

(*a*) Scattering curves for an Al–6 at. % Ag alloy : I—Electropolished and etched ; II—Electropolished only. (*b*) Scattering curves for pure aluminium : I—Electropolished and etched ; II—Electropolished only.

and Davis (1959) noted that surface oxide on aluminium prevented formation of surface pits which were due to condensation of vacancies. Herein are reported small angle scattering studies of foils (25 to 50 microns thick) of Al and an Al–6 at. % Ag alloy quenched from 540°c indicating that a surface film is effective in increasing the magnitude of the double Bragg scattering; escape of vacancies to the surface is reduced.

The small angle scattering was measured using a General Electric XRD–5 diffractometer using a balanced filter technique to isolate the scattering due to CuK_α radiation. The readings obtained were corrected for parasitic scattering. The foils were all capsulated in evacuated pyrex ampules (10^{-6} mm Hg pressure) and drop quenched in water from 540°c.

The figure gives the intensity of the small angle scattering for two conditions: I—Electropolished (in a bath of 817 cm^3 orthophosphoric acid, 40 cm^3 water, 156 g chromic acid, and 143 cm^3 sulphuric acid) and etched in hydrofluoric-nitric acid mixture; and II—Electropolished only. It is to be noted that the small angle scattering below 1° is considerably larger for the unetched samples. Sample foils of Al–6 at. % Ag with the as rolled surface gave curves essentially identical to fig. 1 (*a*)—I. In the case of the alloy the scattering peak between 1° and 2° is due to the presence of Guinier–Preston zones.

The following interpretation of the data in fig. 1 is suggested. In thin foils the surface is a very important sink for quenched-in vacancies. During electropolishing a surface film is presumed to form on the specimen, reducing escape of vacancies. The additional quenched-in vacancies then result in an additional number of dislocation loops or spirals. Etching removes the film and the effect is not observed.

REFERENCES

DOHERTY, P. E., and DAVIS, R. S., 1959, *Acta Met.*, **7,** 111.
SMALLMAN, R. E., and WESTMACOTT, K. H., 1959, *J. appl. Phys.*, **30,** 603.

REVIEWS OF BOOKS

Electrophoresis. Theory, Methods and Applications. Edited by MILAN BIER. (Academic Press Inc., 1959.) [Pp. 563.] 107*s.* 6*d.*

ELECTROPHORESIS has long played a major rôle in the study of colloidal systems and this volume sets out to give an account of the various forms of electrophoresis which have been employed and the systems which have been studied by this technique. The first three chapters are largely theoretical and are devoted to consideration of the distribution of electric potential at interfaces, acid-base equilibria of proteins and the theory of the moving boundary method of electrophoresis. Other chapters deal with the methods and applications of moving boundary, paper, zone and microscopic electrophoresis. The use of electrophoresis as a technique for the separation of mixtures and as a means of studying interacting systems is also discussed. The material, in general, appears to be soundly presented and well illustrated. The text is relatively free of typographical errors, but nomenclature, unfortunately, is not kept quite consistent from chapter to chapter. The emphasis of the book is very much in the direction of biological chemistry, a predominance not suggested by the title, and it is to be regretted that a little more space has not been devoted to the applications of electrophoresis to other large and important fields, such as, mineral dressing, hydrophobic sols, emulsions, and suspensions in non-aqueous media. This book does, however, make a useful and commendable contribution to the subject of electrophoresis.

R. H. O.

Semi-conductors. By R. A. SMITH. (Cambridge University Press, 1959.) [Pp. 494+xvii.] 65*s.*

THE output of work on solid state physics is now so great that the task of keeping up-to-date is an extremely difficult one. It is true that there are various series of summarizing reviews, but many of the articles are written before the subjects they deal with have been properly consolidated, and the student is often forced to read not only the reviews but the original papers as well. It is therefore a pleasure to find a book such as Dr. R. A. Smith's *Semi-conductors* which deals with a well-defined section of solid state physics in a workmanlike fashion.

The first part of the book gives an account of the fundamental principles of carrier concentrations in semi-conductors, of electron transport phenomena including the diffusion of electrons and positive holes, and of optical effects. The treatment is far from devoid of mathematics, but, since the various steps are spelled out in more detail than in most of the standard texts, it should be generally acceptable to physicists and engineers. The second part of the book deals with the methods of determining the characteristic properties of semi-conductors, followed by an account of the properties of elemental and compound semi-conductors and brief accounts of their more important applications. The chapters dealing with the properties of the individual semi-conductors are particularly valuable.

A. H. W.

[*The Editors do not hold themselves responsible for the views expressed by their correspondents.*]

Fig. 2

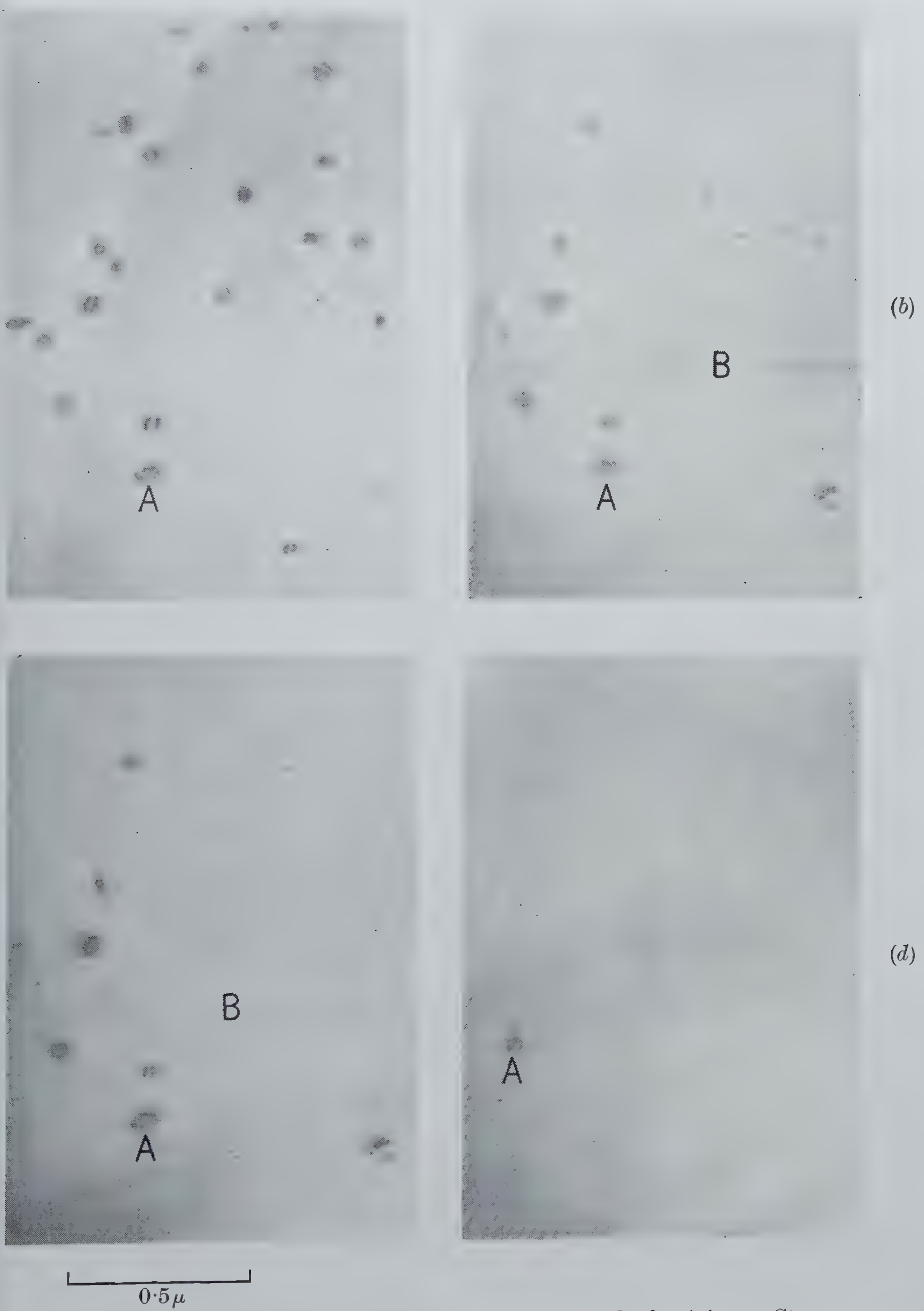

Sequence showing the annealing of loops in quenched aluminium. Stage temperature 187°C. The interval between exposures is ~1 min. Note the loop A which remains through the whole sequence. Note also the slip trace B left by a moving dislocation in (*b*) and (*c*). Mag. ×53 000.

Fig. 3

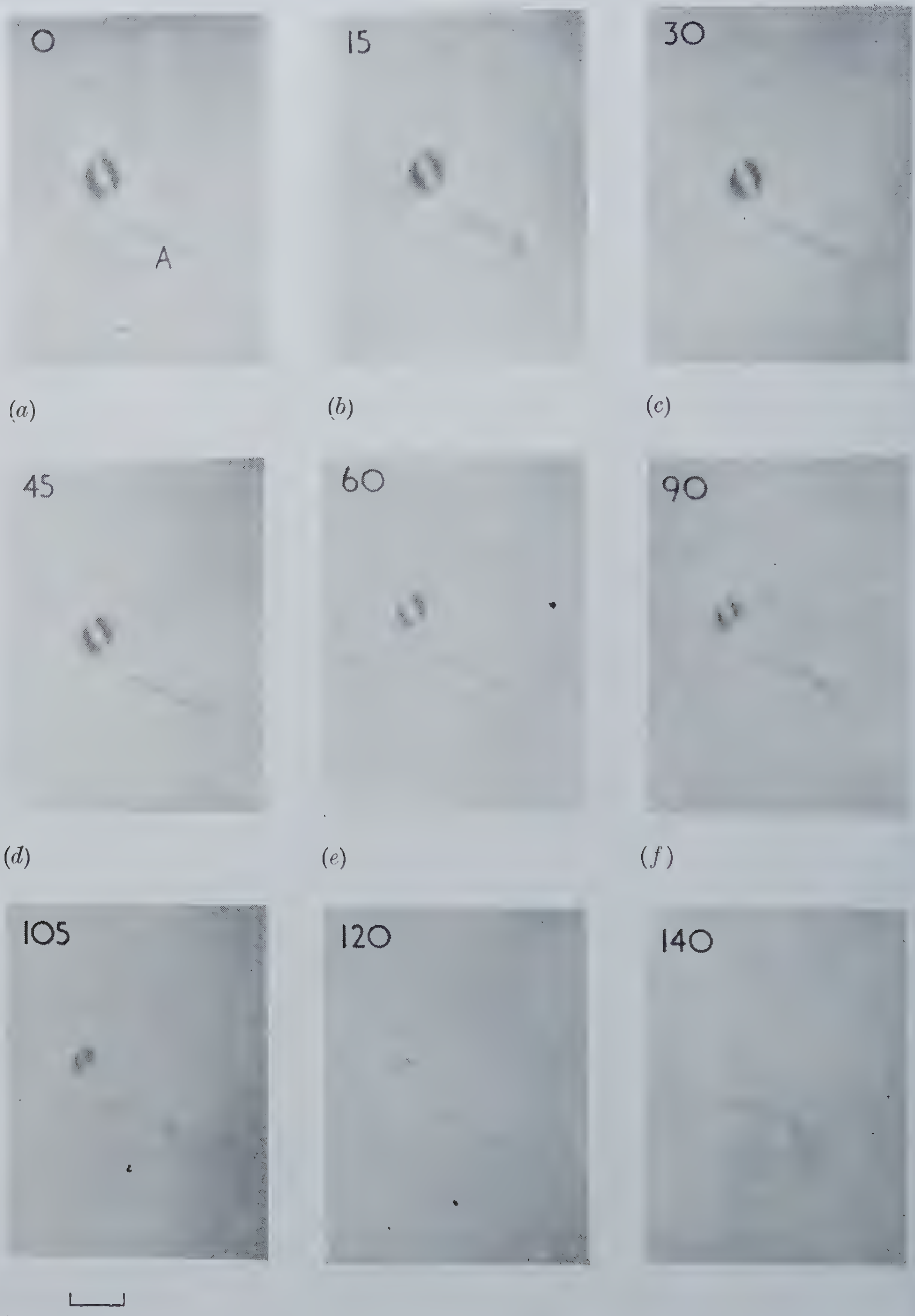

(*a*) (*b*) (*c*)

(*d*) (*e*) (*f*)

(*g*) (*h*) (*i*)

Sequence showing the annealing of an isolated loop near a dislocation A. Stage temperature 197°c. The numbers refer to the time in seconds at which exposures were made. The loop lies on an inclined plane and the more steeply inclined parts are less visible. Mag. × 82 500.

Fig. 5

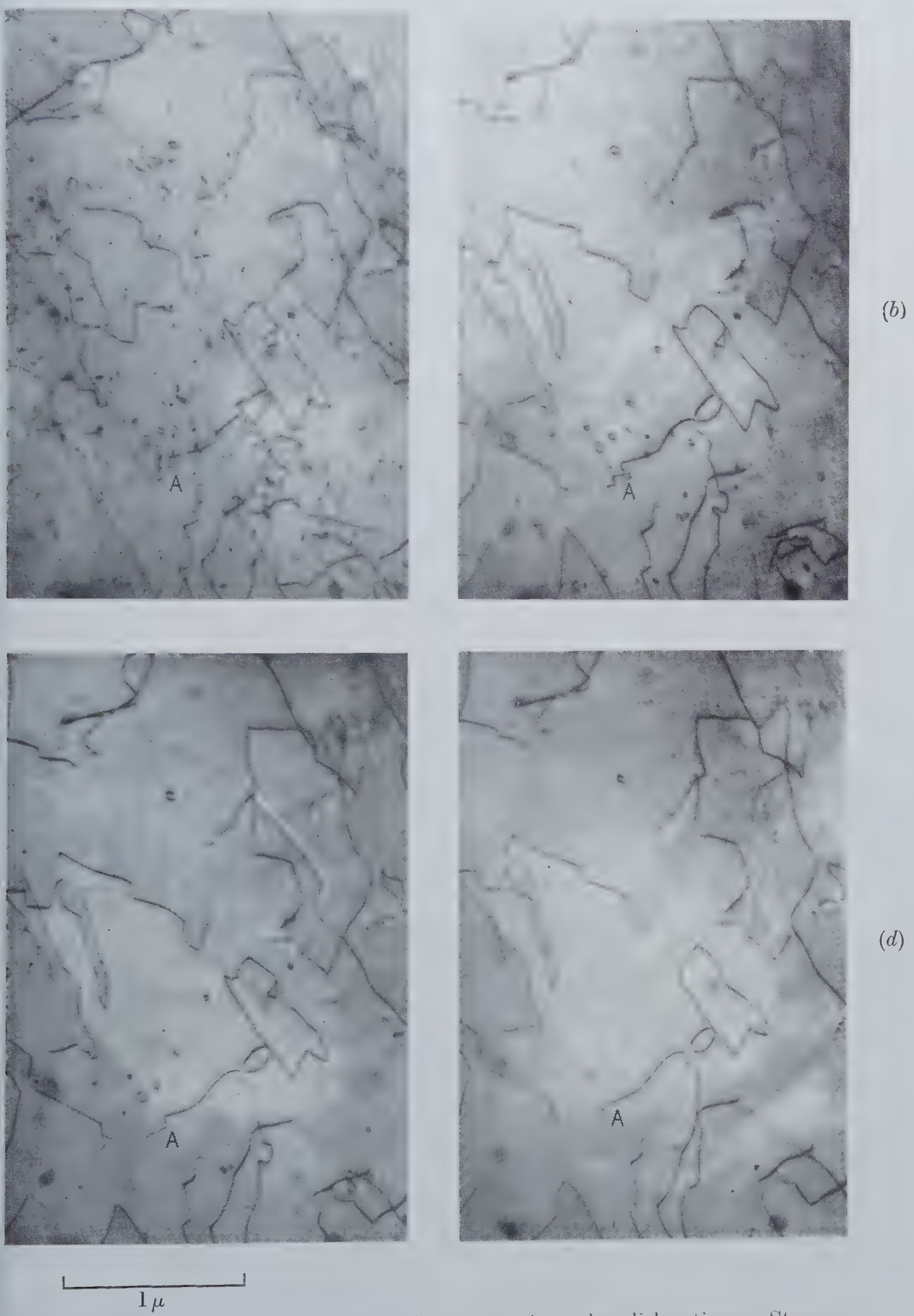

Sequence showing the annealing of loops near irregular dislocations. Stage temperature and time not recorded. As the loops anneal out the irregular dislocations become smoother. This effect is thought to be due at least partly to climb. Mag. ×28 000.

Fig. 6

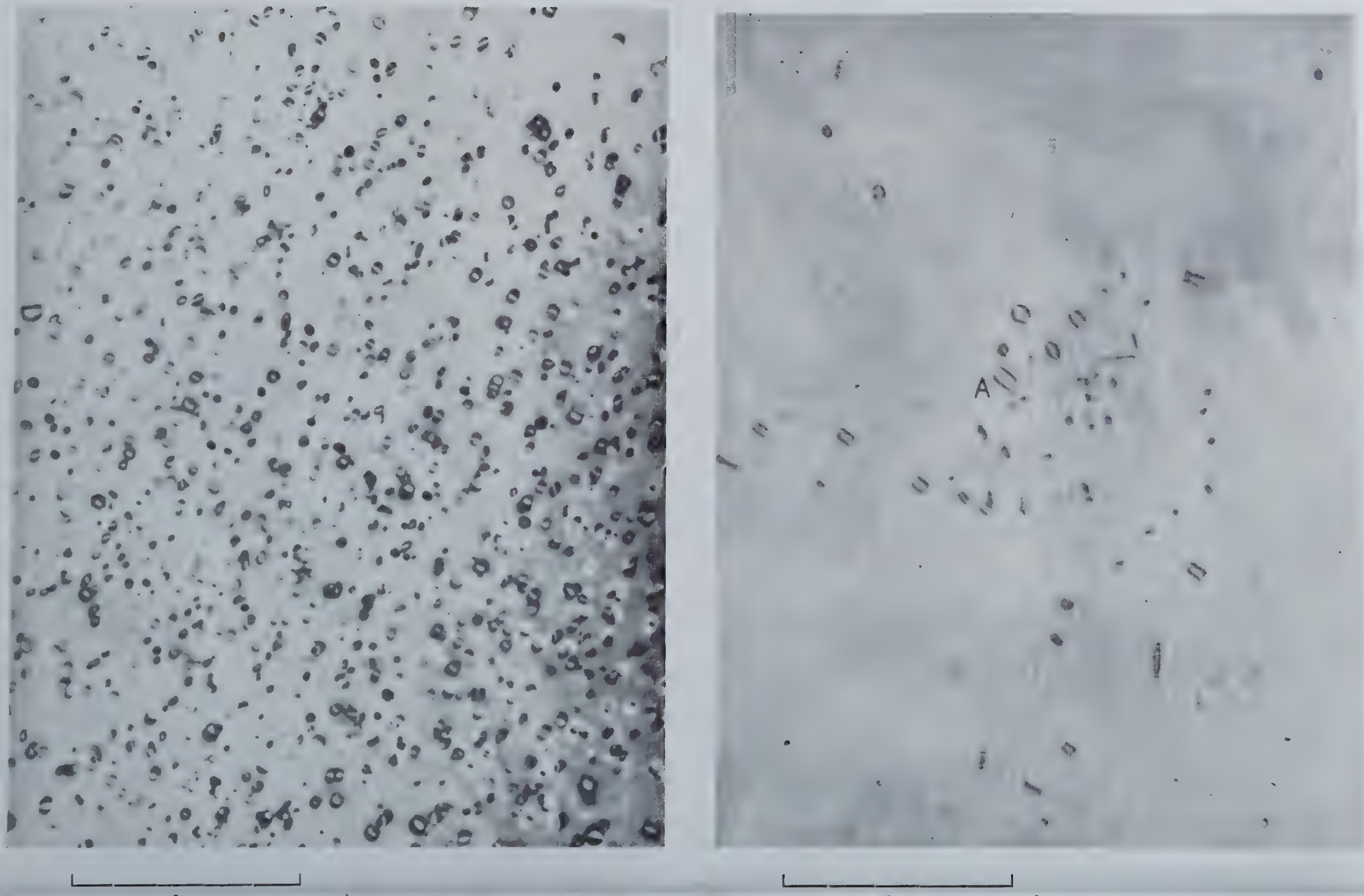

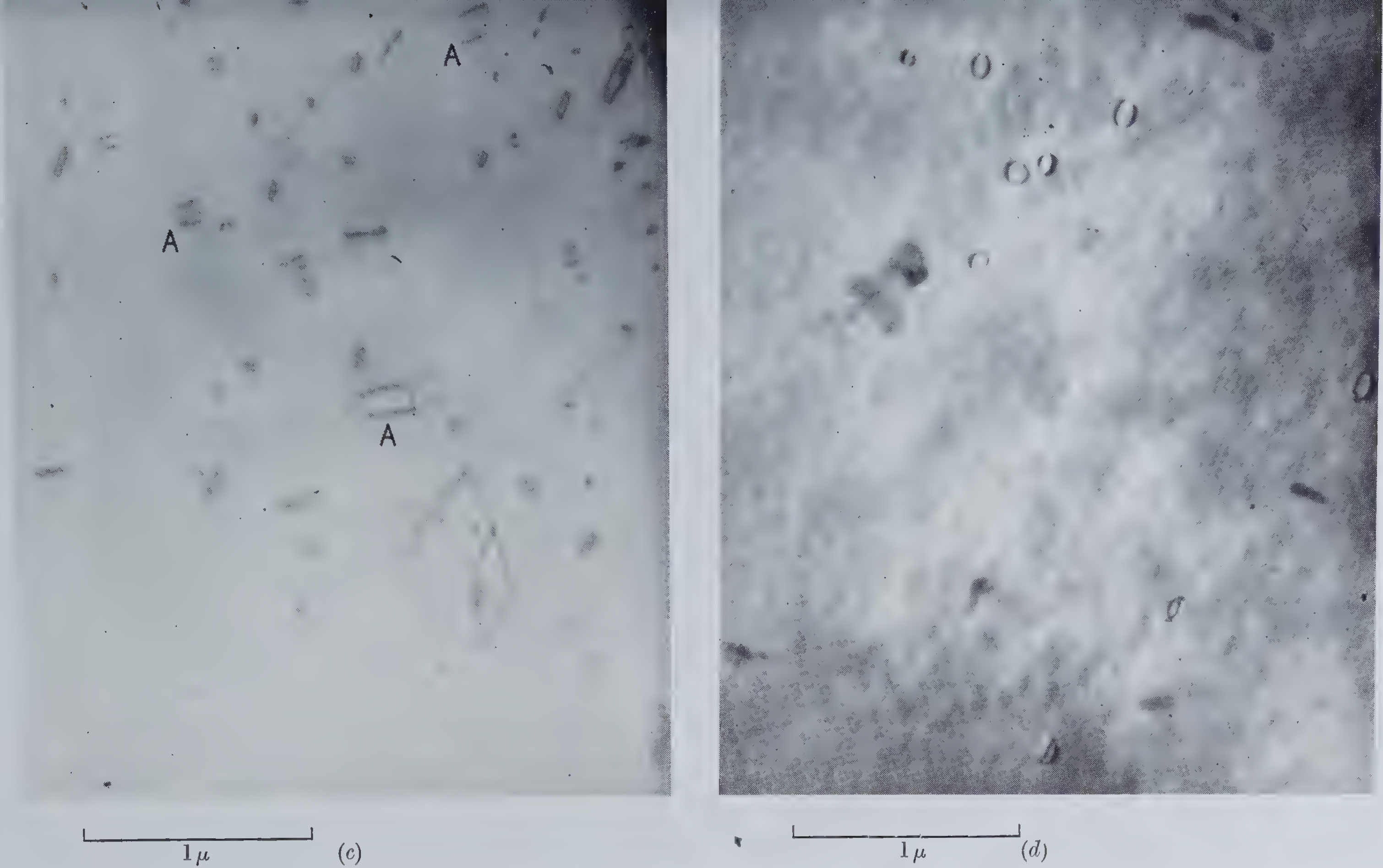

(c) (d)

Typical micrographs showing the annealing of loops in bulk material.

(*a*) Typical micrograph of Al quenched from 600°c—no annealing. (*b*) and (*c*). Micrographs obtained after annealing the bulk material at 190°c for 6 minutes prior to thinning. Note the larger angular shaped loops at A. The small loops remaining are probably the remnants of larger loops which have almost disappeared during the 6-min. anneal. (*d*) Micrograph obtained after annealing the bulk material for 6 min at 200°c. Note the large loops. Mag. ×33 000.

Fig. 2

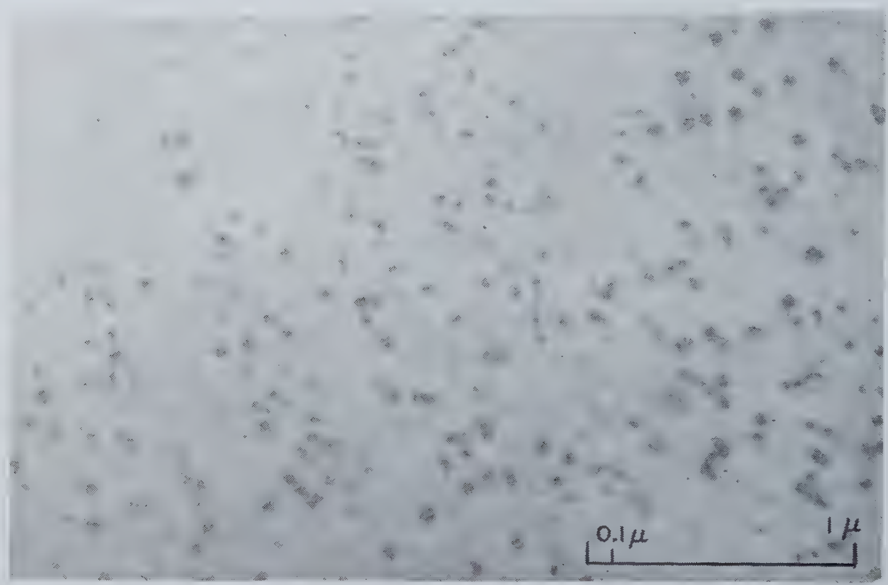

As-quenched dislocation loops.

Fig. 3

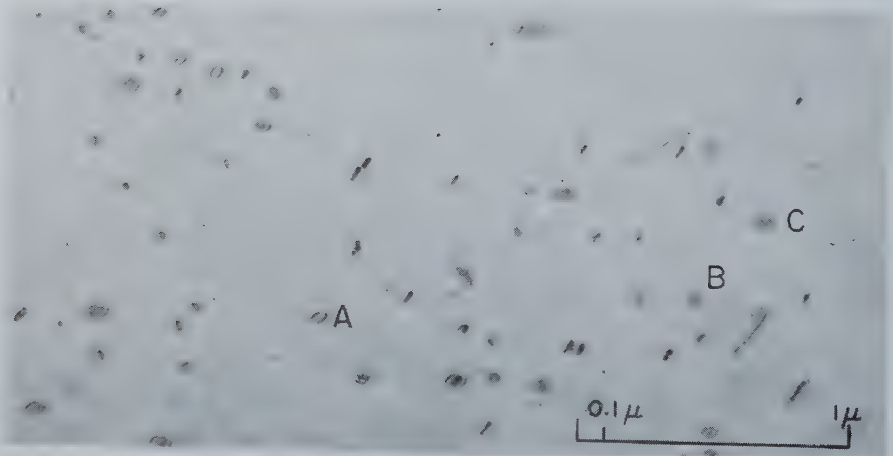

Three types of dislocation loops: (A) single loop, (B) hexagon, (C) double loop. (Note crystallographic alignment of the loops.)

Fig. 4

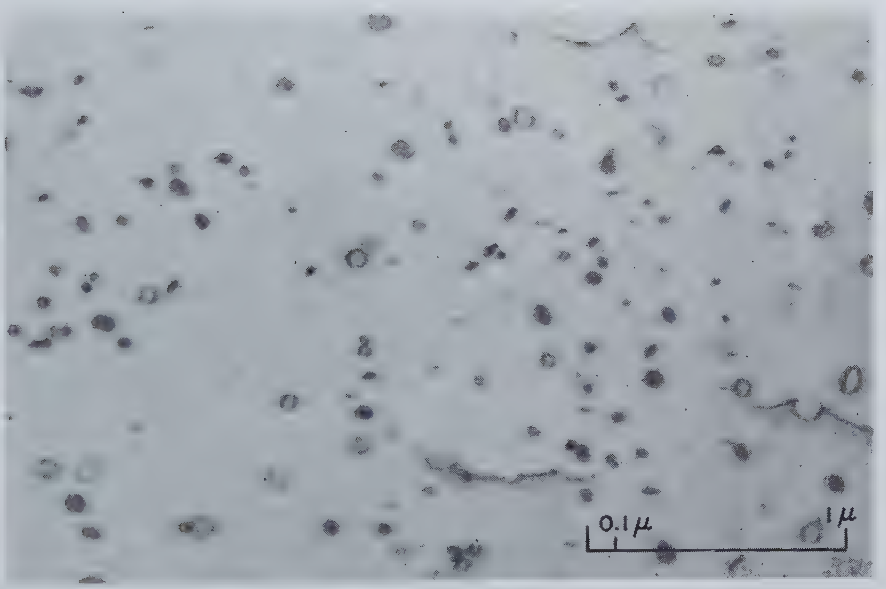

Annealed 10 min at 125°c after quenching.

Fig. 5

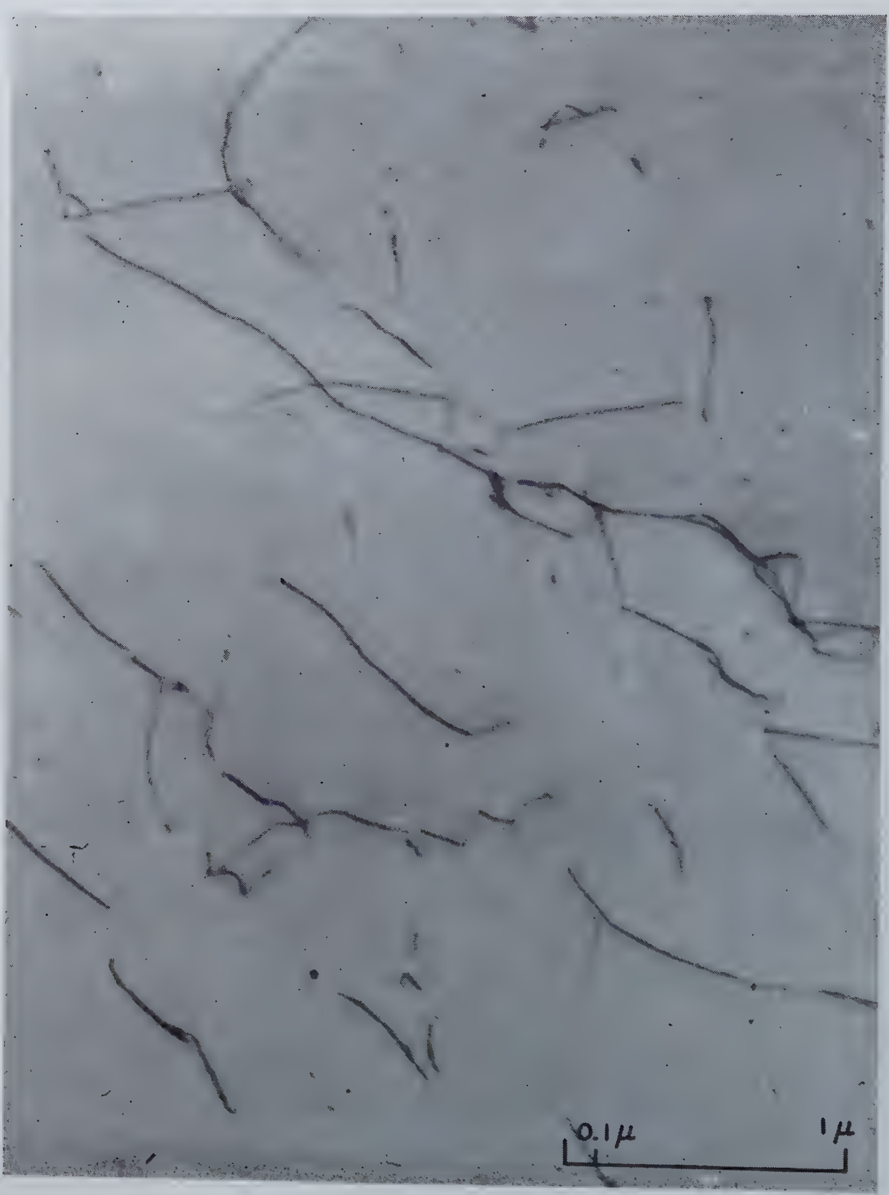

Annealed 10 min at 125°c after quenching.

Fig. 6

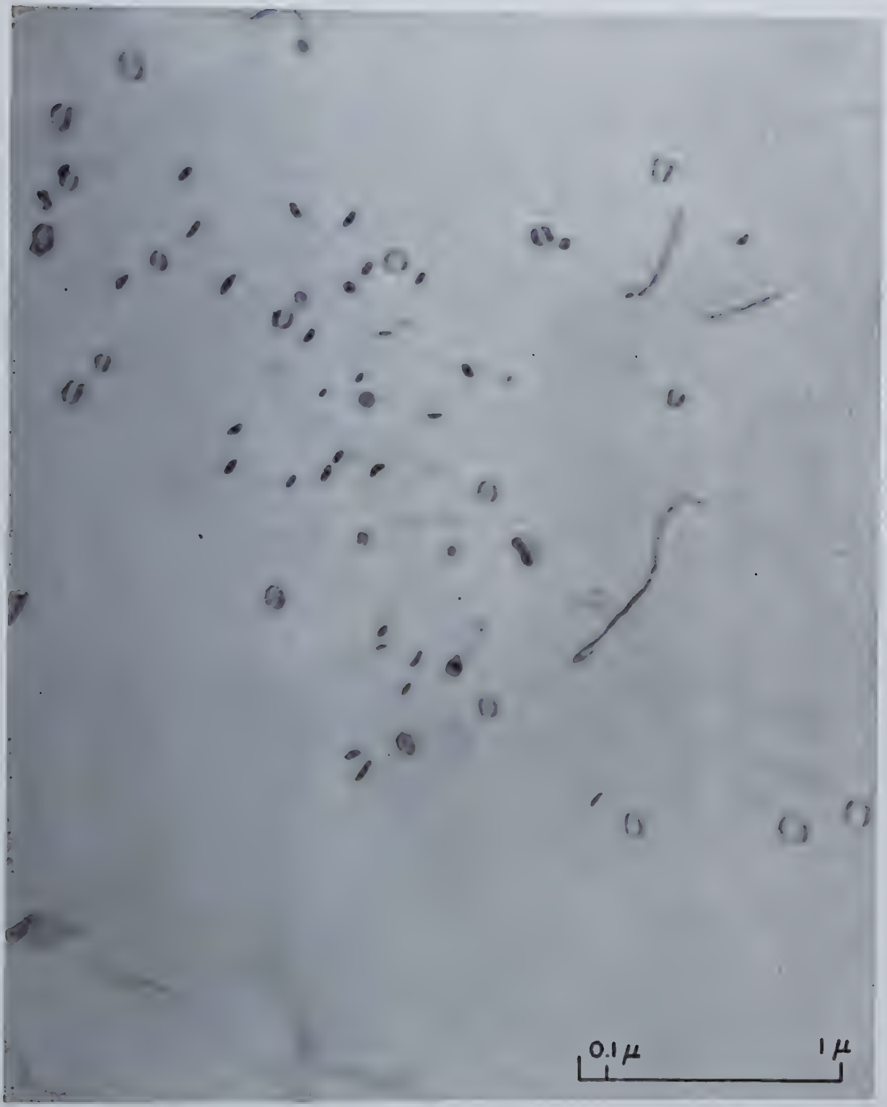

Annealed 10 min at 125°c after quenching.

Fig. 7

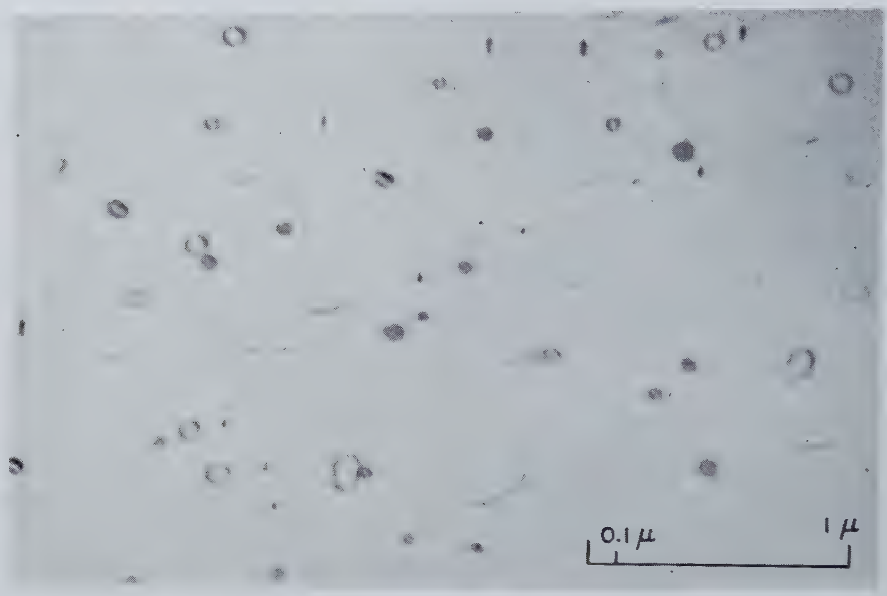

Annealed 10 min at 150°c after quenching.

Fig. 8

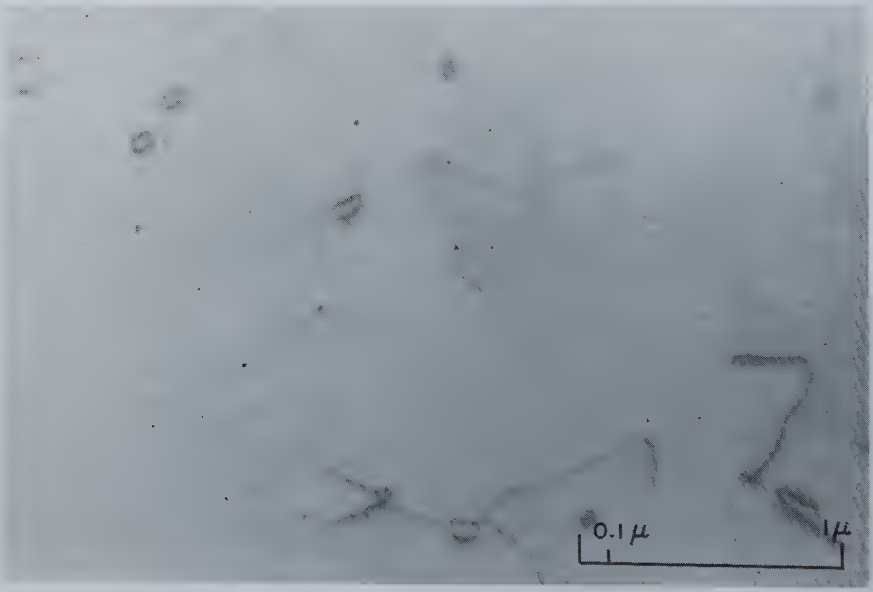

Annealed 10 min at 175°c after quenching.

Fig. 9

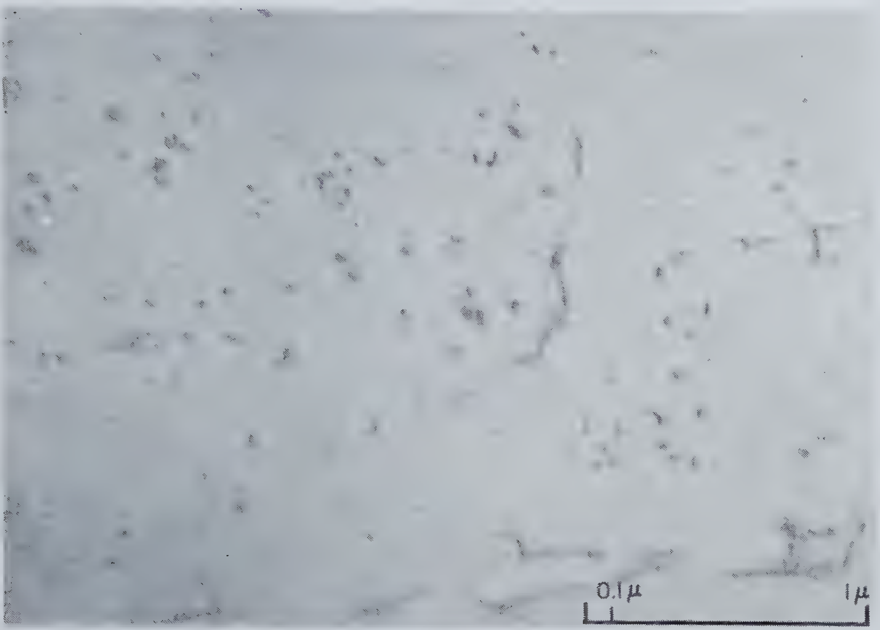

Extended 2½% in tension after quenching.

Fig. 10

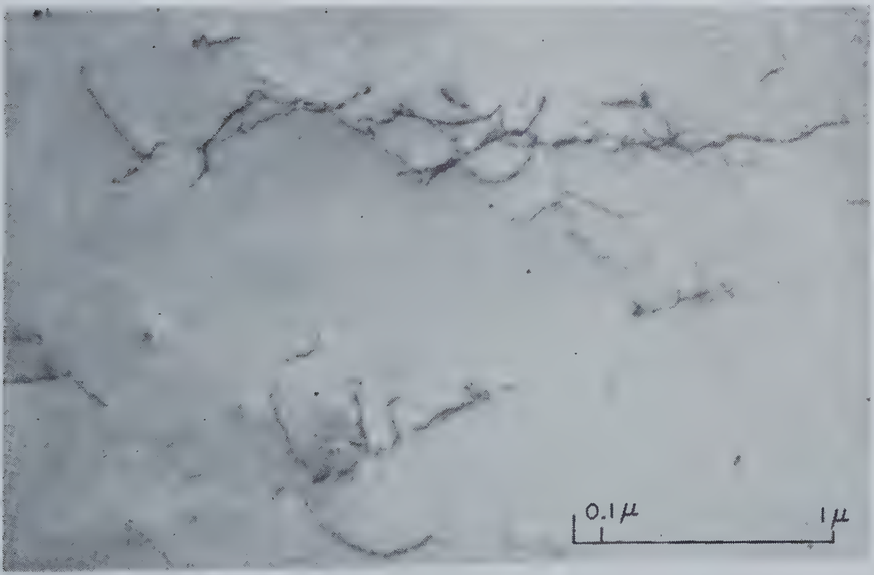

Cold rolled 5% after quenching.

Fig. 11

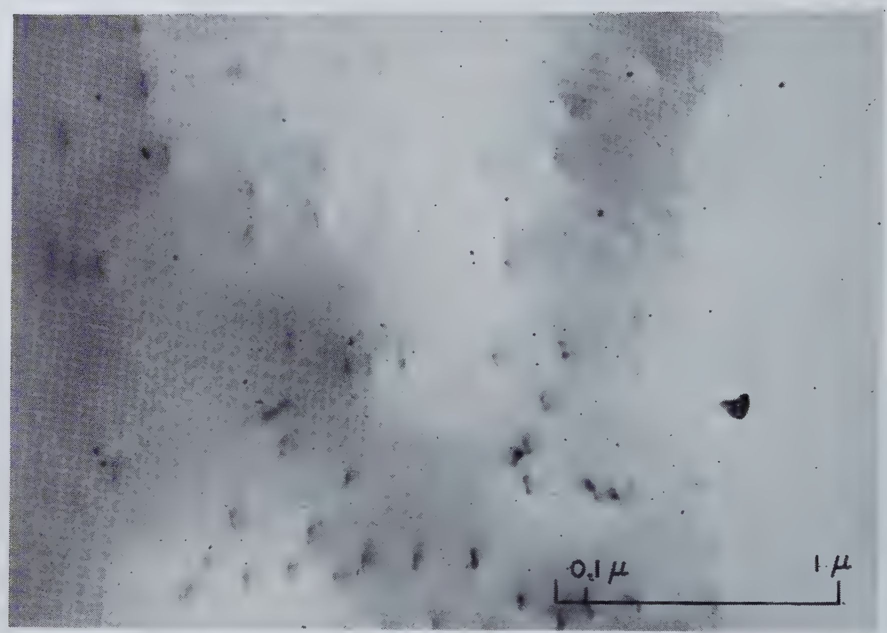

Cold rolled 5% after quenching.

Fig. 12

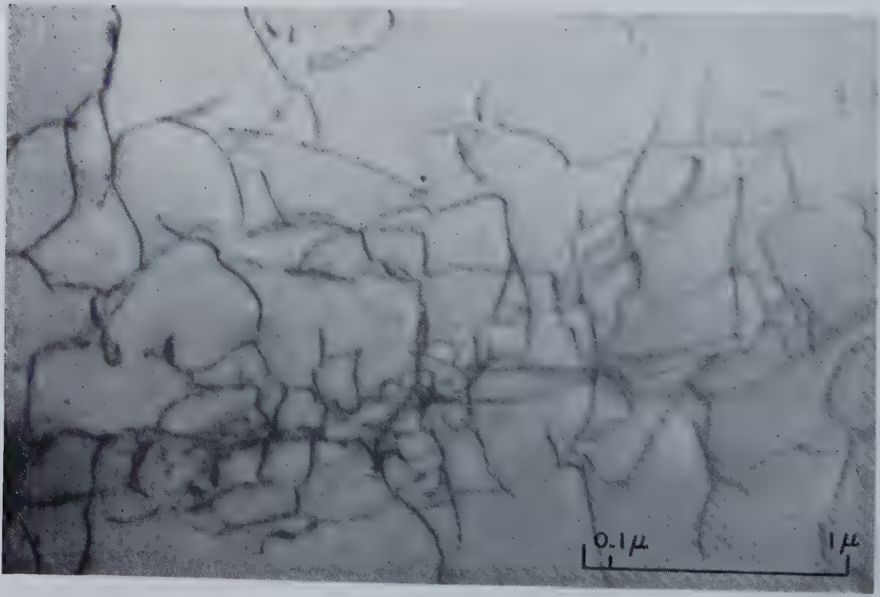

Cold rolled 15% after quenching.

Fig. 13

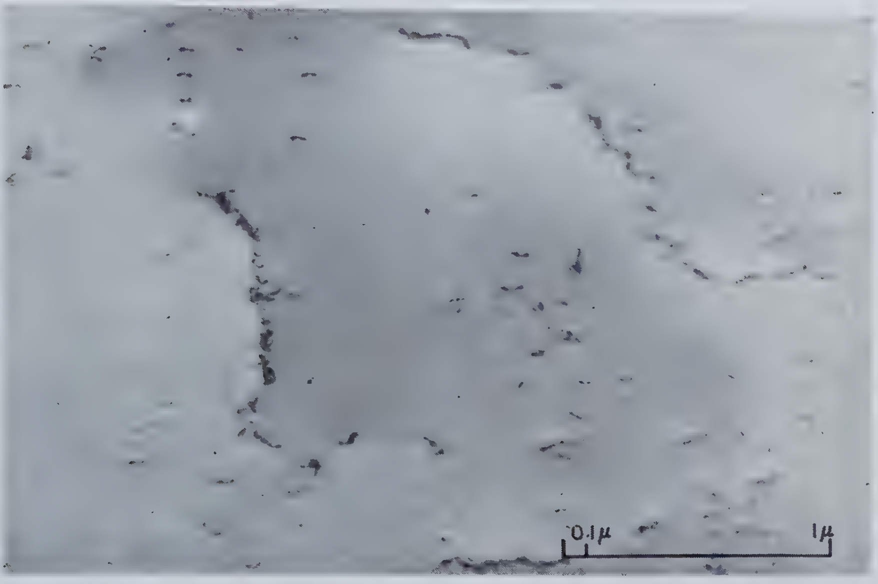

Cold rolled 15% after quenching.

Fig. 14

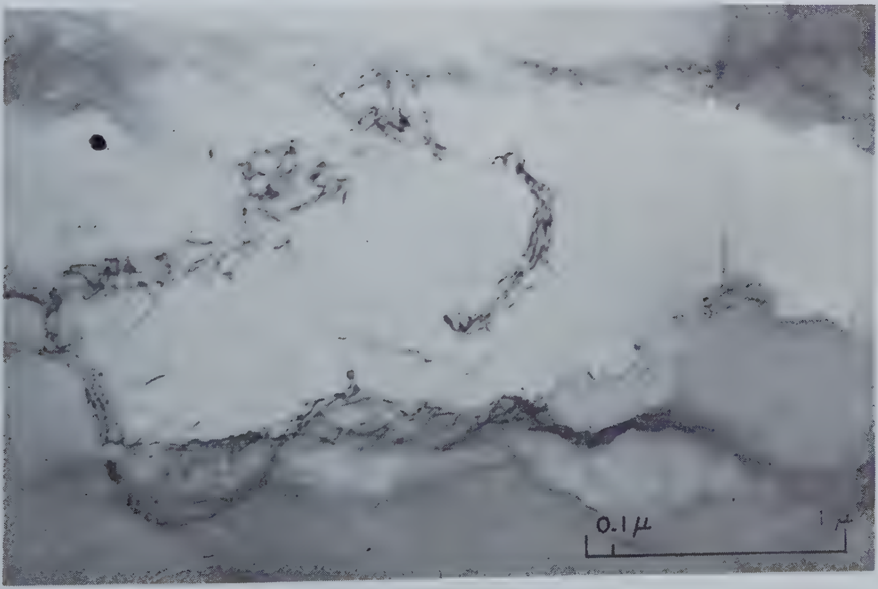

Cold rolled 45% after quenching.

Fig. 15

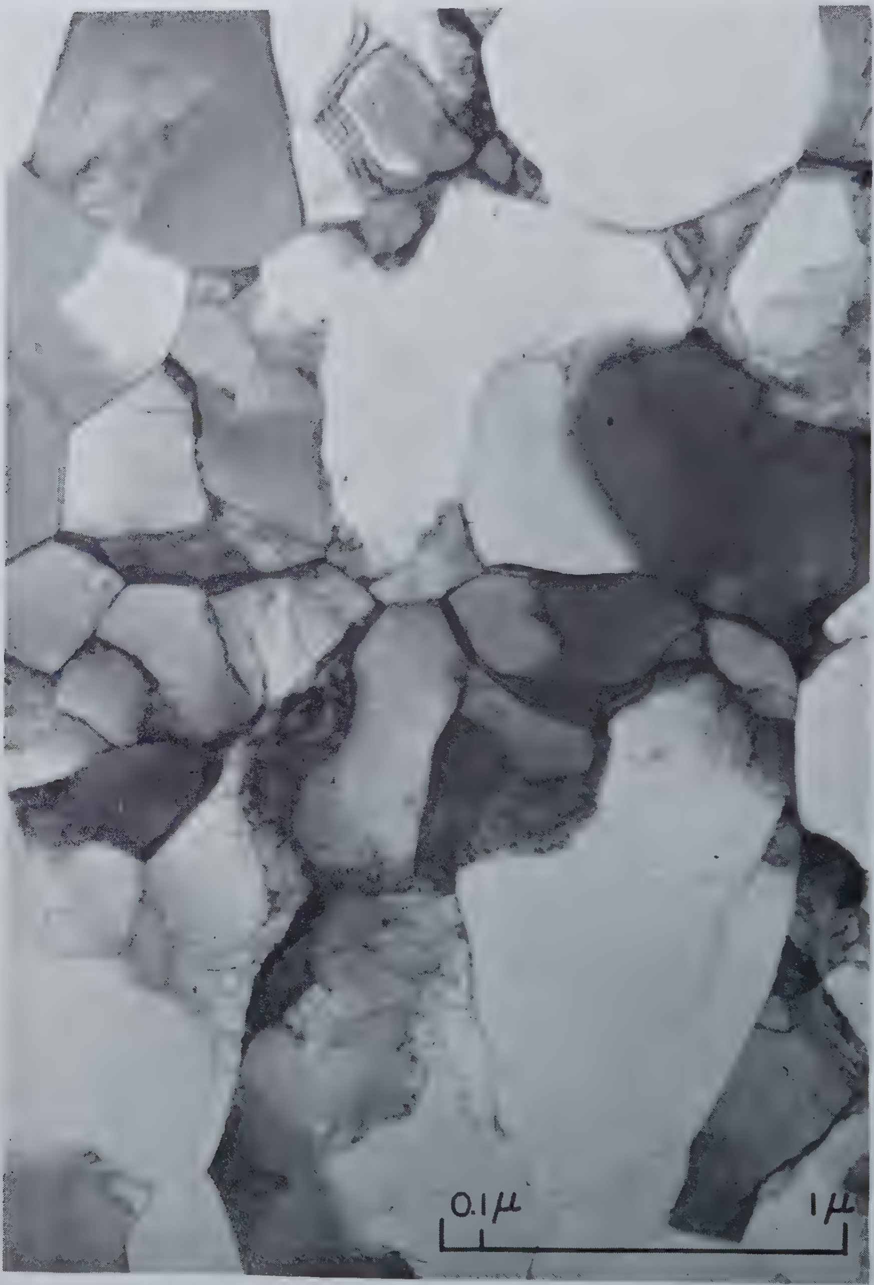

Cold rolled 98% after quenching.

Fig. 1

Natural rubber film. Very little structure is visible.

Fig. 2

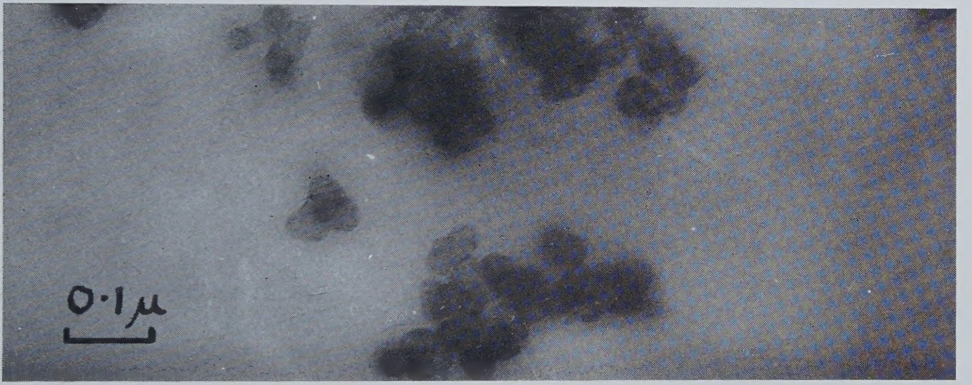

Film of natural rubber with 10% of carbon black (' MPC black ') filler.

Fig. 3

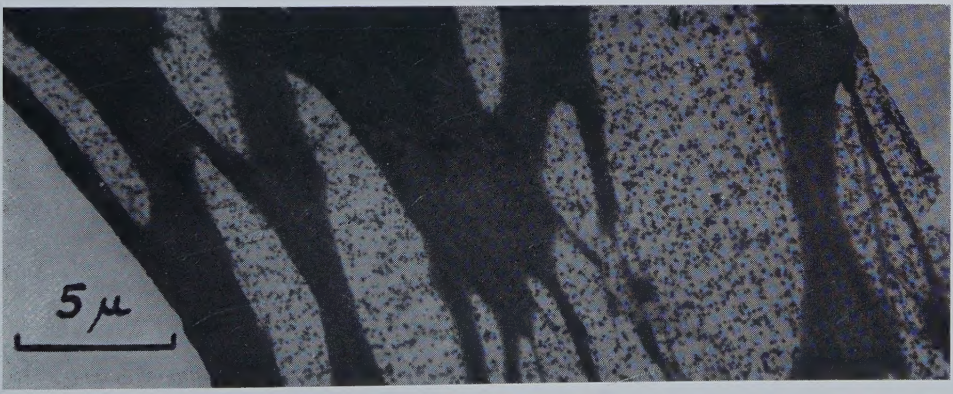

Film of natural rubber with 2% of carbon black (' MPC black ') filler, after being stretched. Numerous thin patches have developed in the film.

Fig. 4

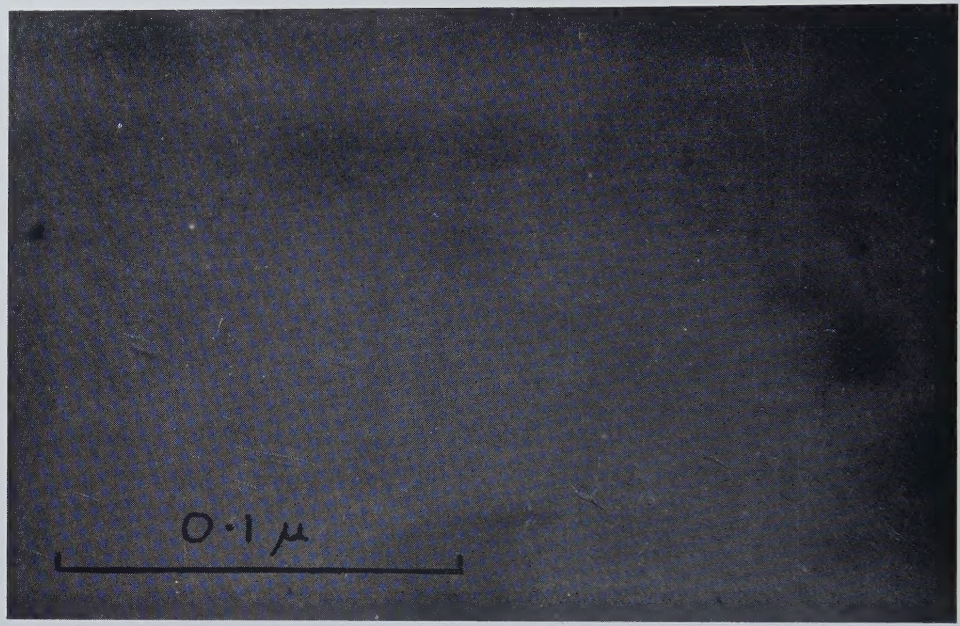

Film of natural rubber containing about 5% neoprene. The dark patches probably represent areas of neoprene, the smaller ones corresponding to individual molecules.

Fig. 5

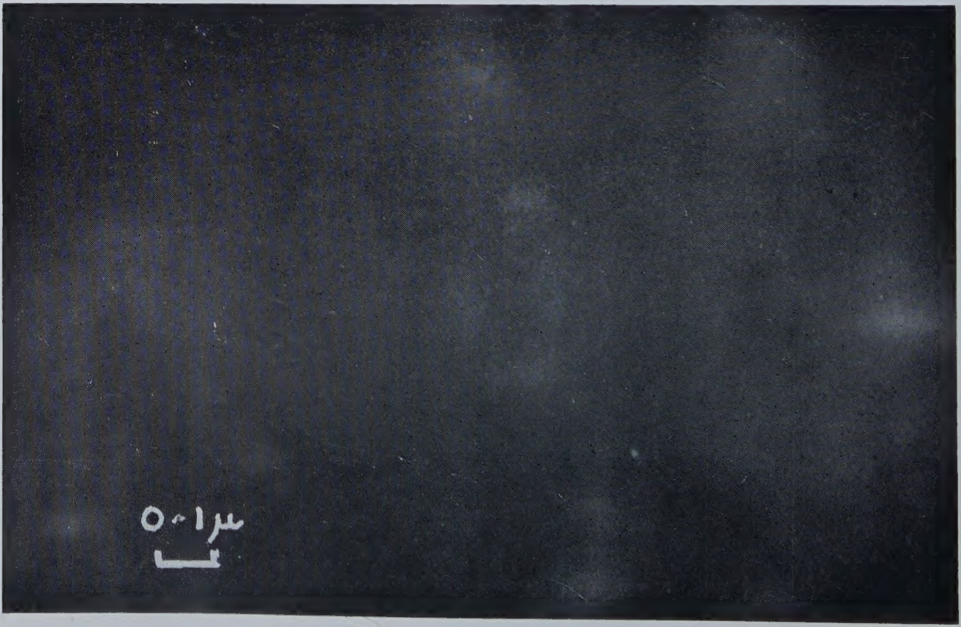

Film of neoprene containing about 5% natural rubber. This shows the expected appearance of light patches on a dark background.

Fig. 6

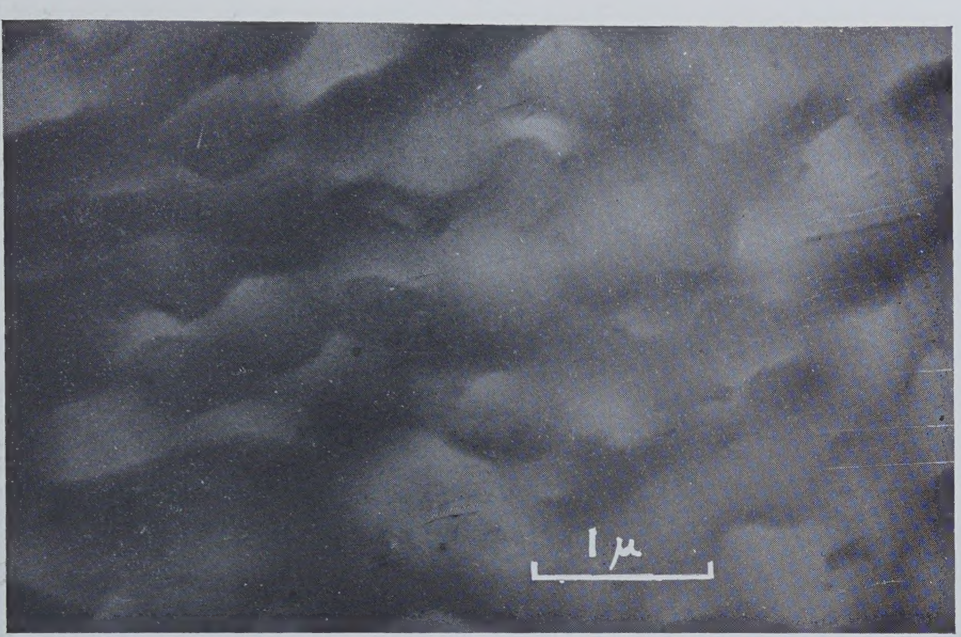

Film of 50% natural rubber, 50% Alloprene. The two polymers have not mixed and the film is inhomogeneous.

Fig. 7

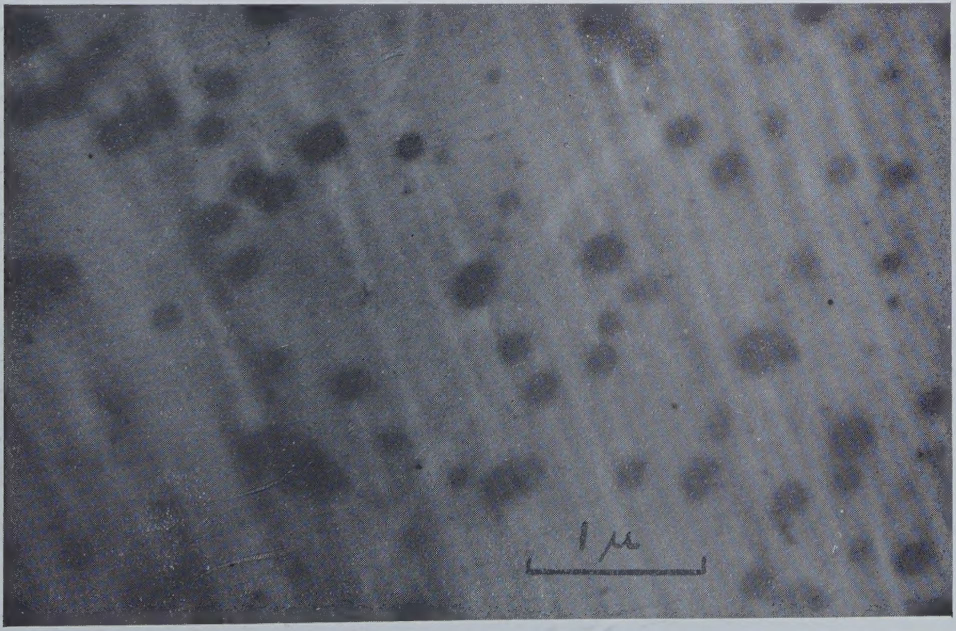

Film of 80% natural rubber, 20% Alloprene. The dark patches are thought to represent globules of Alloprene.

Fig. 8

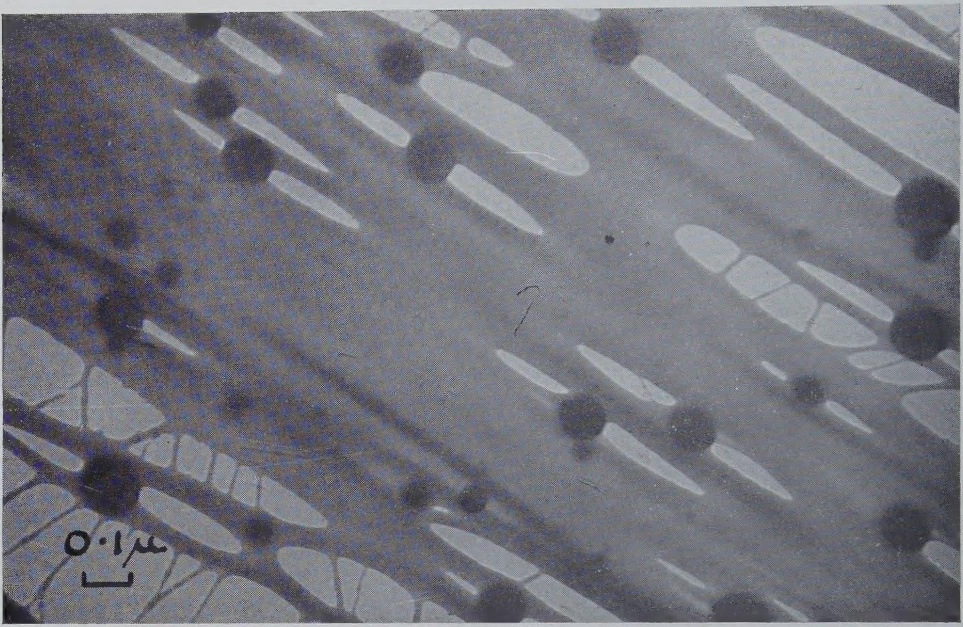

Film of 90% natural rubber, 10% Alloprene, after being stretched. The film has torn at the dark patches and this suggests that the adhesion between the two polymers was weak.

Fig. 9

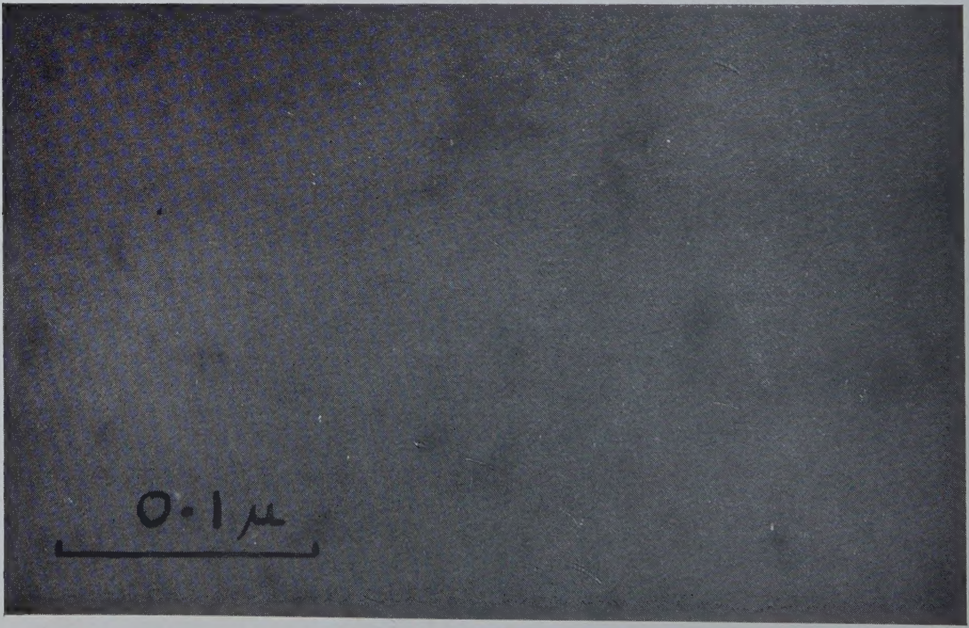

Film of 95% natural rubber, 5% Alloprene. Small dark patches—probably due to individual molecules of the Alloprene—are visible.